LASER STUDIES OF RELAXATION PROCESSES IN SF_6

by

DAVID GEORGE SUTTON

S.B. University of California at Berkeley

(1966)

SUBMITTED IN PARTIAL FULFILLMENT OF THE

REQUIREMENTS FOR THE DEGREE OF

DOCTOR OF PHILOSOPHY

at the

MASSACHUSETTS INSTITUTE OF TECHNOLOGY

(Feb. 1971)

Archives

MASS. INST. TECH.

MAR 2 1971

LIBRARIES

Signature of Author_____

Department of Chemistry

Certified by_____

Thesis Supervisor

Accepted by_____

Chairman, Departmental Committee on Graduate Students

This Doctoral Thesis has been examined by a Committee of the Department of Chemistry as follows:

. . . . . .

Professor John S. Waugh

Chairman of Thesis Committee

. . . . . .

Associate Professor Jeffrey I. Steinfeld

Thesis Supervisor

. . . . . .

Professor John Ross

LASER STUDIES OF RELAXATION PROCESSES IN SF_6

by

DAVID GEORGE SUTTON

Submitted to the Department of Chemistry on September , 1970
in partial fulfillment of the requirement for the
degree of Doctor of Philosophy

ABSTRACT

The infrared spectroscopy of SF_6 relevant to laser experiments is discussed. A computed contour of the ν_3 band is presented which reproduces the prominent Q branch structure. Experiments measuring the saturation of absorption by the ν_3 transition in SF_6 by a CW CO_2 laser and Q-switched pulse transmission in the same medium are described. The results of these experiments are interpreted with the aid of a four state model for energy transfer in SF_6. Machine calculations based on this model reproduce the experimental results and yield cross sections for rotational and vibrational energy transfer.

A double resonance experiment involving two CO_2 lasers which allows the direct, time resolved observation of ground state bleaching, and excited state absorption in SF_6 is described. The experimental results yield rates of vibrational to translational energy transfer in bimolecular collisions between SF_6 and a variety of buffer gases and provide evidence for the validity of the four state model. Finally the direct observation of acoustical pulses generated in SF_6 gas by a coincident Q-switched CO_2 laser is reported. Measurements on these pulses enable us to set a lower limit on the rate at which translational energy is generated in the gas when the laser pumped levels relax.

Thesis Supervisor: Jeffrey I. Steinfeld
Title: Associate Professor of Chemistry

This work is dedicated to Professor Isadore Amdur,

who helped and inspired so many of us.

ACKNOWLEDGEMENTS

Gratitude is insufficient payment for the guidance and inspiration provided by Jeffrey Steinfeld. I can only hope that he receives a small fraction of the satisfaction afforded me in our association. Special thanks are due to Dr. Itamar Burak who worked closely with me and provided much necessary impetus, Irene Platzblatt who contributed in the early stages of this work, and Andrew Nowak who has been a helpful comrade. Finally, I wish to acknowledge the considerable sacrifices made by my wife and son and thank the N.I.H. who made it possible for us to survive.

TABLE OF CONTENTS

Table of Figures.....6

A. Introduction.....8

B. Spectroscopy of SF_6.....11

C. Saturation and Pulse Transmission.....26

D. Double Resonance Experiments.....43

E. Infrared Induced Acoustic Pulse.....61

F. Summary of Results and Evidence for the Four State Model.....72

APPENDICES

Appendix 1: Pulse Transmission Program.....75

Appendix 2: Infrared Saturation in Sulfur Hexafluoride.....80

Appendix 3: Infrared Double Resonance in Sulfur Hexafluoride....103

Appendix 4: Statistical Weights for Rovibrator Levels of SF_6....119

Biographical Note.....121

TABLE OF FIGURES

Figure 1: Absorption Spectrum of SF_6.....12

Figure 2: Energy, Symmetry, Degeneracy and Fractional Populations of Singly Excited Normal Modes of SF_6.....13

Figure 3: Absorption Contour, CO_2 Laser Coincidence, and Laser Absorption Coefficients for the ν_3 Band of SF_6.....15

Figure 4: Computer Synthesized ν_3 Band of SF_6.....21

Figure 5: Some Dipole Allowed Transitions in SF_6 near 947 cm^{-1}....23

Figure 6: Deconvolution of Computer Synthesized Band.....25

Figure 7: Apparatus for Study of Pulse Transmission.....28

Figure 8: Typical Pulse Transmission Data.....30

Figure 9: Four State Model for Energy Flow in SF_6.....32

Figure 10: Beer-Lambert Law Reproduced by Pulse Transmission Program.....36

Figure 11: CW Saturation Calculated Via Pulse Transmission Program.....37

Figure 12: Calculated and Experimental Pulse Shapes.....39

Figure 13: Calculated and Experimental Pulse Shapes.....40

Figure 14: Double Resonance Cell Used with Perkin-Elmer 337 Spectrometer.....44

Figure 15: Infrared Spectrum of Irradiated SF_6.....45

Figure 16: SF_6 Absorption Spectra Near 947 cm^{-1}.....46

Figure 17: Geometry for Heating Calculations in a Laser Pumped Gas.....48

Figure 18: Pump and Monitor Laser Beams Incident on Double Resonance Cell.....51

Figure 19: Detection Circuitry.....57

Figure 20: Detector Time Response for Various Load Resistors.....58

Figure 21: Apparatus for Acoustical Pulse Measurement.....63

Figure 22: Acoustic Signals.....66

Figure 23: Acoustical Pulse from Non-Saturating Excitation.....68

Figure 24: Acoustical Pulse from Saturating Excitation.....69

A. INTRODUCTION

Lasers have not only made possible many studies heretofore impossible, but have stimulated many investigations of processes basic to their operation. Saturation,[1,2] energy transfer,[3,4] gaseous discharges,[5] mode structure,[6] and quantum electronics[7,8] can not only be studied by lasers, but are inherent in laser physics. A host of ancillary processes have also stimulated much research.

The studies described here have centered around the satura-

---

1. I. Burak, J. I. Steinfeld, and D. G. Sutton, J. Quant. Spectrosc. Radiat. Transfer 9, 959 (1969).

2. C. P. Christensen, C. Freed, and H. A. Haus, IEEE J. Quant. Electronics OE-5, 276 (1969).

3. James T. Yardley and C. Bradley Moore, J. Chem. Phys. 46, 4491 (1967).

4. R. Taylor and S. Bitterman, Reviews of Modern Physics 41, 26 (1969).

5. G. Francis, Handbuch Der Physik, 22, 53 (1956).

6. H. W. Kogelnik, Modes in Optical Resonators, in "Advances in Lasers," Volume 1, A. K. Levine (ed.), Dekker, New York, 1966.

7. C. K. N. Patel and R. E. Slusher, Phys. Rev. Letters 19, 1019 (1967).

8. J. P. Gordon, C. H. Wang, C. K. N. Patel, R. E. Slusher, and W. J. Tomlinson, Phys. Rev. 179, 294 (1969).

tion of molecular infrared absorption and energy transfer, the rationale being that novel laser techniques could be applied fruitfully in these areas. Both processes are accessible for experimentation with laser techniques and can straightforwardly be related to the fundamental parameters of molecular physics, therefore facilitating the extraction of these quantities with a minimum of abstraction.

A secondary goal of developing a double resonance technology for application at infrared and optical frequencies served as an added stimulus. The incentive for development of the technique has grown out of the demonstrated power of the microwave and infrared-microwave double resonance experiments[9-13] and the inherent facility of the technique to resolve highly specific energy transfer events and complex optical spectra.

The body of this thesis will mainly handle experimental details and describe procedures used to obtain and reduce data. The bulk of the results are available in several papers which are included as appendices. The infrared double resonance apparatus is fully des-

---

9. T. Oka, J. Chem. Phys. 49, 4234 (1968) and references therein.

10. A. M. Ronn and E. B. Wilson, Jr., J. Chem. Phys. 46, 3262 (1967).

11. A. M. Ronn and D. R. Lide, Jr., J. Chem. Phys. 47, 3669 (1967).

12. J. Lemaire, J. Houriez, J. Bellet, and J. Thibault, Compt. Rend. B268, 922 (1969).

13. T. Shimizu and T. Oka, Symp. Mol. Structure and Spectry., Columbus Ohio, September 1970.

cribed in Section D and Appendix 3.

B. I. R. SPECTROSCOPY OF SF_6

Sulfur hexafluoride was originally chosen as the appropriate molecule to study for two reasons. It was demonstrated to be saturable by attainable fields[14] and was easy to handle with conventional vacuum techniques.

The SF_6 molecule conforms to the octahedral symmetry of the point group O_h. An infrared transition must have F_{1u} symmetry to be infrared active in the dipole approximation. Only two fundamental modes have this symmetry: the ν_3 mode at 947 $cm.^{-1}$ and the ν_4 at 617 $cm.^{-1}$ Both of these modes are triply degenerate and between them account for six of the fifteen vibrational internal degrees of freedom. These modes give rise to the two strong absorption bands in the infrared spectrum shown in Figure 1. The weak absorption peaks are assigned to various combination bands which have components of F_{1u} symmetry. Figure 2 shows all of the fundamental modes together with their assigned frequency, degeneracy, and fractional Boltzman population at 300° K. The form of the fundamental modes is illustrated on page 122 of reference 15.

---

14. O. R. Wood and S. E. Schwarz, Appl. Phys. Letters 11, 88 (1967).

15. G. Herzberg, Infrared and Raman Spectra, (D. Van Nostrand Co., Princeton, N. J., 1945).

Absorption Spectrum of SF_6 (∿ 6 torr)

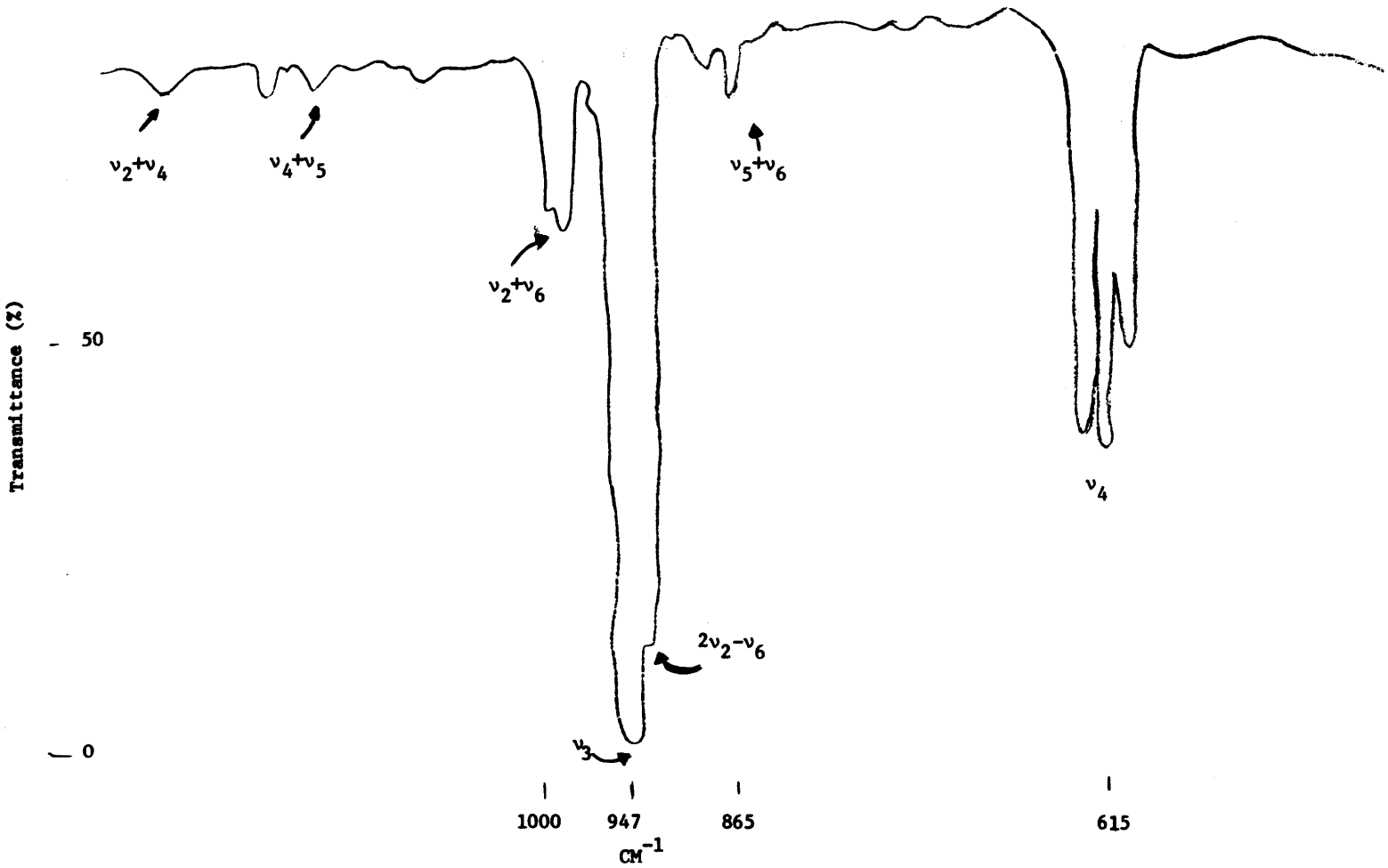

Figure 1

Energy, Symmetry, Degeneracy and Fractional

Populations of Singly Excited Normal Modes of SF_6

Mode	$E(cm^{-1})$	Degeneracy	Symmetry	Fractional[(a)] Population at 292° K.
3	947	3	F_{1u}	.0096
1	775	1	A_{1g}	.0076
2	644	2	E_g	.028
4	615	3	F_{1u}	.049
5	363	3	F_{2u}	0.17
ground state 0		1	A_{1g}	0.33

Figure 2

(a) Combination and multiply excited levels account for the remainder of the population.

The CO_2 laser, when oscillating on the P branch of the transition 001→100, has output which coincides with the ν_3 [000100←000000] absorption band of SF_6. Figure 3 shows a high resolution (.1 cm^{-1}), low pressure (<1 torr) spectrum of the ν_3 band.[16] Superimposed on this spectrum are vertical lines representing the laser output. The height of these lines is proportional to the gain exhibited by a laser operating CW under conditions typical of these experiments.[17] Below alternate laser lines is the transition assignment. The low power (non-saturated) absorption coefficient for each CO_2 laser line is indicated by a circle.[18]

Figure 3 illustrates several extraordinary features of this band. The fact that all laser lines, P(16) excepted, give absorption coefficients similar to those obtained with a spectrometer indicates that the absorption band is rather structureless. In fact several experiments have indicated that the absorption is continuous or nearly so, at least in the immediate frequency region of several CO_2 laser lines.[19,20,21]

---

16. H. Brunet and M. Perez, J. Mol. Spec. 29, 472 (1969).

17. I. Burak, J. I. Steinfeld, and D. G. Sutton, J. Appl. Phys. 39, 4464 (1968).

18. Absorption Coefficient supplied by A. Szöke and C. Rhodes in a private communication.

19. C. K. Rhodes and A. Szöke, Phys. Rev. 184, 25 (1969).

20. F. Shimizu, Appl. Phys. Letters 14, 378 (1969).

Absorption Contour, CO_2 Laser Coincidence, and Laser

Absorption Coefficients for the ν_3 Band of SF_6

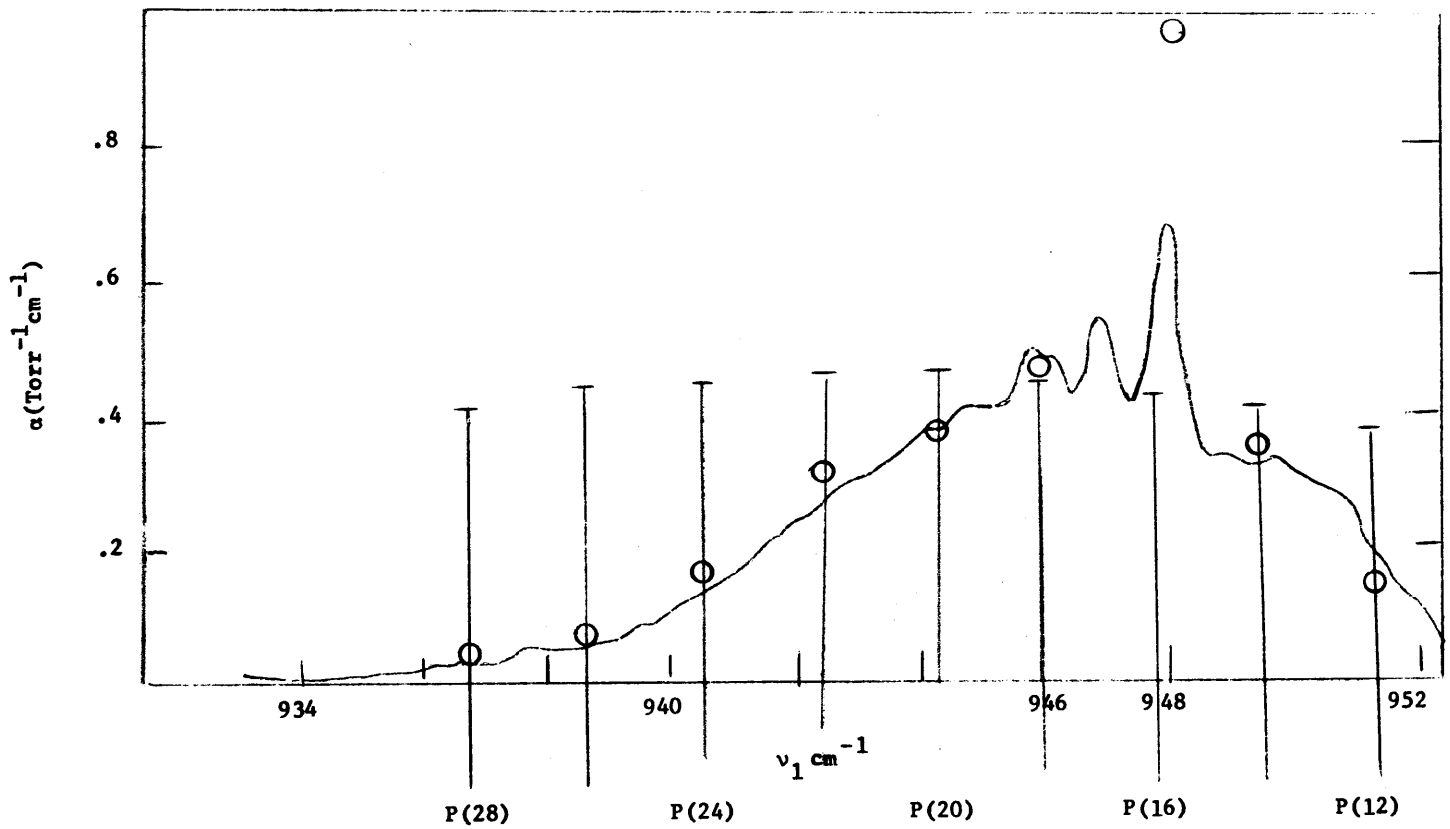

Figure 3

This result can be explained by the following considerations. The energy spacing between two consecutive vibrational-rotational transitions in the R and P branch of the ν_3 band is, assuming no change in the rotational constant on excitation,[22]

$$2B\,[1 - \zeta] = .045\ \mathrm{cm}^{-1} = 1350\ \mathrm{Mhz}.$$

where

B is the rotational constant = .089 cm^{-1} as calculated from electron diffraction data;[23]

and

ζ is the coriolis coupling constant = 0.75 as calculated from the separation in the maxima of the P and R branches in the infrared spectrum of the ν_4[24] band and the sum rule for the ζ_i.[25]

The doppler width of these lines at 300° K. is approximately 20 MHZ. However, if coriolis interactions lift the (2J + 1) fold K degeneracy, then assuming J = 50 (the level of maximum population at 300° K.), we have $1.4 \times 10^9/100$ = 14 MHZ per line. This predicts

---

21. E. D. Hinkley, Appl. Phys. Letters 16, 351 (1970).

22. G. Herzberg, op. cit., p. 454.

23. L. Brockway and L. Pauling, Proc. Nat. Acad. Sci. U. S. 19, 68 (1933).

24. W. F. Edgell and R. E. Moynihan, J. Chem. Phys. 27, 155 (1957).

25. R. S. McDowell, J. Chem. Phys. 43, 319 (1965).

1 line per doppler width. The line spacing in the Q branch region (945-949 cm^{-1}) is equal to zero in this approximation. In regions of the band corresponding to higher J values, the number of lines per doppler width would increase. Higher approximations in the calculation of energy levels decrease the spacing of R branch lines and increase the spacing of Q and P branch lines.

The Lorentz line width under similar conditions (300° K., 1 torr) is Z/π Hz.,[26] where Z is the gas kinetic collision number. Defining a collision in terms of a cross section derived from viscosity data, one gets ∿10 Megaherz. The use of Patel's dephasing cross section[27] to define the collision yields a line width at one torr of ∿1000 Megaherz. If Lorentz broadening were dominant, the absorption coefficient would be expected to vary with pressure. Rhodes and Szöke have pointed out,[19] however, that the absorption coefficient of SF_6 for several P branch lines of the 10.6 μ laser transition is independent of pressure in the range 0 to 17 torr, indicating that the absorption properties of SF_6 are not influenced by pressure broadening.

From the integrated absorption coefficient of the ν_3 band, one can compute the average radiational lifetime of the excited

---

26. A. Mitchell and M. Zemansky, Resonance Radiation and Excited Atoms, (Cambridge Univ. Press, N.Y., 1961) p. 160.

27. C. Patel and R. Slusher, Phys. Rev. Letters 20, 1087 (1968).

vibrational state.[28] This has been done and yields τ = 25 msec.

The structure of the band around 947 cm^{-1} has been attributed to hot band absorption.[27] This is unsatisfactory, however, because the intensities of this series of peaks don't correlate quantitatively with the equilibrium populations of the excited vibrational levels.[29] It would be highly desireable to explain this structure and analyze the J structure of the entire band, since this information is crucial to the understanding of the self-induced transparency and photon echo experiments[30] and would facilitate the interpretation of the saturation and double resonance work.

With these two goals in mind, an attempt was made to synthesize the entire band utilizing the IBM 360/65 computer and the following procedure.[31] The exact frequency at which each infrared transition occurred was computed for each branch according to the formulae given below.[32] These equations include first order coriolis effects and the change in rotational constant with vibrational excitation.

---

28. Mitchell and Zemansky, op. cit., p. 95.

29. See Figure 2.

30. C. Rhodes, A. Szöke, and A. Javan, Phys. Rev. Letters 21, 1151 (1968).

31. For further detail see Platzblatt, I. M., Infrared Band Contour Analysis, Senior Thesis, M.I.T. Chem. Dept. 1969.

32. See page 454 of Reference 2.

$$R(J) = \nu_0 + 2\,B_v'\,(1 - \zeta) + (\Delta B + 2B_v'[1 - \zeta])\,J + (\Delta B)\,J^2$$

$$Q(J) = \nu_0 + (\Delta B)\,J + \Delta B\,J^2$$

$$P(J) = \nu_0 - (-\Delta B + 2B'[1 - \zeta])\,J + \Delta B\,J^2$$

where

ν_0 = the frequency for the transition $\begin{matrix} v' = 1 \\ J' = 0 \end{matrix} \leftarrow \begin{matrix} v'' = 0 \\ J'' = 0 \end{matrix}$

$\Delta B = B_v' - B_v''$ = the difference between rotational constant in the ground vibrational state and first excited vibrational state

ζ is the coriolis coupling constant

J is the quantum number of the rotational state in the ground vibrational state which gives rise to the absorption.

The line strength of each line was then computed as follows.

$$\alpha_p = \frac{g_J \cdot (e^{-B_V' J(J+1)\,hc/kT})}{Q_{rot}\,\sigma^*} \quad \frac{\Theta}{2J + 1}$$

g_J is the rotational degeneracy of the Jth level due to the rotational equivalence of the six fluorine atoms (spin 1/2). These values were calculated by the method of Wilson[33] and are tabulated in Appendix 4.

Q_{rot}, the classical rotational partition function, =

$$e^{Bhc/4kT}\sqrt{\pi/B^3(kT/hc)^3} \rightarrow 1.027\,(T/B)^{3/2} \text{ as } \frac{hcB}{kT} \rightarrow 0$$

---

33. E. B. Wilson, Jr., J. Chem. Phys. 3, 276 (1935).

σ^* = Total nuclear spin multiplicity ÷ classical symmetry number = $[2(1/2) + 1]^6/24 = 8/3$

Θ arises from the difference in matrix elements for the various branches = 2J - 1 for the P branch
2J + 1 Q
2J + 3 R

The entire band width of the 000100←000000 transition was divided arbitrarily into equally spaced zones roughly corresponding to the resolving power of the Perkin-Elmer 521 spectrometer; i.e., 0.2 $cm.^{-1}$ The width of these divisions was large enough to encompass several lines but small compared to the width of the band. The line strength of all the lines in each division was summed and plotted at the center frequency of that division by the computer. The contour thus derived was compared to the infrared absorption band obtained with the use of the Perkin-Elmer spectrometer. The rotational constant in the vibrationally excited state (B_v'), V, and ζ were varied independently to obtain a "best" fit.

First it was noticed that the Q structure (the three prominent peaks between 946 and 948 cm^{-1} in Figure 3) could be reproduced without invoking hot band absorption. See Figure 4. However, when this was done the wings of the band were not reproduced satisfactorily. Conversely, when the wings were fit preferentially, the computer generated Q structure was not comparable to experiment. We concluded that this failure was due to one or both of two considerations not included in the calculations. Either hot band

Computer Synthesized ν_3 Band of SF_6

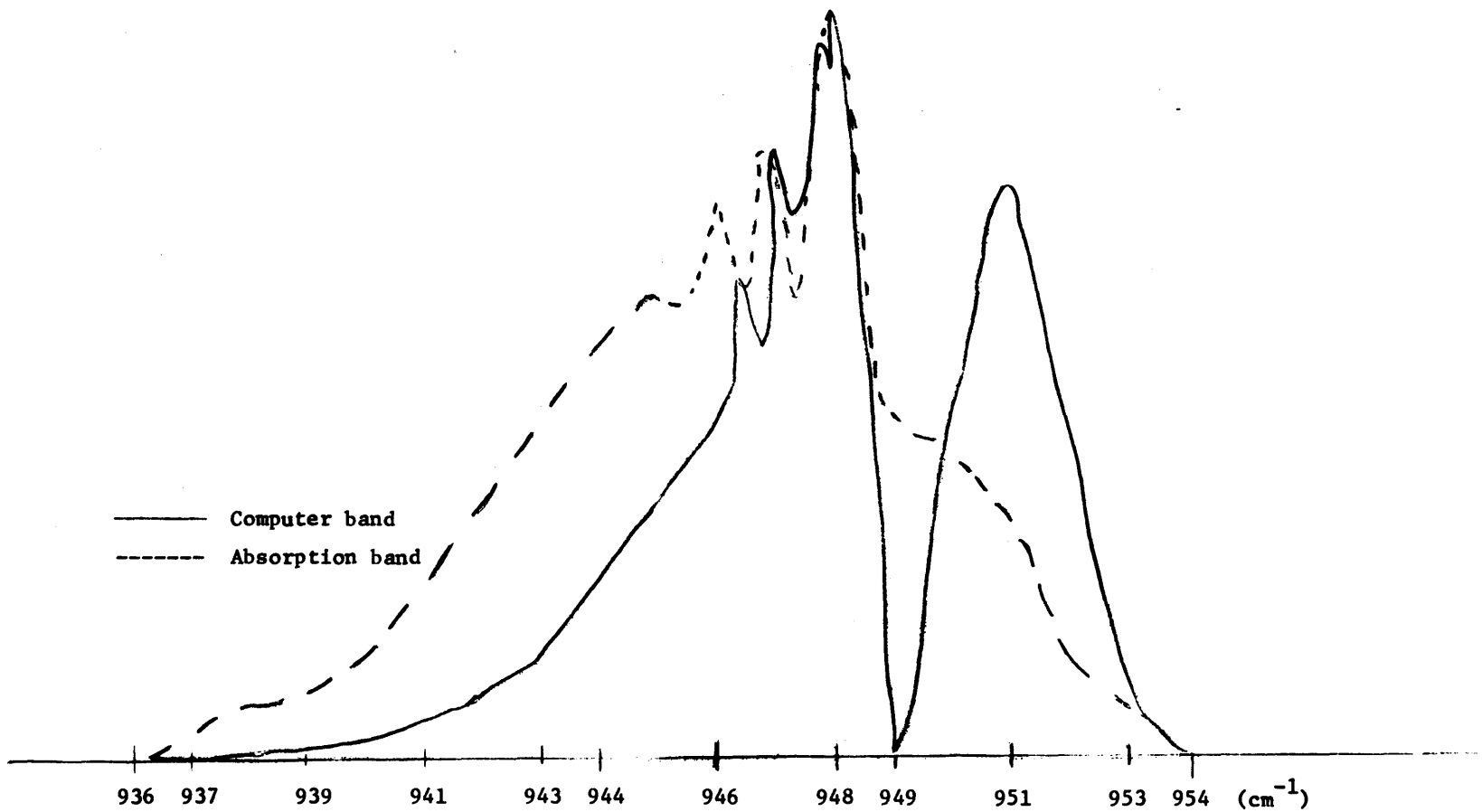

Figure 4

absorption is significant or second order coriolis interactions affect band shapes to a measurable degree or both. Absorption from the ν_6 level is allowed and this level is populated to 50% of the ground state value. This implies that the transition (000101←000001) may be contributing to the absorption spectrum near 947 $cm.^{-1}$ Several other hot bands and combination bands may also contribute; see Figure 5.

Childs and Jahn have shown how second order coriolis effects can affect band shapes in methane.[34] We expect similar perturbations to be active in SF_6. Consequently we have calculated the form of the matrix elements between the various normal modes that interact,[31] but these matrix elements have not yet been evaluated or included in the formulas of line position. The decision to proceed awaits a low temperature, low pressure, high resolution infrared absorption spectrum which should be free of hot band absorption and allow straightforward estimation of the importance of second order coriolis splitting. This data will then be used as the contour to which the synthetic band will be forced to conform.

By shifting the origin of the synthetic band one can match the Q branch peaks to those of the absorption band. Then the computer data can be deconvoluted to assign probable J values to the

---

34. W. Childs and H. Jahn, Proc. Roy. Soc. London Ser. A 169, 451 (1939).

Some Dipole Allowed Transitions in SF_6 near 947 cm^{-1}

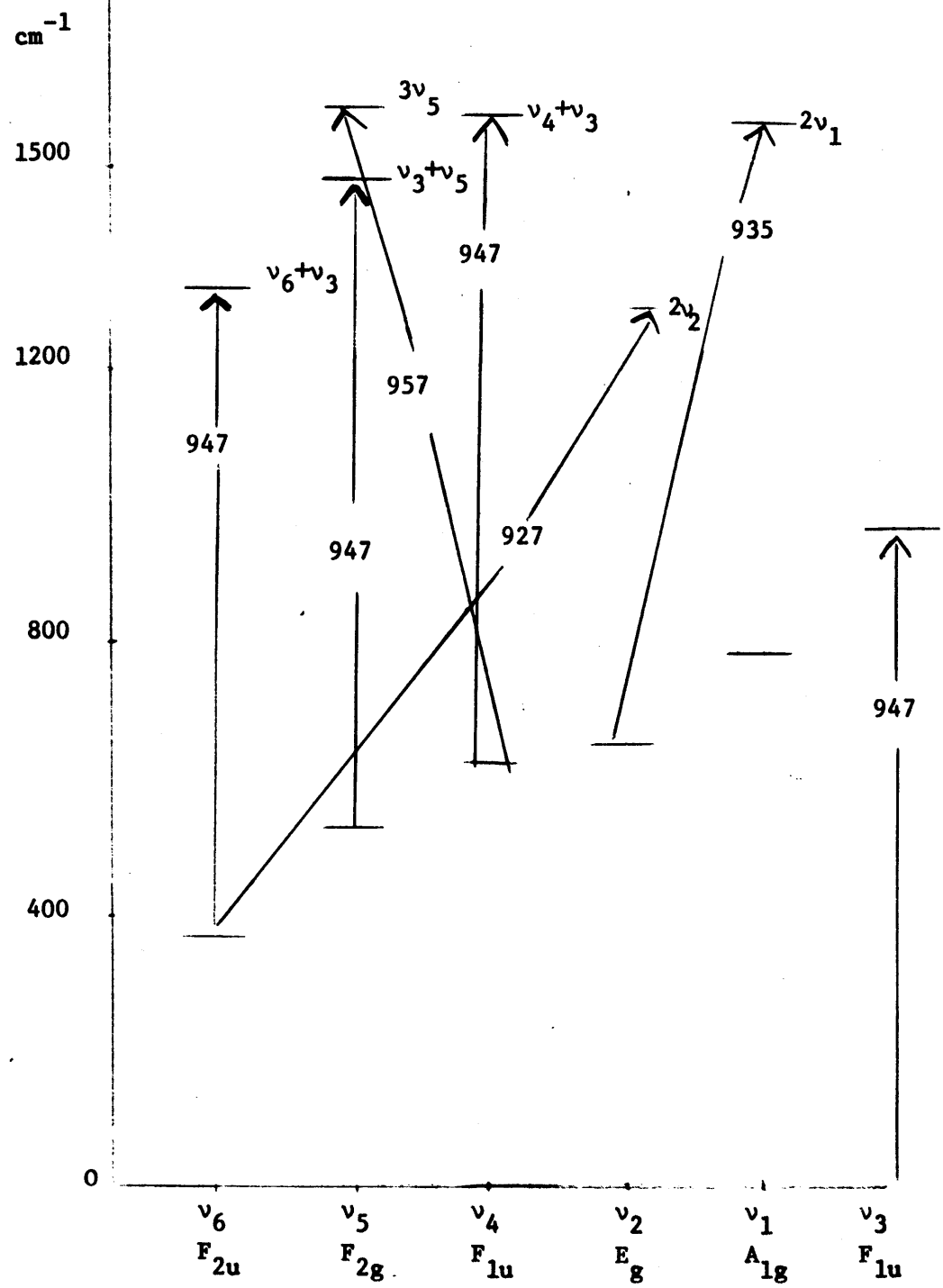

Figure 5

regions of the spectrum responsible for absorption of the CO_2 laser lines. The density of lines can also be estimated for these regions. These data are critical for understanding pulse transmission experiments in SF_6.[19,30] Therefore, the table shown in Figure 6 has been prepared from the computer calculations performed in the generation of the synthetic band shown in Figure 4. These results are highly speculative, given the preliminary stage of the contour synthesis.

However, the following tentative conclusions may be drawn. For any one laser line, the fraction of molecules affected varies from .03 → .0007. This range brackets the value of β = .003 used in our saturation model (Appendix 2). Second order coriolis splittings would tend to reduce both limits of this range by reducing the number of molecules interacting with the field per homogeneous band width. Only medium to high J levels are involved in the absorption of radiation. This conclusion is buttressed by the fact that only a very small fraction (<.04%) of the molecules populate the first few rotational levels.

Deconvolution of Computer Synthesized Band

$\nu(cm^{-1})$	CO_2 Laser Transition	Most Probable J" Value Coincident With Laser		# of lines per 10^{-2} cm^{-1} (a)		Fraction of Mol. in Ground State Responsible for Absorption	
		P	Q	P	Q	P	Q
947.7	P(16)	24	52	1	1	1.03%	1.74%
945.9	P(18)	53	83	1	1	1.68	.65
944.2	P(20)	76	104	1	1	.93	.18
942.4	P(22)	97	122	1	1	.29	.04
940.5	P(24)	117	139	1	1	.062	.007

Figure 6

(a) Corresponds to homogeneous linewidth of SF_6; see page 101 of Appendix 2.

C. SATURATION AND PULSE TRANSMISSION

The apparatus, model, experimental results, and computational results of the saturation of SF_6 by a high power continuous wave CO_2 laser are fully described in Appendix 2. The topic to be treated in this section is pulse transmission through SF_6 in the pressure region where coherent effects are negligible. A host of papers have dealt with the optical analogues of radio frequency phenomena in SF_6;[35] there exists, however, a dearth of studies on saturation effects despite its obvious importance to communications research and pollution monitoring schemes. As a first step to remedy this situation, the program utilized in the CW calculations (Appendix 2) was modified to provide time resolution of the transmission of high field (>10 watts/cm^2) pulses through gaseous SF_6. A listing of the program used to generate theoretical envelopes for pulses modulated by transmission through SF_6 is included as Appendix 5. This program is written in Fortran IV and utilizes the Calcomp plotting subroutines, NEWPLOT, PICTUR, and ENDPLOT.

In order to neglect coherent effects, especially self-induced transparency, the width of the pulse, τ_p, must be greater than T_2',

---

35. See the references cited in Appendix 3, page 104.

the inverse of the collision induced homogeneous line width.[36,37] This criterion sets lower limits on the pressures of SF_6 and foreign gases necessary if saturation is to be studied to the exclusion of coherent effects. Utilizing the parameters reported in references 36 and 37, the following criteria are obtained:

$$PT_2' \ (SF_6\text{-}SF_6) = 22 \times 10^{-9} \text{ sec-torr}$$

$$\tau_p \sim 200 \times 10^{-9} \text{ sec} > T_2' = \frac{22 \times 10^{-9} \text{ sec-torr}}{P \text{ (torr)}}$$

or

$$P_{SF_6} > \frac{22}{200} = .11 \text{ torr}$$

$$PT_2' \ (SF_6 - He) = 33 \times 10^{-9} \text{ sec-torr}$$

or

$$P_{He} > .16 \text{ torr if } P_{SF_6} < .1 \text{ torr}$$

Experiments were carried out under the requisite pressure conditions, utilizing the apparatus shown in Figure 7. The laser was tuned to emit single 300 nanosecond pulses every 5 milliseconds consisting of approximately 90% P(18) and 5% each P(16) and P(20) CO_2 [001-100] laser lines. The peak power was calculated from the average power (measured by the Coherent Radiation Laboratories model 201 Power meter), pulse shape, and repetition rate of

---

36. C. K. N. Patel and R. E. Slusher, Phys. Rev. Letters 19, 1019 (1967).

37. C. K. N. Patel and R. E. Slusher, Phys. Rev. Letters 20, 1087 (1968).

Apparatus for Study of Pulse Transmission

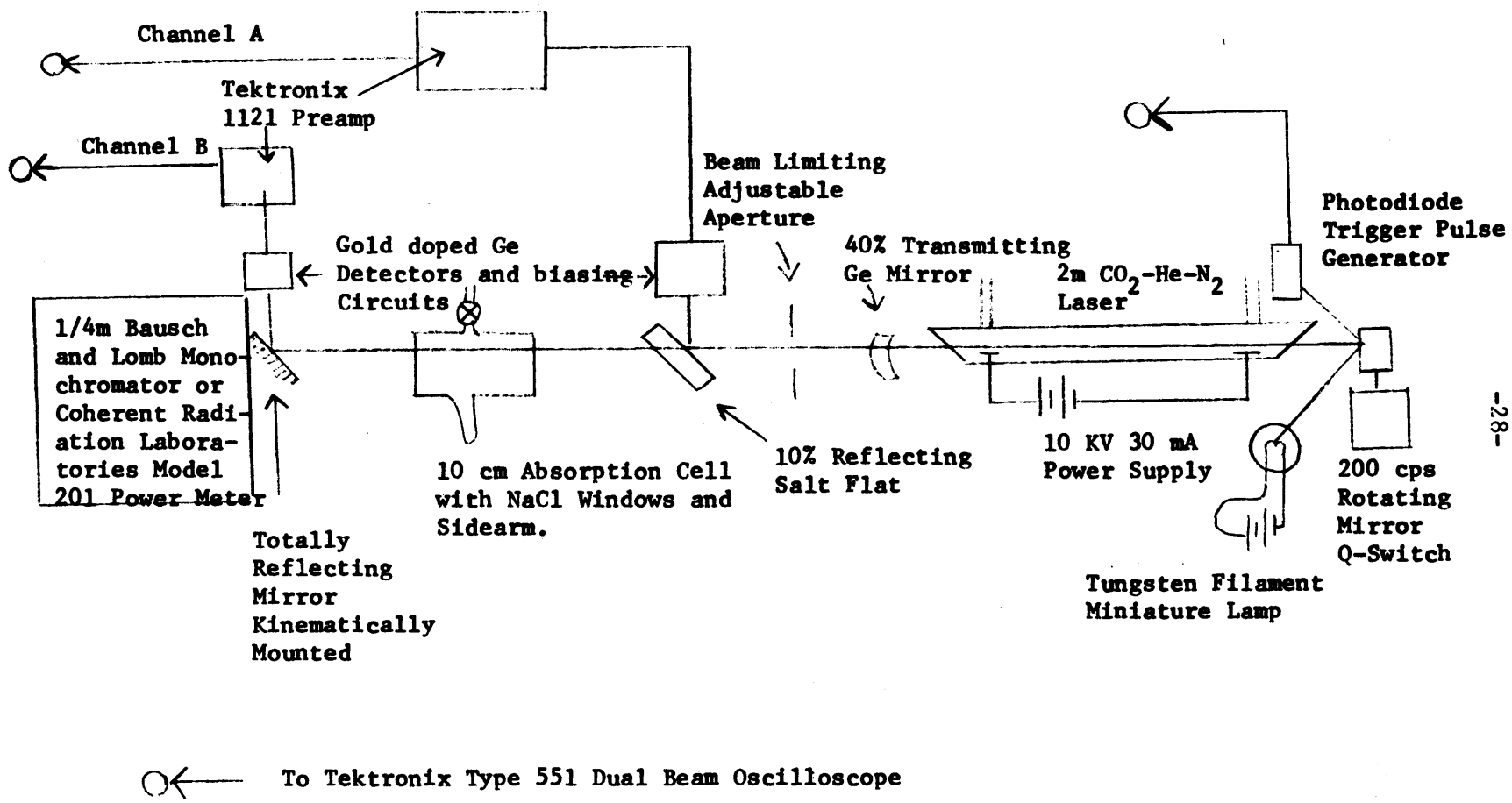

Figure 7

the Q-switched laser. The limiting aperture was adjusted to less than 1/2 inch diameter to insure a homogeneous radial power distribution in the beam. A 10% reflecting salt flat served as a beam splitter so that the incident pulse could be monitored by Channel A. A Raytheon (QKN1568) gold-doped germanium detector operated at 77° K. and a Tektronix 1121 (5 Hz to 17 Mhz bandpass) preamplifier completed this channel. Channel B monitored the transmitted pulse via a similar detector (Santa Barbara Research Corp.) and an identical preamplifier. The outputs of both channels were monitored by a Tektronix 551 dual beam oscilloscope which was triggered by the output generated by an RCA photodiode-tungsten lamp network coupled through the Q-switching mirror. The gain in channels A and B were adjusted to produce identical traces on the scope with the absorption cell in place, but with the SF_6 frozen in the sidearm. The SF_6 was then allowed to sublime and a photograph was taken of the resulting dual trace on the scope.

The SF_6 used in these experiments was supplied by Lif-O-Gen-Inc. and guaranteed 99.9% pure. The Helium was Matheson research grade guaranteed 99.995% pure. Both gases were employed without further purification.

A typical photograph is shown in Figure 8. The output of Channel A appears on the upper trace. The vertical scale of Channel B is expanded 10 times relative to Channel A. No delay in the transmitted pulse is apparent. Peak power is 3200 watts/cm.^{2}

Typical Pulse Transmission Data

Upper trace is incident pulse

Lower trace is transmitted pulse amplified 10 times relative to incident pulse

Pressure SF_6 = 1.32 torr

Pressure He = 7.4 torr

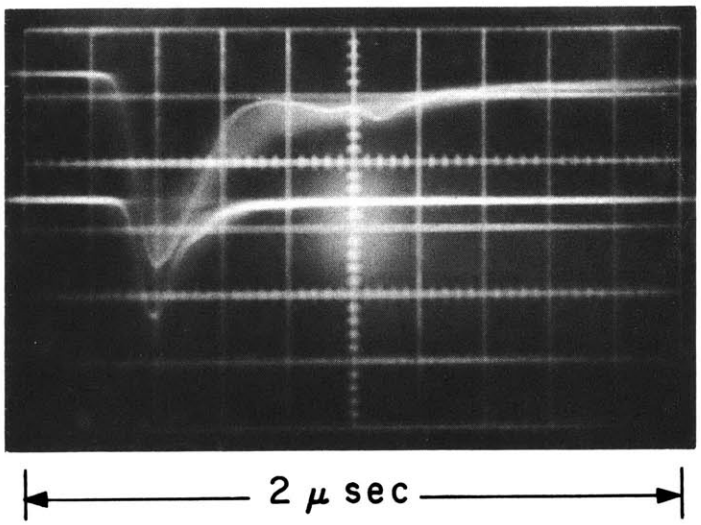

Figure 8

The pressures of SF_6 and He are 1.32 and 7.4 torr respectively. The time scale is .2 microseconds/div.

The computer was asked to simulate the output of Channel B using the output of Channel A, several model parameters, and the gas pressures as input. A schematic of the four state model[38] which defines the rate equations solved by the computer program is shown in Figure 9.

All SF_6 molecules are assigned to one of the four subsets N, N_o, N*, or N' according to the following functional definitions. N is the number of molecules in the ground vibrational state which are incapable of interacting with the perturbing field. N_o is the number of molecules in the ground vibrational state capable, by virtue of their rotational state, of absorbing the laser radiation. N* is the number of molecules which differ from N_o only in that they have absorbed one quantum of laser radiation. N' is the number of molecules not in the ground vibrational state and which cannot interact with the laser radiation. These numbers can be calculated for the case of zero field from the partition function and line-width data and are read into the program as initial conditions. β' is defined to be N_o/N under the same conditions.[39] B, the

38. Figure 7 of Appendix 3 defines the four states shown here in terms of the actual SF_6 energy levels; the rate equations derived from this model are shown in Appendix 2, page 85.

39. The parameters β and $\delta\nu$ are intimately related. For a discussion of this relationship and methods used to calculate $\delta\nu$, see Appendix 2, pages 101-102.

Four State Model for Energy

Flow in SF_6

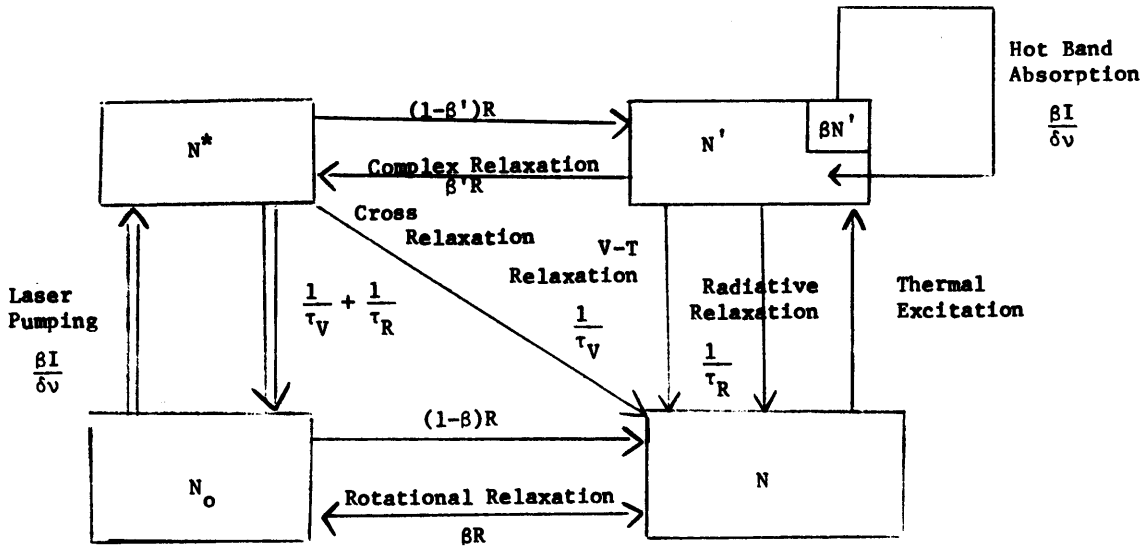

Figure 9

Einstein coefficient for induced absorption, and τ_R, the inverse of the Einstein A coefficient, were calculated from the known relations connecting B to the integrated absorption coefficient for the ν_3 transition and A to B. $\delta\nu$ is estimated as 10^9 Hz.[39] τ_v is taken to be equal to the collisional relaxation time of the lowest vibrational mode, ν_6, to the ground level. $p\tau$ for this transition is known to be 100 microsec-torr from the double resonance experiments. The results of the pulse transmission calculations are exceedingly unresponsive to this parameter; therefore, its precise value is inconsequential for these experiments. The thermal excitation time is taken to be equal to $\tau_v \cdot 3e^{-h\nu_6/kT}$ to satisfy the principle of detailed balancing.

R is now defined as the rate at which bimolecular collisions remove SF_6 molecules from the states N_o and N* (which are coupled by the laser) to the noninteracting states N or N' respectively. The greater energy level density for the transition $N^* \rightleftarrows N'$ is reflected in the inequality $\beta' < \beta$. In terms of cross sections

$$R = \sqrt{2}\,\pi\,(n_1{}^R\sigma_{SF_6}\,\bar{v}_1 + n_2{}^R\sigma_{He}\,\bar{v}_2)$$

where

n_1 = molecular density of SF_6 molecules

n_2 = molecular density of He atoms

$\bar{v}_1$ = mean relative velocity between SF_6 molecules

$\bar{v}_2$ = mean relative velocity between SF_6 molecules and He atoms.

This equation thus defines the relevant cross sections, ${}^{R}\sigma$, for SF_6-SF_6 and SF_6-He collisions. These values were varied to provide the best fit to the experimental data over a wide range of He and SF_6 pressures.

The computer program reads the varying input intensity, I, and reshapes the pulse according to the following procedure. The pulse intensity as a function of time was fit to the analytical expression

$$I(t) = D\, t^2 \exp\,(t^2/A^2)$$

where

$$D = I_{max} \cdot e/A^2$$

and

$$A = t \text{ when } I = I_{max}$$

This function was found to fit the Q-switched waveform adequately over two-thirds of its duration; the actual pulse decays more slowly than its analytical representation. The cell was divided into several equal zones normal to the axis of the light path such that the length of each division, Δl, was much less than $(\alpha p)^{-1}$

where

α = SF_6 absorption coefficient for P(18) laser radiation in the low power limit

and

p = pressure of SF_6 in the cell.

The pulse was similarly divided into time sections such that

$$I(t) = I(L \cdot \Delta t) = I(L)$$

where

$$\Delta t = \Delta l/c \text{ and } L = \text{integer}; \; 0 \leq L \leq \tau_p \cdot C/\Delta l.$$

An iterative procedure was then employed whereby I(0) was applied to the first cell zone and the difference equations derived from the model incremented to redefine N, N', N_o, N*, and I(0) in this zone. I(1) was then applied to the first zone, while the redefined I(0) was applied to the second zone. The incrementation was then executed in the first two zones. This iteration continued until the pulse was transmitted completely through the cell, reshaped, and reduced in intensity. Transmitted pulse shapes, calculated as described, served as the parametric touchstone to the experimental data, the cross sections being varied to maximize the fit with experimental pulse shapes recorded under a variety of experimental conditions. The program was run with I(0) = .01 watts/cm^2 and 100 watts/cm^2, using a step function pulse shape and checked against the Beer-Lambert Law and the CW saturation experiments respectively. Figures 10 and 11 are the outputs from these calculations. The top line represents the input pulse as a function of time; the bottom curve represents the transmitted pulse. The arrow on the vertical axis indicates the experimental transmitted power. Figure 10 shows that under appropriate conditions the program predicts Beer-Lambert behavior to within 10%. Figure 11, however, shows that the program

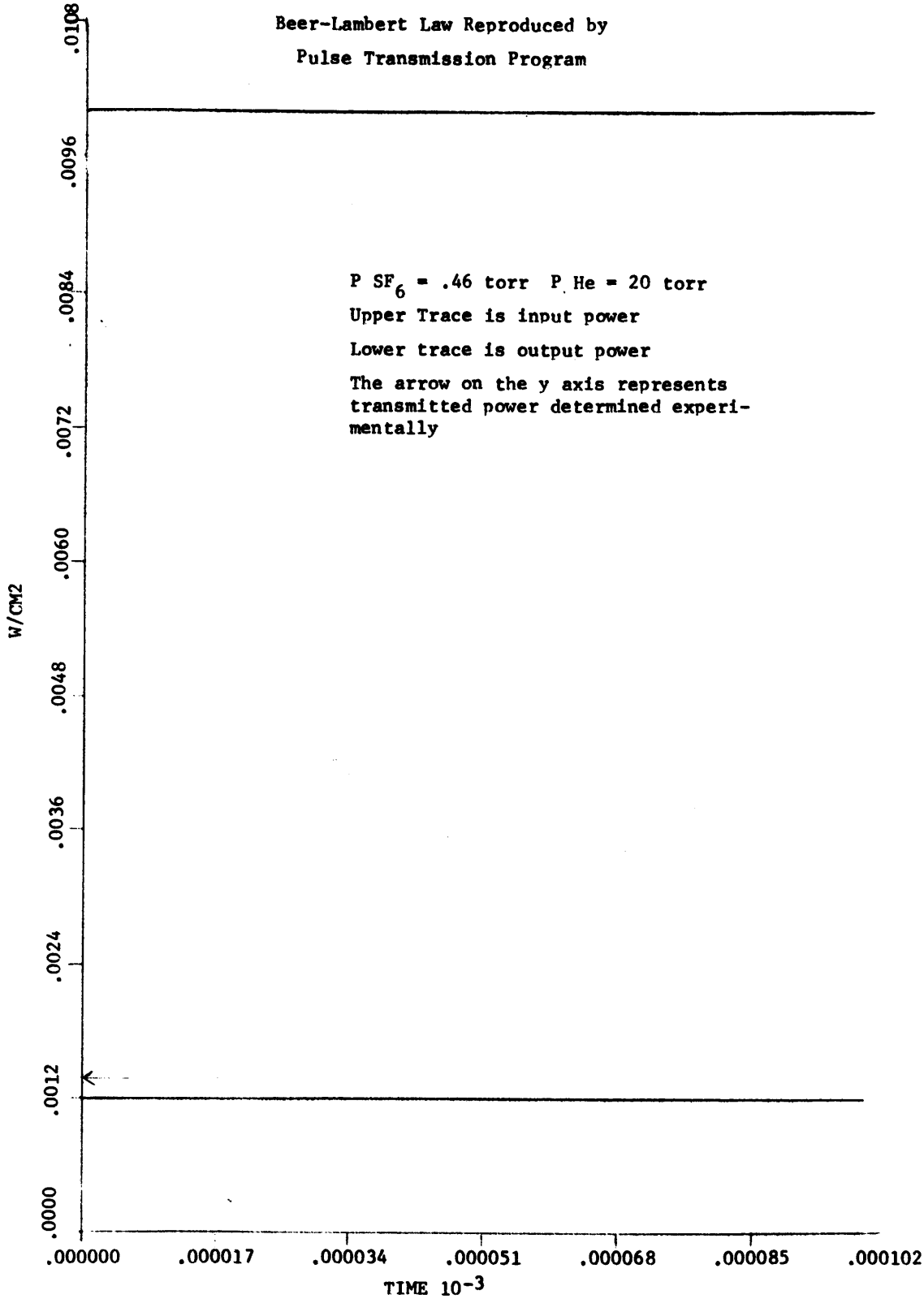
Beer-Lambert Law Reproduced by
Pulse Transmission Program
P SF6 = .46 torr P He = 20 torr
Upper Trace is input power
Lower trace is output power
The arrow on the y axis represents transmitted power determined experimentally
W/CM2
.0108
.0096
.0084
.0072
.0060
.0048
.0036
.0024
.0012
.0000
.000000
.000017
.000034
.000051
.000068
.000085
.000102
TIME 10-3

Figure 10

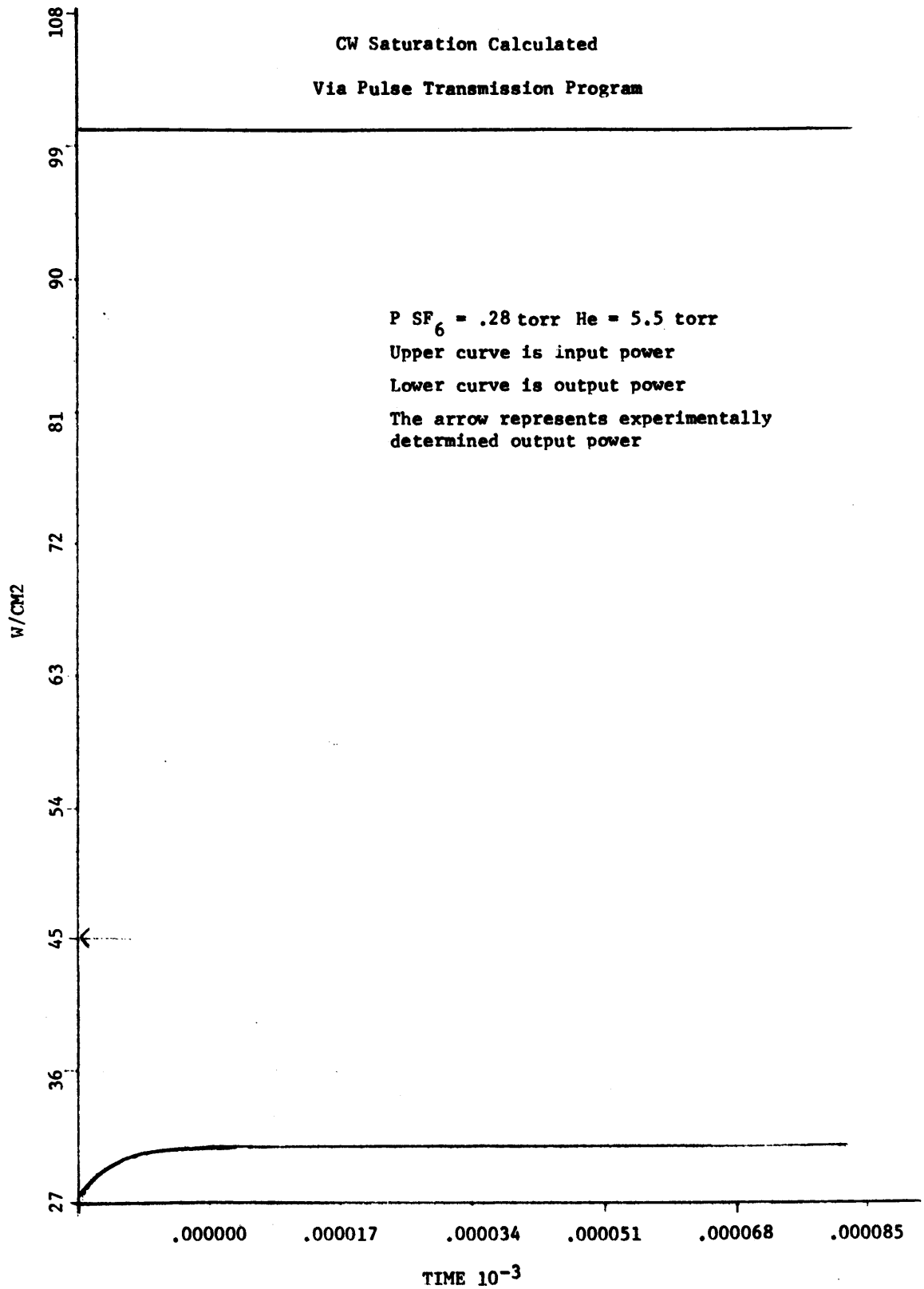
CW Saturation Calculated
Via Pulse Transmission Program
P SF6 = .28 torr He = 5.5 torr
Upper curve is input power
Lower curve is output power
The arrow represents experimentally determined output power
W/CM2
108
99
90
81
72
63
54
45
36
27
.000000
.000017
.000034
.000051
.000068
.000085
TIME 10-3

Figure 11

used in these calculations predicts saturation, but yields a transmission 30% lower than experimental.[40] The difference indicates the importance of the heating effects, which were included in the program used in Appendix 2 to calculate CW transmission, but were eliminated in the present program. The great reduction in average power incident on the cell in going from CW to Q-switch operation reduces heating effects to a level where they can be ignored.[41]

The input pulse shape previously described was then used to calculate pulse shapes, transmitted through a 10 cm cell containing the following gas mixtures:

1.02 torr SF_6	0.0 torr He
1.32	0.0
1.32	7.44
0.48	5.93
0.46	20.0
0.48	38.0
0.99	10.9

Figures 12 and 13 show the computer output for two runs. Experimental points extracted from the photographs are plotted on the

---

40. The data point representing the experiment relevant to the calculation shown in Figure 11 is plotted in Figure 8, Appendix 2. 45% transmission was measured under conditions identical to those used in the calculation of Figure 11.

41. See Appendix 2, page 98 for a discussion of heating effects.

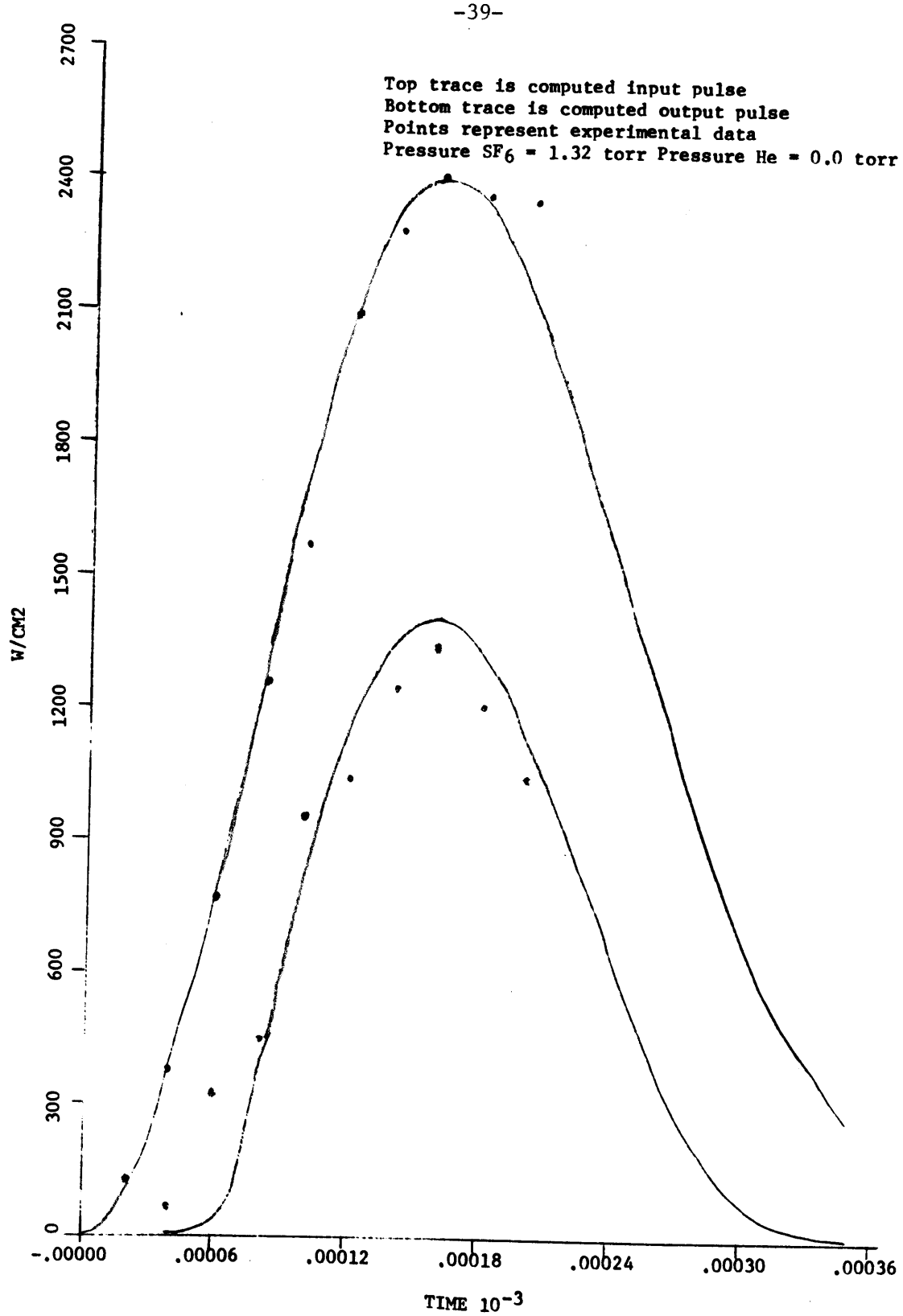
Top trace is computed input pulse
Bottom trace is computed output pulse
Points represent experimental data
Pressure SF6 = 1.32 torr Pressure He = 0.0 torr
W/CM2
0
300
600
900
1200
1500
1800
2100
2400
2700
-.00000
.00006
.00012
.00018
.00024
.00030
.00036
TIME 10-3

Figure 12

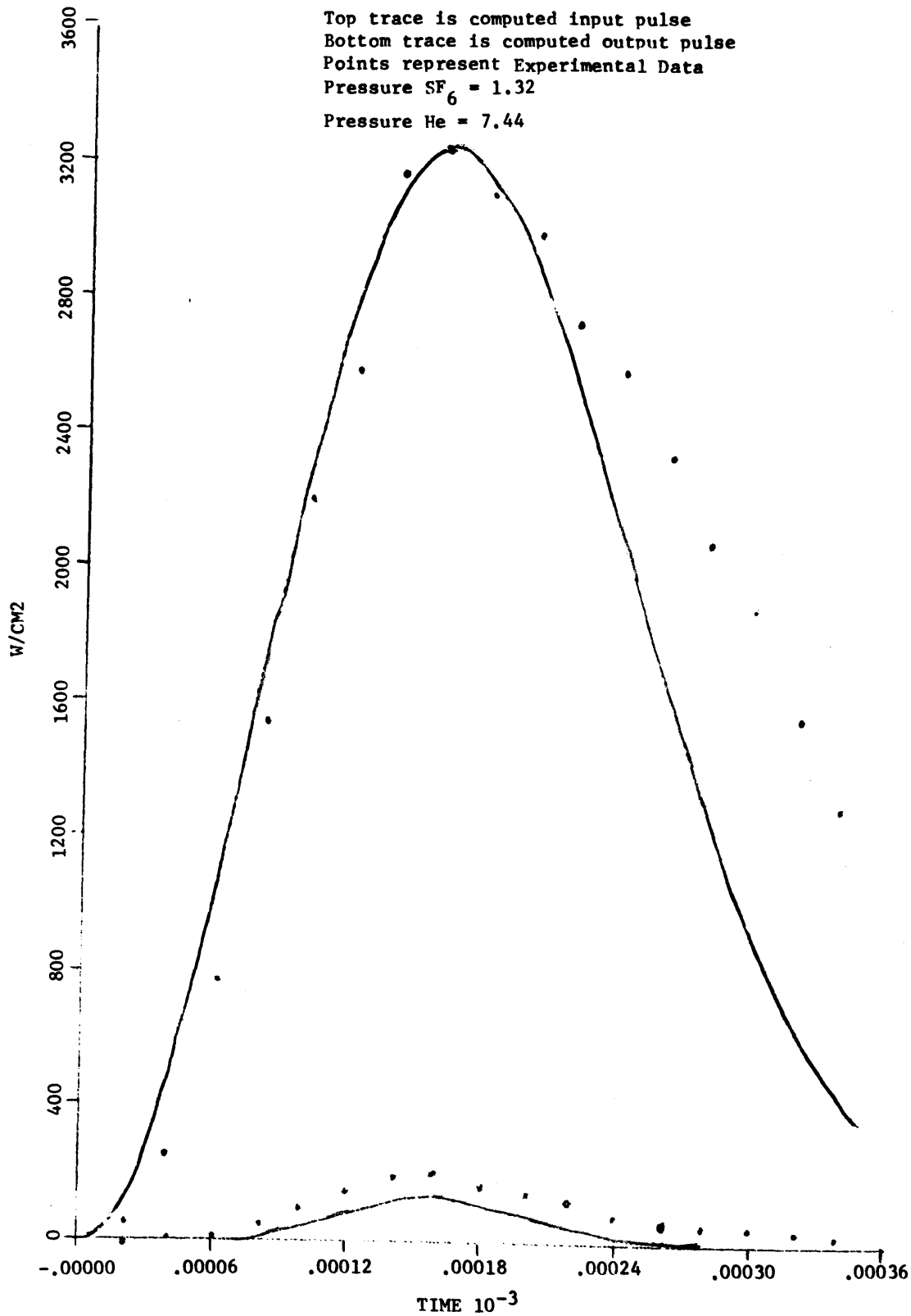
Top trace is computed input pulse
Bottom trace is computed output pulse
Points represent Experimental Data
Pressure SF_6 = 1.32
Pressure He = 7.44
W/CM2
3600
3200
2800
2400
2000
1600
1200
800
400
0
-.00000
.00006
.00012
.00018
.00024
.00030
.00036
TIME 10^{-3}

Figure 13

same figures. The data for all the experiments can be fit with equal accuracy using the set of parameters in the following table. These parameters were also used in the generation of Figures 10 and 11.

Fixed Parameters

β	β'	τ_R	$\delta\nu$	α
.003	.001	.025 sec	10^9 Hz	.46 $torr^{-1}$ cm^{-1}

Variable Parameters[42]

${}^{v}\sigma_{SF_6}$	${}^{v}\sigma_{He}$	${}^{R}\sigma_{SF_6}$	${}^{R}\sigma_{He}$
.1A$^{\circ 2}$	.01A$^{\circ 2}$	100A$^{\circ 2}$	20A$^{\circ 2}$

The parameters ${}^{v}\sigma_{SF_6}$ and ${}^{v}\sigma_{He}$ are defined, analogous to the ${}^{R}\sigma$, by the following equation:

$$\frac{1}{\tau_v} = \sqrt{2}\,\pi\,(n_1\,{}^{v}\sigma_{SF_6}\,\bar{v}_1 + n_2\,{}^{v}\sigma_{He}\,\bar{v}_2),$$

n_1, n_2, $\bar{v}_1$, and $\bar{v}_2$ were defined previously.

---

42. These parameters must be considered indeterminate to $\pm 50\%$ due to the uncertainty in β (see Appendix 2, p.101) and the strong interdependence of β, ${}^{R}\sigma_{SF_6}$ and ${}^{R}\sigma_{He}$.

The computed output was found to be very insensitive to the vibrational cross sections, ${}^{V}\sigma$, over a range of .1 to 10 times the values listed in the table. Such behavior is not unexpected at these pressure and time scales. The determinate factors then are ${}^{R}\sigma_{SF_6}$ and ${}^{R}\sigma_{He}$. This implies that the rate determining step for pumping SF_6 molecules with saturating pulses less than 1 μsec in duration is the R-T and V-V processes which transport molecules into and out of the levels which interact with the laser. The fact that almost identical pressures of He and Xe quench the SF_6 passive Q-switching of the CO_2 laser, even though their respective efficiencies for relaxing the lowest vibrational mode of SF_6 differ by at least a factor of 100, can be understood given the dominant role of rotational energy transfer in the absorption rate.

The increase in signal in the double resonance experiments upon addition of several torr of krypton can also be understood in relation to this model. The krypton increases the pumping rate for the duration of the pulse, thus increasing the number of molecules in excited vibrational states which give rise to the signal.

D. DOUBLE RESONANCE EXPERIMENTS WITH SF_6

Once the saturation experiments had clearly established that a substantial fraction of the molecules existed in vibrationally excited states, we attempted to monitor them directly utilizing the technique of infrared-infrared double resonance. Our first attempts were made utilizing CW laser pumping and conventional spectrometric-detection. A 10 cm stainless steel absorption cell suitable for use in a Perkin-Elmer infracord was constructed with provision to introduce pumping power as detailed schematically in Figure 14.

With this apparatus, spectra of SF_6 were obtained at various pressures and with continuous CO_2 pumping power from 0-10 watts. A typical result is shown in Figure 15. One-third of the change in absorption at 948 cm^{-1} is due to scattered laser radiation, but the change in the wings of the band is real.

Figure 16 consists of two conventional spectra of the ν_3 band of SF_6 taken at 30° C. and 103° C. These spectra were obtained using the same infracord (Perkin-Elmer 337) as those shown in Figure 15. The temperature was regulated by a heating tape wound around the cell and powered by a variac. A copper-constantan thermocouple placed between the tape and outside wall of the cell served as a convenient monitor. A multiple reflection cell providing

Double Resonance Cell Used

With Perkin Elmer 337 Spectrometer

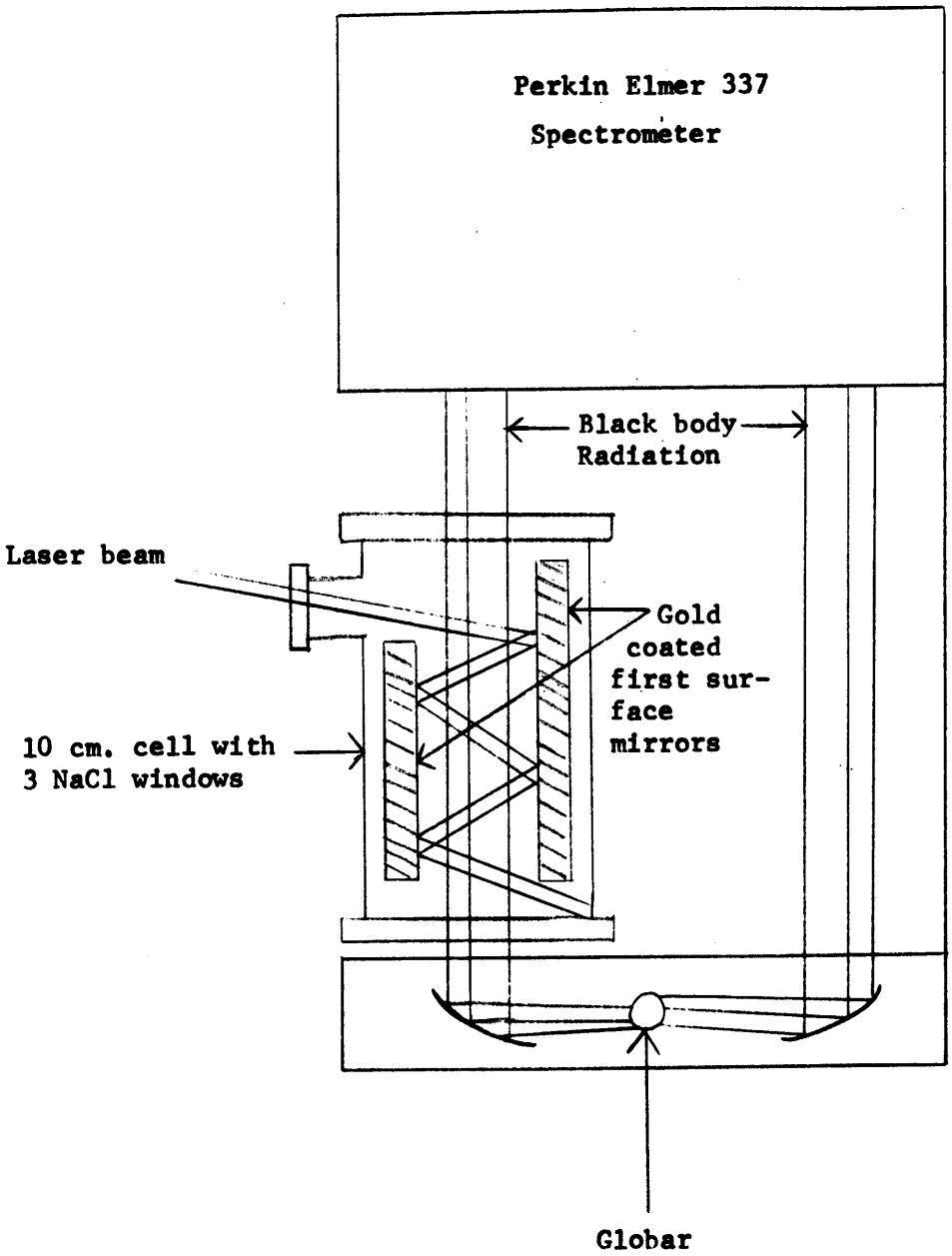

Figure 14

Infrared Spectrum of Irradiated SF_6 Presurre SF_6 = 0.39 torr

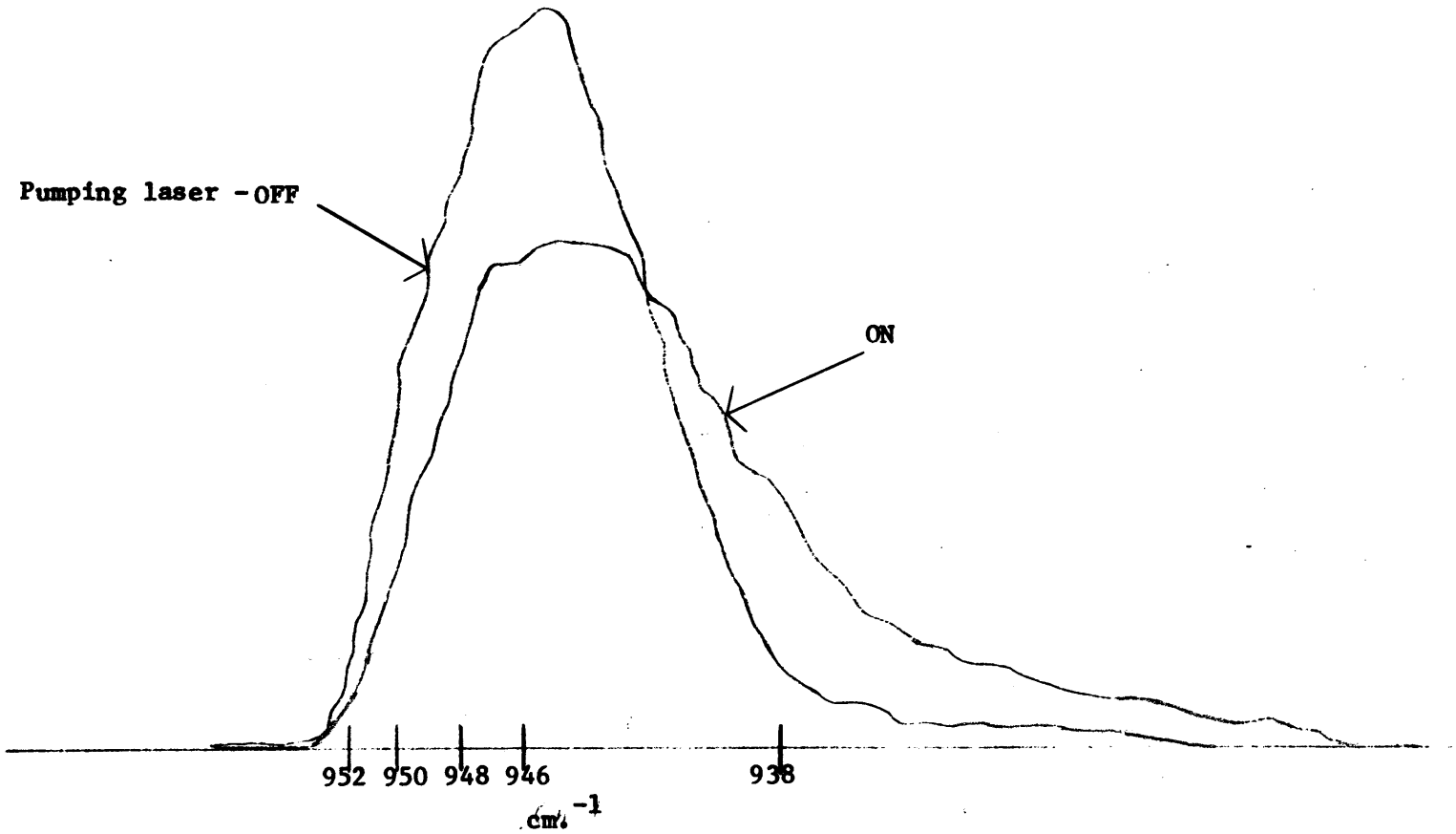

Figure 15

SF_6 Absorption Spectra Near 947 cm^{-1}

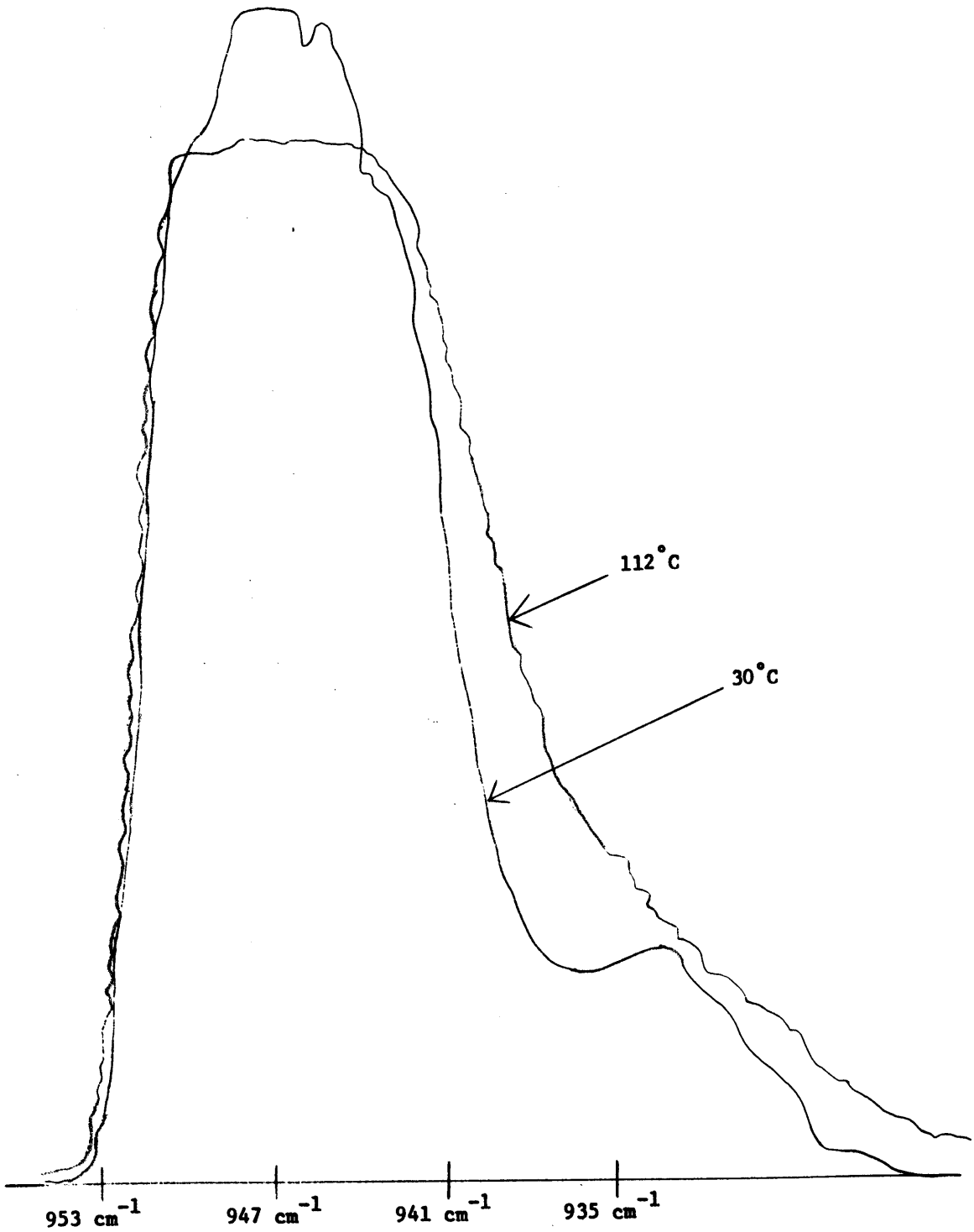

Figure 16

for a 1 meter absorption length was used. SF_6 pressure was 65 microns.

A comparison of Figures 15 and 16 shows than, except for the bleaching in the region 948 cm^{-1} to 952 cm^{-1}, the features of the double resonance spectrum can be reproduced simply by heating the gas. In other words, the major detectable effect of CW laser pumping is to raise the temperature of the gas. This heating effect apparently masks any increased absorption due to excited states. This is not an unreasonable conclusion, for if one calculates the per cent change in population of a high J state (J=100) due to a rise in temperature from 30° C. to 100° C., a value of 560% is obtained.

These conclusions were taken into account in the computer model of SF_6 saturation. In Appendix 2 it is shown that the temperature of a pumped system with cylindrical geometry is equal to

$$T(r) = \frac{P_{abs}(2.39)\ \ln(a/r)}{\pi L\ 2K} + T(a),\ b \leq r \leq a$$

where end effects are ignored and

P_{abs} = Power absorbed in watts

L = Length of the cell in cm

K = thermal conductivity of the gas in cal/deg.-cm-sec

a, b, r are defined with reference to Figure 17

A simple computation using numbers typical of these experiments,

Geometry for Heating Calculations in a Laser Pumped Gas

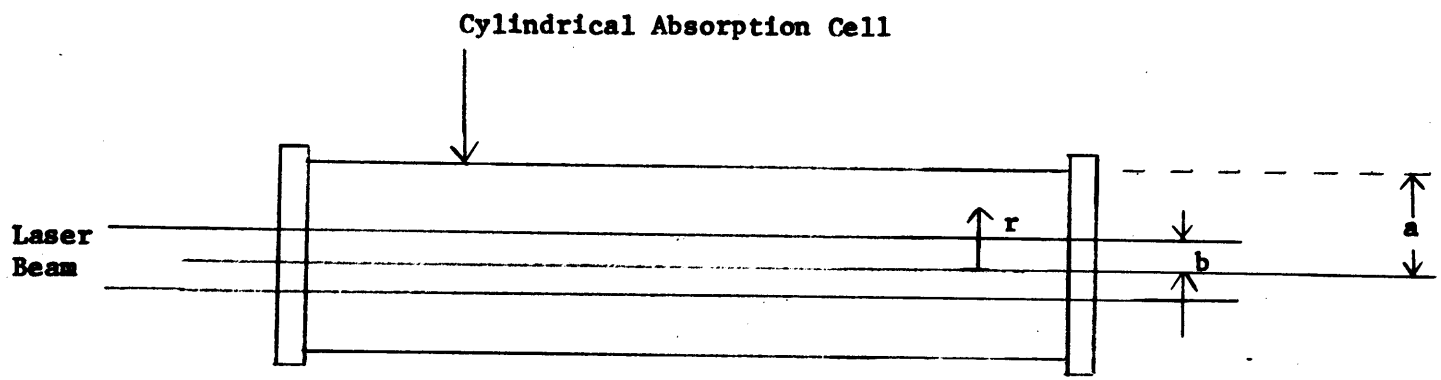

Figure 17

[P_{abs} = 1.0 watt, L = 10 cm, $K(SF_6) = 23 \times 10^{-6}$ cal/deg.-cm-sec, a = 2.0 cm, b = 0.2 cm, T(a) = 300° K.] yields the following results.

r = 0.3 cm T(r) = 609° K.

r = 0.5 cm T(r) = 526° K.

r = 1.5 cm T(r) = 347° K.

An experimental check was made to verify these results using an absorption cell with calibrated thermistor probes sealed in at two different radii. The resistance of the thermistors was monitored with a Wheatstone bridge. The measured temperatures were found to be T(0.5 cm) = 510° K. and T(1.5 cm) = 410° K. This experiment was run under conditions identical to those listed in the calculation above; so, direct comparison can be made. The conclusion to be drawn is that temperature increases of 200° C. do occur, and these induce changes in the distribution of rotational level populations which in turn mask hot band absorption. Experimentally these difficulties were overcome by using a Q-switched pumping source (which reduces the average power coupled into the system by an order of magnitude), and a low power laser probe beam to monitor excited state absorption. Furthermore, a fast, gold-doped germanium diode detector enabled us to time resolve changes in the absorption so that the vibrational relaxation and the relaxation of rotational and translational temperatures could be resolved on the basis of their respective decay times.

Figure 3 of Appendix 3 shows how these decay times were resolved from the experimental data. In the following paragraphs the theoretical foundation for the data reduction method used in Appendix 3 is derived, the rotational-translational temperature relaxation is predicted and compared to experiment, and the instrumental response time is evaluated.

Figure 1 of Appendix 3 diagrams schematically the complete apparatus used in the double resonance experiments. The crucial part of the apparatus for these calculations is the 30 cm absorption cell which is labeled S in that Figure. Figure 18 is an expanded drawing of that cell and the two laser beams coincident on it, which illustrates the near cylindrical symmetry of the experimental configuration. The calculations assume perfect cylindrical symmetry for the sake of tractability. The effect of the monitor beam is ignored, since its low power (<5 watts/cm^2) is insufficient to cause significant heating or saturation over a 30 cm path length at the pressures of SF_6 utilized in these experiments. End effects are also ignored; in effect we assume an infinite cylinder of radius 2 cm pumped by a coaxial beam .3 cm in diameter. Uniform excitation along the entire length of the cell and within the pumped beam is postulated, since the power (up to 5 Kilowatts) of the pulse is sufficient to effect almost complete saturation. At any rate the monitor beam effectively averages any differential excitation over the length of the cell or within the pump beam circum-

Pump and Monitor Laser Beams Incident on Double Resonance Cell

Top View

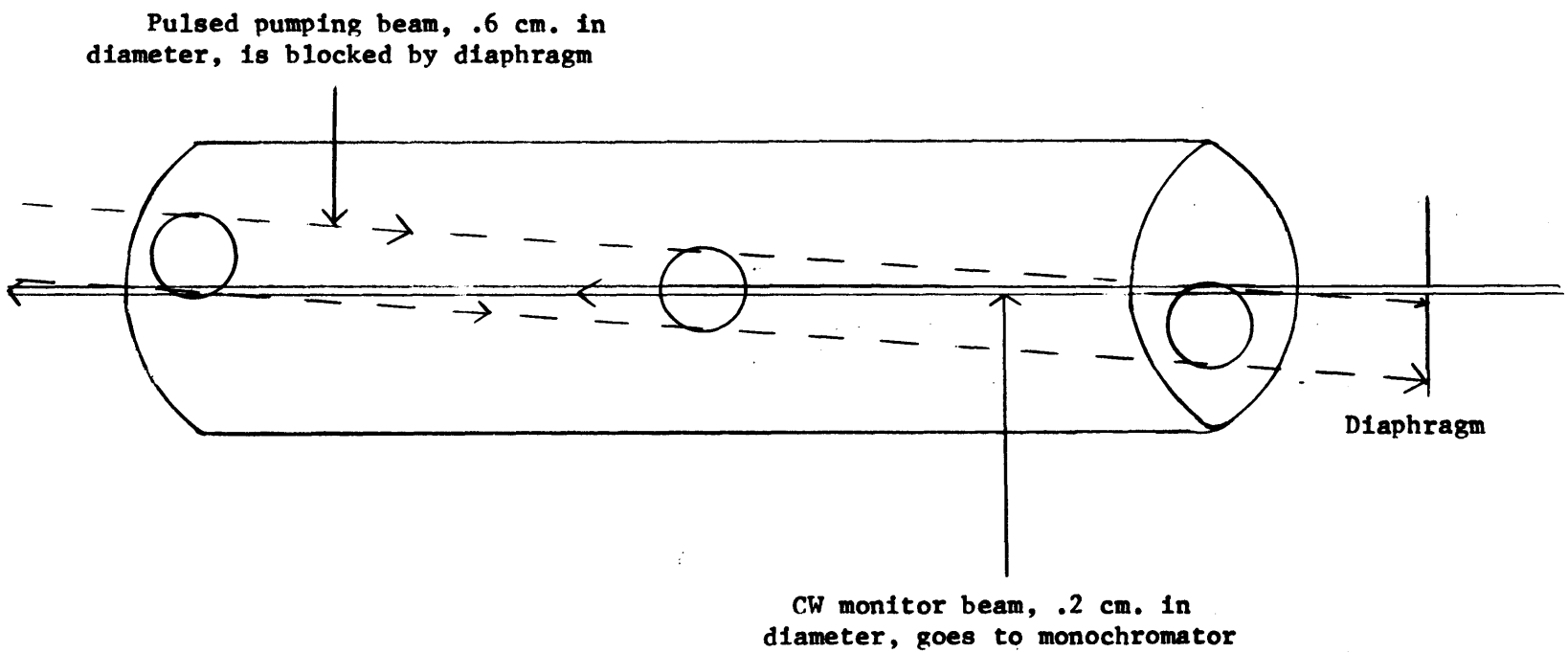

Figure 18

ference.

If we further impose the isothermal boundary condition $T\ (r = 2\ cm) = 300°\ K.$, we have a well defined problem. The solution has already been obtained,[43] but is outlined below.

The differential equation of heat conduction is

$$\nabla^2 T = \frac{1}{k} \frac{\partial T}{\partial t}$$

where

k is the temperature conductivity.

This goes over, in cylindrical coordinates, to

$$\frac{\partial^2 T}{\partial r^2} + \frac{1}{r} \frac{\partial T}{\partial r} = \frac{1}{k} \frac{\partial T}{\partial t}$$

where

r = the radial distance from the cell axis

and

$$\frac{\partial T}{\partial z} = \frac{\partial T}{\partial \theta} = 0 \text{ by symmetry.}$$

The solution to this equation is well known to be

$$T(r,t) = \sum_{m=1}^{\infty} A_m\ I_o(\lambda_m r) e^{-\lambda_m^2 kt}$$

where the coefficients, A_m, are determined from the initial condition

$$T(r,t = 0) = \sum_{m=1}^{\infty} A_m\ I_o(\lambda_m r) = T^o\ (r)$$

---

43. Arnold Sommerfeld, Partial Differential Equations in Physics, (Academic Press, New York, N.Y., 1949), p. 102.

to be

$$A_m = \frac{\int_o^a T^o(r) I_o(\lambda_m r)\, r dr}{\frac{a^2}{2}[I_o'(\lambda_m a)]^2}$$

and

I_o = Bessel function of the first kind of order 0

$\lambda_m a$ = m^{th} root of the zeroth order Bessel function

a = radius of the cylinder = 2 cm, and the prime denotes differentiation with respect to $(\lambda_m r)$.

The quantities of interest are the amplitudes, A_m, of the various Bessel functions and their characteristic decay times, $\tau_m = 1/\lambda_m^2 k$. The ratio A_m/A_1 can be calculated by assuming

$$T^o(r) = T$$

for

$$r \leq r^*$$

and

$$T^o(r) = 0$$

for

$$r > r^*$$

r^* = .3 cm, the radius of the pumping beam.

If the above assumptions are made and the equation for A_m is utilized, we have

$$\frac{A_m}{A_1} = \frac{\int_o^{r^*} I_o(\lambda_m r) r dr}{\int_o^{r^*} I_o(2.4r) r dr} \left[\frac{I_o'(2.4a)}{I_o'(\lambda_m a)} \right]^2$$

Furthermore, making use of the identities[44]

$$\frac{dI_o}{dr}(\lambda_m r) = -\lambda_m I_1(\lambda_m r) = \lambda_m I_o'(\lambda_m r)$$

and

$$\frac{d}{dr}[rI_1(\lambda_m r)] = \lambda_m r I_o(\lambda_m r)$$

which implies that

$$[rI_1(\lambda r)]_o^{r*} = \int_o^{r*} \lambda_m r I_o(\lambda_m r)dr$$

We finally get

$$\frac{A_m}{A_1} = \frac{(\lambda_1)}{\lambda_m} \frac{[rI_1(\lambda_m r)]_o^{r*}}{[rI_1(\lambda_1 r)]_o^{r*}} \frac{[I_1(\lambda_1 a)]^2}{[I_1(\lambda_m a)]^2} = \frac{\lambda_1}{\lambda_m} \frac{I_1(\lambda_m r*)}{I_1(\lambda_1 r*)} \left[\frac{I_1(\lambda_1 a)}{I_1(\lambda_m a)} \right]^2$$

τ_m can be determined trivially by noting that

$$\lambda_1 a = 2.40 \qquad \lambda_m a \sim (m-1/4)\pi$$

and

$$k \text{ (the temperature conductivity)} = \kappa/C_v\rho$$

where

κ = heat conductivity = 23.4×10^{-6} cal/deg.-cm-sec st 300° K.

C_v = constant volume heat capacity of $SF_6 \sim 20 \frac{\text{calories}}{\text{mole-deg}}$

ρ = density in moles/cm^3.

Note that $\tau \propto \rho \propto$ pressure which enables one to differentiate heat effects from collisional effects, where $1/\tau \propto$ pressure is the expected relationship. One may also freeze out temperature modula-

---

44. F. B. Hildebrand, Advanced Calculus for Applications, (Prentice Hall, Englewood Cliffs, New Jersey, 1962), p. 151.

tion by adding large amounts of buffer gas, thereby raising the heat capacity of the system enough to damp any temperature modulation. These techniques were used with considerable success; see Appendix 3 and Figure 18.

The following table summarizes the computed results for several values of m.

m	A_m/A_1	τ_m (P = pressure of SF_6 in torr)
1	1	31.6 msec • P
2	2.16	5.99 msec • P
3	3.04	2.44 msec • P
4	3.41	1.31 msec • P
5	3.16	.82 msec • P

The conclusion then is that the cooling exhibits a complex non-exponential relaxation. The rationale for taking the long time as a pure exponential is that only one or two times will be observable under the limitation imposed by the total intrumental sweep time. The breakdown of this approximation probably accounts for the considerable scatter in the data obtained by this method (see Figure 4 of Appendix 3). The following table compares calculated and measured relaxation times for the heating effect. Clearly the observed decay time is dependent on the duration of the observation.

Calculated and Measured Temperature Relaxation Rates

Sweep Rep Rate 10 msec

Photo #	P torr	msec $\tau_2(1)$	$\tau_2(2)$	$\tau_2(3)$	$\tau_2(4)$	$\tau_2(5)$	(meas)	Total sweep time
143	.25	7.9	1.5	.61	.329		.6	.6
162	.25	7.9	1.5	.61	.329		1.2	1.2
21 a	.6	1.9	3.6	1.5	.79		1	.8
184	.87			2.1	1.1	.7	.5	.5
82	1.15			2.6	1.5		1.2	.8
185	1.56			3.8	2	1.3	.7	.5
85	1.98			4.8	2.6		2	1.8
183	2.4				3.1	2	1.4	.35

The response time of the detector-amplifier circuit (see Figure 19) could be easily measured by tuning the Q-switch laser to produce a 5 microsecond pulse train and by shunting it into the monochromator. The resultant pattern on the scope screen was a good measure of the RC time constant inherent in the total detector-amplifier system. Figure 20 shows several photographs taken with different load resistors, R. Several features are readily apparent. For load resistors greater than 10 K Ω the decay characteristics of the curve are determined by the RC characteristics of the network. For the case of no load resistor, the 1/e time of ∿ 20 microsec corresponds to the input RC of the amplifier. With 1 K load struc-

Detection Circuitry

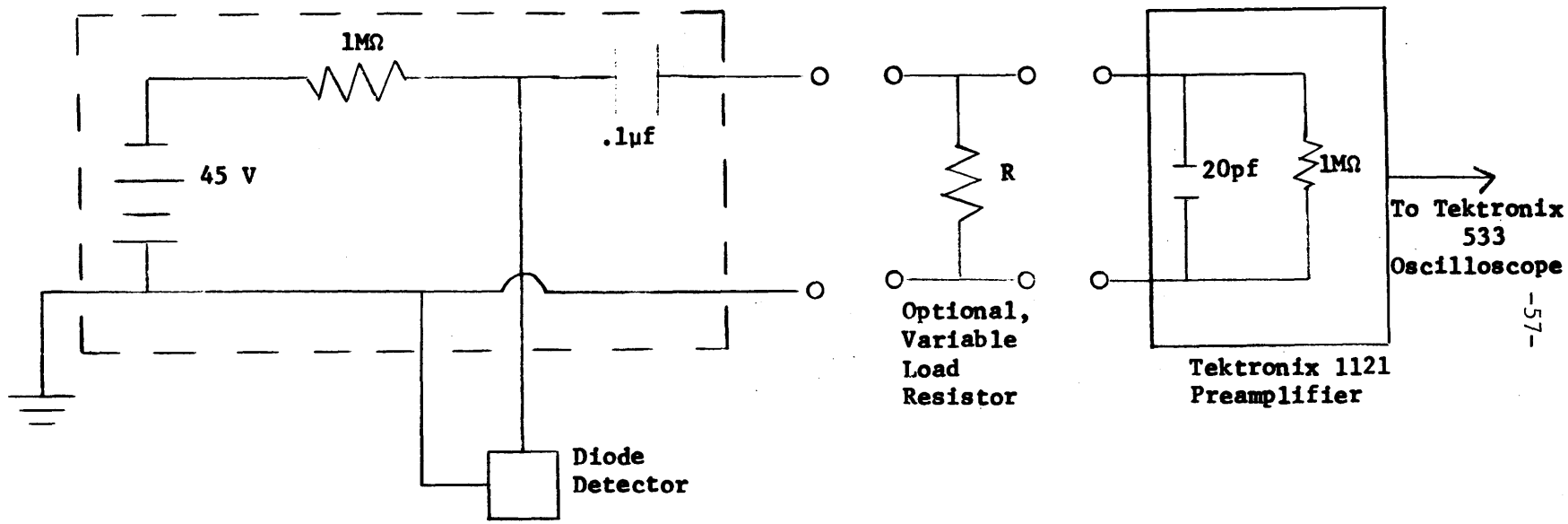

Figure 19

DETECTOR TIME RESPONSE FOR VARIOUS LOAD RESISTORS

a. No load Resistor

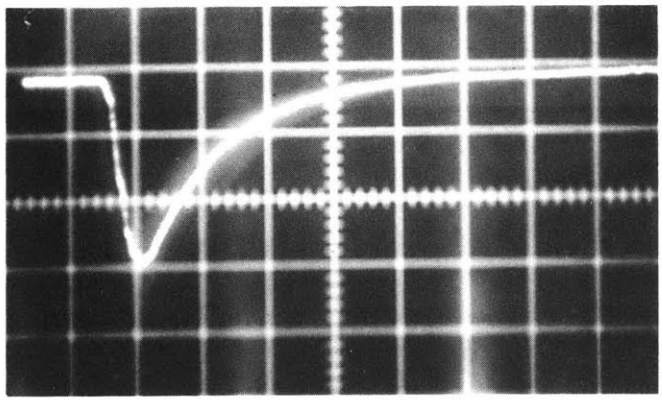

b. R = 10K Ω

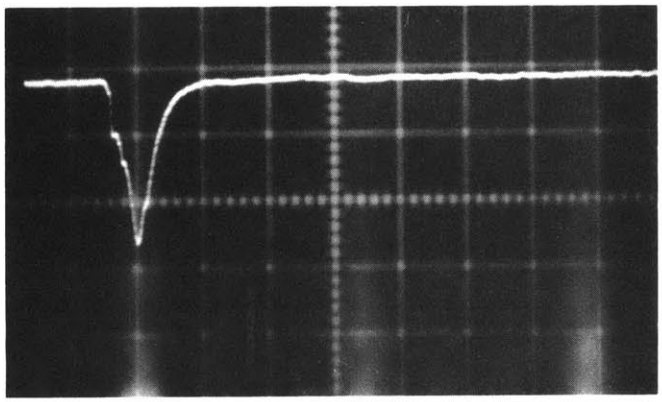

c. R = 1K Ω (vertical scale expanded 10x relative to a and b)

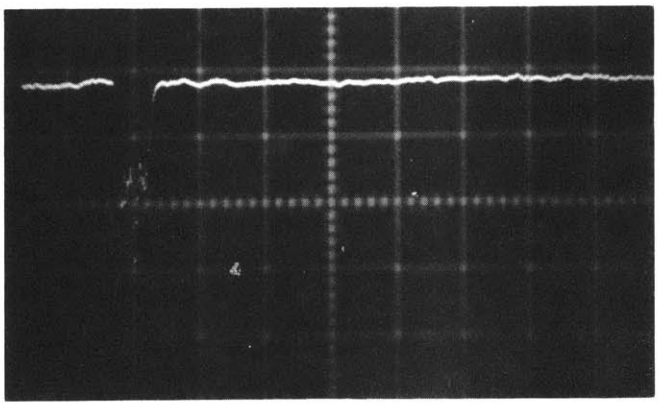

Input is Q-switched Pulse Train

Horizontal Scale = 10 μsec/div

Figure 20

ture in the pulse train can be resolved indicating a response time of $\sim$ 1 microsecond. Note, however, the trade-off between response time and signal amplitude (load resistors intermediate to those shown in Figure 20 gave intermediate decay times and signal amplitudes). For this reason we used the highest load resistor compatible with the criterion that the measured response time be less than 1/10 of the double resonance relaxation time under consideration.

Alignment Effect

As noted in Appendix 3, three different types of signal were observable depending on whether the probe beam wavelength was greater than, equal to, or less than the pumping wavelength. These signals were interpreted as a transient absorption arising from vibrationally excited molecules, a hole burned into the ground state rotational band, and a transitory bleaching of the ground state absorption respectively. Spurious double resonance signals could also be produced if the pump beam was allowed to enter the cavity of the probe laser. In addition to these effects, the double resonance signal for the case $\lambda_{probe} < \lambda_{pump}$ was shown to have a curious dependence on the relative alignment of the two beams.

Under ordinary operating conditions, the two beams were aligned in a near coaxial geometry. The pumping beam was slightly skewed about a vertical axis, while both beams remained in the

same horizontal plane. Diaphragms were then positioned to isolate the pumping beam from the probe laser cavity (see Figure 1 of Appendix 3). Under these geometrical constraints, the signals described in Appendix 3 were observed consistently. However, if the pumping beam was aligned to pass through the absorption cell parallel to the probe beam (a simple adjustment of the gimbal mounted beam splitter, M4 in Figure 1 of Appendix 3), the excited state absorption disappeared, but the bleaching changed to an increased absorption.

This effect is distinguishable from the spurious double resonance signal, because it has been observed only for $\lambda_{pump} < \lambda_{probe}$, and it disappears when the SF_6 is frozen in the sidearm. By adjusting the gimbal the original signal could be reinstated. The duration of both signals was equivalent. Upon addition of 20 torr Krypton, both the double resonance and the parallel alignment signal increased.

Given these experimental observations several possible explanations can be eliminated. Bulk heating and diffusion effects, for example, would be damped, not enhanced, by addition of Kr. The spurious effect due to cavity coupling has already been ruled out. The possibility of a radial acoustic pulse raising the rotational temperature of the gas exists, but any definitive conclusions will have to await more systematic study.

E. LASER INDUCED ACOUSTICAL PULSES IN SF_6

During the course of the double resonance experiments, it was discovered that if a cell filled with SF_6 was opened to the atmosphere while Q-switched pulses were incident upon it, a low pitched buzzing was clearly audible. The buzzing could be stopped by interrupting the Q-switched beam, and the pitch could be varied by changing the rotational velocity of the rotating mirror. Shortly thereafter, Flynn et. al., reported structure in the decay of fluorescence from SF_6 vapor pumped by a Q-switched CO_2 laser, which they interpreted in terms of an acoustic wave propagating in the gas.[45] It became apparent that a measurement of the rise time of the acoustical pulse could determine a lower limit for the rate at which vibrational energy is converted into translational energy. This information could in turn be used to distinguish between our model of vibrational relaxation in SF_6 and alternative models proposed in the literature.[46]

The experiment consisted of passing the output from a Q-switched carbon dioxide laser through an absorption cell equipped

---

45. Thomas Knudtson, Richard D. Bates, Jr., George W. Flynn, and A. M. Ronn, Bul. Am. Phys. Soc. 14, 953 (1969).

46. O. R. Wood, P. L. Gordon, and S. E. Schwarz, I.E.E.E. J. Quantum Electronics, QE-5, 502 (1969).

with a condenser microphone. A block diagram of the apparatus is shown in Figure 21.

The IR pulse train, produced by a 2-m CO_2 laser described in Appendix 3, consisted of 1-2 microsec duration pulses occurring every 10 msec. Triggering for the electronics was produced by a tungsten lamp and photo diode (RCA845TL) arrangement. The triggering was stable to .1 microsec because of the small size of the diode. The pulses from the laser passed through an iris, a fast shutter, the absorption cell, a monochromator (Bausch and Lomb 250-mm, with 30 line/mm grating), and fell onto a detector (Raytheon QKN1568, gold-doped germanium at liquid nitrogen temperature). The shutter could be fired rapidly (10 msec) allowing only one pulse to pass through the cell. By using this technique the effect of interference of acoustic waves from different pulses was eliminated.

Two different acoustic cells were used. The first, shown in Figure 21 (b), was 10 cm long and had the microphone mounted in a sidearm 3.5 cm from the front window. In this arrangement the surface of the microphone was parallel to the laser beam. The end windows were of NaCl and were mounted perpendicular to the beam. The second absorption cell, shown in Figure 21 (a), was 45 cm long and had the microphone mounted at one end with its surface perpendicular to the beam. The entrance window was, again, of NaCl mounted perpendicular to the beam.

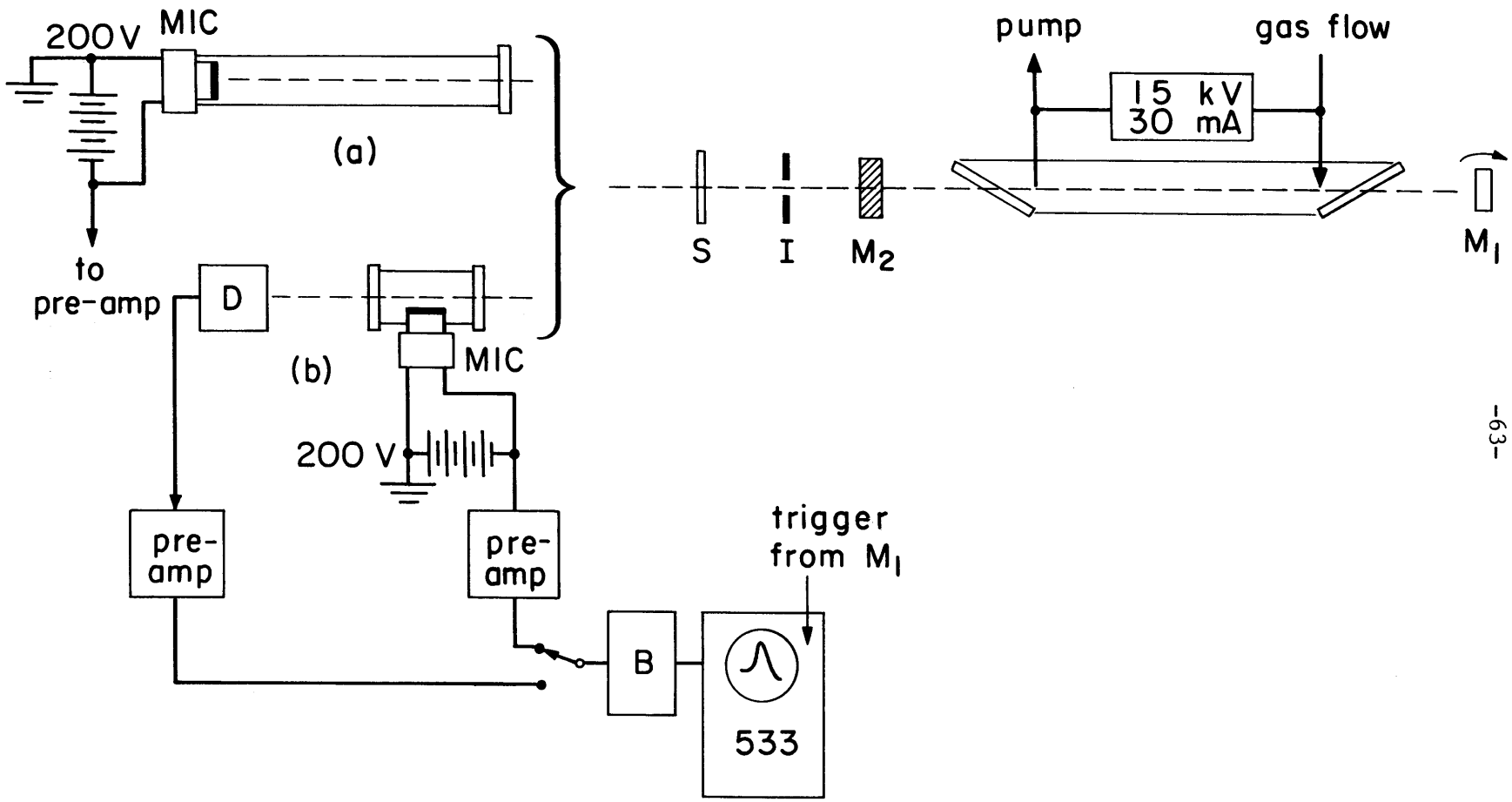

Apparatus for Acoustical Pulse Measurement

Figure 21

When the first cell was used, the arrival of the light pulse was detected as the light passed through the monochromator, while when the second cell was used, the light pulse was detected from the partial (∿1%) reflection of the beam from a salt window. In either case, the signal from the detector was capacitor-coupled (0.1 μf) to a Tektronix 1121 preamplifier (60 db gain, 10 Mhz bandwidth). The amplified signal then passed into a Tektronix 533 oscilloscope with a type B preamplifier.

The acoustic wave was detected by a microphone of the solid dielectric condenser type.[47] In these microphones a sheet of 0.00025 inc. thick mylar coated on one side with aluminum acts as the movable plate of a parallel plate capacitor. The microphone used in our experiments was very similar to that described by Barmatz and Rudnick[48] and had a flat response to at least 100 kHz. The microphone was biased by 200 v. dc and the signal was then passed through a Tektronix 1121 preamplifier and into the oscilloscope.

Sulfur hexafluoride was supplied by the Matheson Company 98% pure and was further purified by a freeze-pump-thaw-cycle before use.

The acoustic signals received by the microphone situated at

---

47. W. Kuhl et. al., Acustica 4, 519 (1954).

48. M. Barmatz and I. Rudnick, Phys. Rev. 170, 224 (1968).

one end of the cell are shown in Figure 22 (a) - (c). The initial ripples in Figure 22 (b) are produced by a portion of the laser pulse striking the surface of the microphone. The shape of the rise of the pressure wave up to the maximum is just a map of the energy absorption profile in the gas cyclinder, and can be predicted by an exceedingly simple model.

We assume that the signal at the transducer is proportional to the translational energy of SF_6 molecules at that point, and that this energy is derived from a complex V-T process that occurs at each point in the cell where surplus vibrational energy is deposited by the laser pulse. We further assume that translational energy is released at a rate $R = \gamma e^{-t\gamma}$ and that this energy propagates homogeneously toward the transducer at a rate v equal to the speed of sound in the cell. Since the beam and transducer have radii comparable to the cell radius, radial propagation of the acoustic energy is ignored.

The signal at a time t will be proportional to the sum from all points (where $\frac{z-\ell}{v} < t$) of the product of the initial vibrational energy at that point times the rate of the V-T process at the retarded time $(\frac{z-\ell}{v})$, i.e.,

$$S(t) = S(\frac{\ell}{v}) \int_{o}^{t<\frac{\ell}{v}} f\,(\ell - v\,\tilde{s})\,\gamma e^{-(t-\tilde{s})\gamma}\,d\tilde{s}$$

where

z = axial distance from the transducer

Acoustic Signals

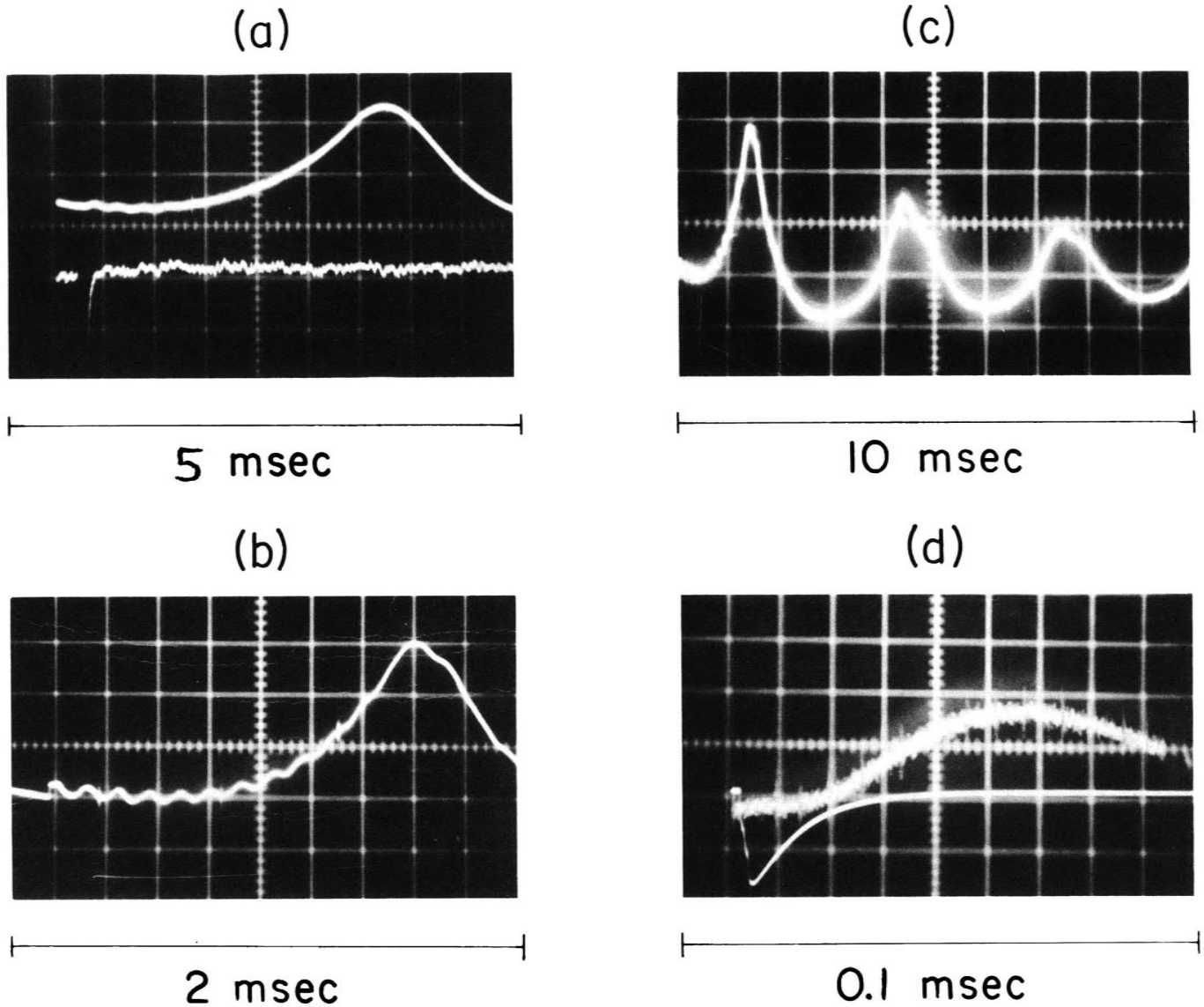

Figure 22

ℓ = length of cell

f = initial excitation function

If Lambert's Law holds, $f = e^{-(\ell - v\tilde{s})\alpha P}$

where

α = the absorption coefficient of SF_6 in the low power limit,

and

P = pressure of SF_6

Using this expression for f and integrating, one obtains

$$S(t) = S\left(\frac{\ell}{v}\right) \frac{\gamma e^{-\ell\alpha P}}{v\alpha P + \gamma} \left[e^{v\alpha Pt} - e^{-t\gamma}\right]$$

The expression in brackets, suitably scaled, is plotted for $\gamma = 10^2$ and $\gamma = 10^6$ sec^{-1} in Figure 23. V is set equal to 3.3×10^4 cm/sec [as calculated from Figure 22 (c)] and P = .35 torr in this plot. The circles correspond to experimental points from Figure 22 (b). The excellent fit implies that Lambert's Law is obeyed. Contrast this with Figure 24, where the same expression is plotted with $\gamma = 10^4$, P = .8 torr, and $V = 1.73 \times 10^4$ cm/sec for pure SF_6. The circles are experimental points defining the curve shown in Figure 22 (a). Here it is evident that saturation broadens the initial excitation function, giving an elongated acoustical pulse. Note that with the given experimental parameters, the shape of the acoustical pulse is nearly independent of γ.

It is also clear from these figures why the phase shift

Acoustical Pulse from Non-Saturating Excitation

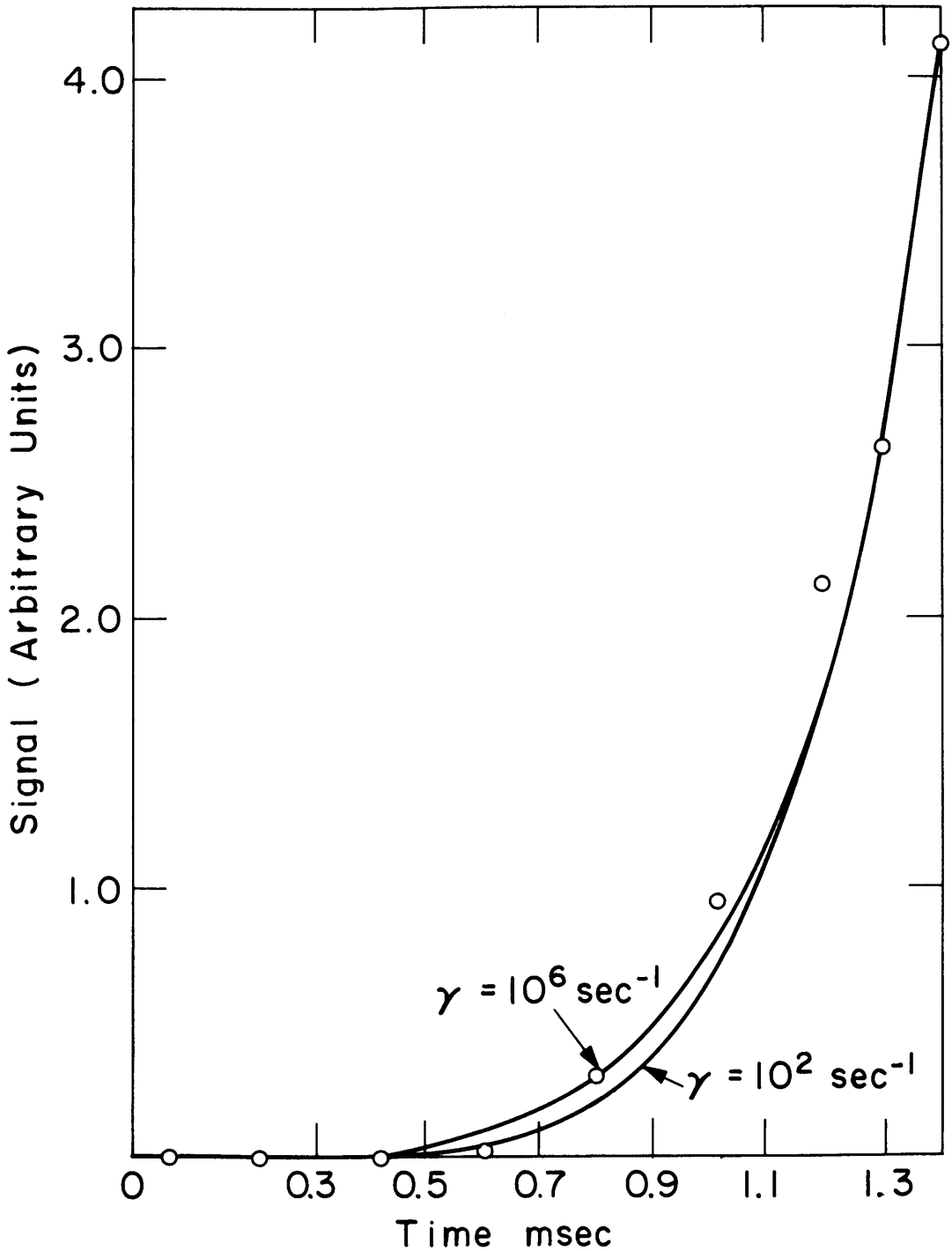

Figure 23

Acoustical Pulse from Saturating Excitation

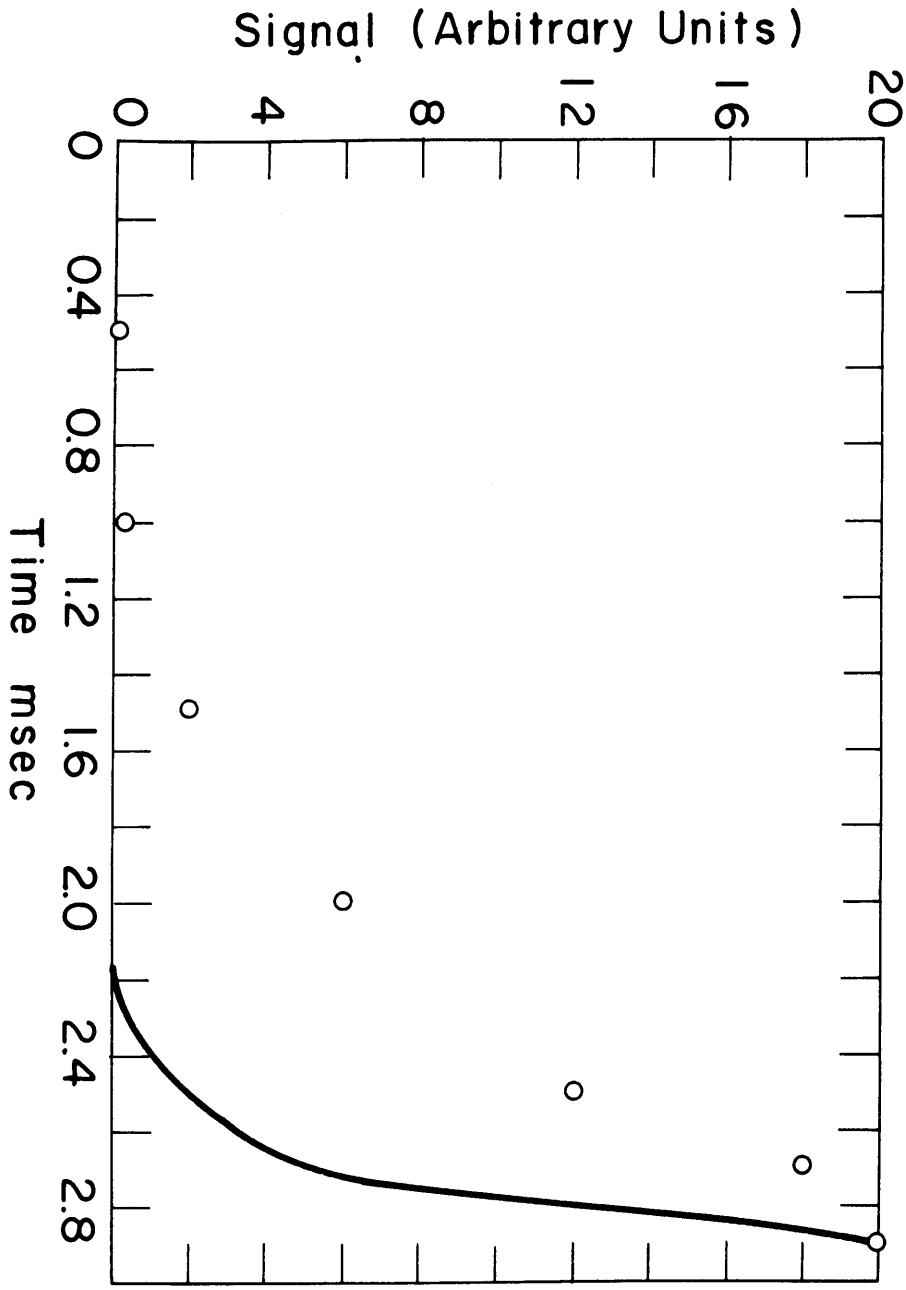

Figure 24

obtained in a conventional spectrophone experiment in SF_6 has the wrong sign:[49] as the pressure of SF_6 is increased, more energy is absorbed near the entrance window, and thus it takes a longer time for the wave to reach the microphone in the cell, leading to a phase shift increasing rather than decreasing with pressure. In Figure 22 (c), we show the same acoustic wave at a longer time scale, in which the successive reflections are evident. This is just a direct map of the fluorescence "bumps" reported in Reference 45; there is a slight broadening of successive reflections, not observable in the fluorescence experiment, which is attributed to the dispersion of the different frequency components on the sound wave.[50]

At higher pressures of added gas (e.g., 90 torr of air), the acoustic profile becomes steeper than that predicted by this simple theory and the sound speed as measured from the interval between reflections becomes slightly higher. This indicates the formation of a shock wave in the higher density gas.

The detailed time development of the acoustic wave turns out to be quite complicated, and work on understanding it is proceeding at both our laboratory and Columbia. The most important observation from the signal recorded by the microphone located at the side of the cell [Figure 22 (d)] is that sufficient energy to produce an

---

49. T. L. Cottrell, I. M. MacFarlane, and A. W. Read, Trans. Faraday Soc. 62, 2664 (1966).

50. E. U. Haebel, Acustica 20, 65 (1968).

acoustic wave is released at essentially the same instant that the light enters the cell. The 10-20 microsec delay between the laser pulse and the start of the pressure rise just corresponds to the propagation time from the edge of the illuminated region of the gas radially outward to the surface of the microphone. The observation of an acoustic wave at a gas pressure of 50 microns enables us to set a lower limit on the vibration-vibration transfer rate in SF_6 of 2×10^6 sec^{-1} $torr^{-1}$ which corresponds to an inelastic event at approximately every collision. This, it should be noted, is just opposite to the conclusion reached by Wood and Schwarz,[47] who felt that energy in the ν_3 vibrational mode relaxed very slowly, with a time constant of 70,000 microsec torr. We feel that the acoustic evidence and the infrared double resonance results definitely precludes this possibility.

F. SUMMARY OF RESULTS AND EVIDENCE FOR THE FOUR STATE MODEL

All of the experiments described here rely on the four state model for interpretation. This summary will recapitulate the basic features of the model and list the contributions that each experiment has made toward its development.

The four state model was originally conceived to provide a basis for machine calculations designed to reproduce saturation experiments described in Appendix 2. Its nascent features are best described with reference to Figure 1 of Appendix 2, page 85. There is a one-to-one correspondence between the respective states N_o, N^*, N', and N in this figure and the states n_1, n_2, n_3, and n_4 used in the rate omitted from this model a priori is the cross relaxation between N' and N_o. This could safely be done because N_o contains only a small fraction of the rotational levels of the ground vibrational state. The radiative relaxation rate, $1/\tau_R$, calculated from the integrated absorption coefficient of the ν_3 band was determined to be negligible (25 sec^{-1}). The pumping rate as a function of intensity was determined by this same calculation and the known relation between the Einstein A and B coefficients.

The uncertainty in the model at this stage centered on the role of the vibrational states other than the $\nu_3 = 1$ and ground states. The resolution of this problem provided by the double

resonance experiments affected the definitions of N' (n_3), the vibrational relaxation rate ($1/\tau_v$), and the rotational relaxation, R, between the excited states N* and n' (n_2 and n_3).

The double resonance experiments provided evidence (summarized on pages 112-114 of Appendix 3) for a more detailed interpretation of the model:

1) n_3 was redefined to include all molecules with excess vibrational energy. These levels were assumed to be in rapid equilibrium (see Figure 7 of Appendix 3, page 112).
2) The vibrational relaxation was determined to take place through the lowest vibrational level, ν_6, 363 cm^{-1} above the ground state.
3) Relaxation from the pumped state, n_2, was determined to involve V-V as well as R-T processes. This necessitated a redefinition of β for this rate to take account of the increased level density.

The experimental data obtained with the double resonance technique determined the vibrational relaxation time explicitly and set upper limits on the relaxation times for the processes connenting n_1 to n_4 and n_2 to n_3. These are, respectively, 122 microsec-torr, < 3 microsec-torr, and < 3 microsec-torr. The .3 microsec-torr relaxation time for the n_2 state has been corroborated by observation of the rise time of the acoustical pulse generated in SF_6 when the pumped levels n_2 equilibrate with n_3 dumping much of

their excess energy into the translational modes in the process (see Section E).

The model and its associated rates have since been used in machine calculations that have successfully reproduced the results of passive Q-switching[51] and infrared pulse transmission experiments (see Section C).

---

51. I. Burak, Paul Houston, and J. I. Steinfeld, Symp. on Molecular Structure and Spectroscopy, Columbus, Ohio, 1970.

Appendix 1

PULSE TRANSMISSION PROGRAM

```
C      PULSE TRANSMISSION (SF6) HOLE BURNING MODEL
C READING IN DATA ON THE GASES AND THE PULSE AND THE TEMPERATURE
C    TEMP(DEG), FREQ(CM-1), DELTL AND ALENG(CM), COEFF(TORR-1,CM-1), TAUR(SEC),
C      TPK(SEC),   SIGXX(ANGSQXE16), AMAS(AMU), BETA(NUMERIC)
C    NDIV(NUMERIC)=ALENG/DELTL, PRES(MICRONS)
       CALL NEWPLT('M7395','2440','GRAPH ','BLACK')
  300  READ(5,110,END=999) TEMP,FREQ,DELTL,ALENG,COEFF,TAUR,TPK
       READ (5,111) SIGV1,SIGV2,SIGR1,SIGR2,AMAS1,AMAS2,BETA
       READ (5,112,END=999) PRES1, PRES2
       READ (5,109) WATTPK, TPULSE, NDIV
C    INPUT FORMATS
  109  FORMAT (2E10.3,I10)
  110  FORMAT (7E10.3)
  111  FORMAT (7E10.3)
  112  FORMAT (2E10.3)
  101  WRITE (6,102)
  102  FORMAT('0WATTPK    TPULSE            NDIV')
       WRITE (6,109) WATTPK, TPULSE, NDIV
       WRITE (6,104)
  104  FORMAT('0TEMP      FREQ      DELTL     ALENG     COEFF     PTAUR
     P   TPK')
       WRITE (6,110) TEMP,FREQ,DELTL,ALENG,COEFF,TAUR,TPK
       WRITE (6,105)
  105  FORMAT ('0SIGV1     SIGV2     SIGR1     SIGR2     AMAS1     AMAS2
     P    BETA')
       WRITE(6,111) SIGV1,SIGV2,SIGR1,SIGR2,AMAS1,AMAS2,BETA
       WRITE (6,106)
  106  FORMAT('0PRES1     PRES2')
       WRITE (6,112) PRES1,PRES2
C DEFINING SOME BASIC CONSTANTS
       H = 6.62517E-27
       BOLTZ = 1.38044E-16
       PI=3.14159
       AVOG =6.023E+23
       GAMMA=1.0-BETA
       CL= 2.998E10
```

```
C   GENERATING SOME CONSTANTS USED INTERNALLY
      DFREQ=1.0E+09
      ULAMB = EXP(-1.0*COEFF*ALENG*PRES1/1000.)
      EXPON=3*EXP(-1.0*H*CL*947/(BOLTZ*TEMP))
      BEPR = BETA*EXPON
      GAMPR = 1.0-BEPR
      DELT=DELTL/CL
      II=NDIV+1
      ASQ = (CL*TPK   /DELTL)**2
      D=WATTPK*EXP(1.)/(ASQ)
      JJ=TPULSE/DELT
      JJJ=JJ+1
      JJJJ=JJ+NDIV
      GASN = (9.65E+15)*PRES2/TEMP
      TOTN = (9.65E+15)*PRES1/TEMP
      AMU1 = (AMAS1/2.0)/AVOG
      AMU2 = (AMAS1*AMAS2/(AMAS1+AMAS2))/AVOG
      VEL1=SQRT(8.0*BOLTZ*TEMP/(PI*AMU1))
      VEL2=SQRT(8.0*BOLTZ*TEMP/(PI*AMU2))
      ZCOLL = 1.414*PI*(TOTN*SIGR1*(1.0E-16)*VEL1 + GASN*SIGR2*(1.0E-16)
     P*VEL2)
      ZVIB = 1.414*PI*(TOTN*SIGV1*(1.0E-16)*VEL1 + GASN*SIGV2*(1.0E-16)
     P*VEL2)
      BABS = (COEFF*PRES1/1000.)*DFREQ/(BETA*TOTN*H*FREQ*CL)
      FACTOR =    DELTL*COEFF*PRES1/1000./(BETA*TOTN)
C  ZERON, PLAIN, STARN, DW, WCELL, C, PRIME, AND Q ALL HAVE DIM=NDIV+1
C   DIM W=DIM PULSE=DIM T=(JJ+NDIV+10)
      DIMENSION ZERON(100), PLAIN(100), STARN(100), DW(100)
      DIMENSION Q(100) C(100), PRIME(100), WCELL(100)
      DIMENSION T(22000), W(22000), PULSE(22000)
C   THE FOLLOWING DO LOOPS INITIALIZE SOME OF THE INTERNAL VARIABLES
      DO 5 I=1,II
      Q(I) = C.C
      DW(I)=0.0
      WCELL(I)=0.0
      PRIME(I)=0.0
```

```
      ZERON(I)= BETA*TOTN
      PLAIN(I)= TOTN*GAMMA
    5 STARN(I)= 0.0
C   THE FOLLOWING DO LOOP GENERATES THE INPUT PULSE
C   THIS PULSE HAS THE SHAPE OF A BOLTZMAN DISTRIBUTION
      DO 10 L=1,JJJJ
   10 W(L)  = D*L*L*EXP(-1.0*L*L/(ASQ))
C   THE FOLLOWING ARE RATES WHICH ARE INDEPENDENT OF POWER
      R=ZCOLL
      A=1.0/TAUR
      Z=ZVIB
C   THE FOLLOWING TWO NESTED DO LOOPS MOVE THE PULSE THROUGH THE CELL
C   AND RESHAPE IT... COMPUTING TRANSITORY POPULATION VALUES  AS IT GOES
      DO 200 J=1,JJJJ
      WCELL(1) = W(J)
      DO 100 K=1,NDIV
      WCELL(K+1)=Q(K)-DW(K)
      Q(K) = WCELL(K)
      C(K)=BABS*WCELL(K)*1.E+7/(DFREQ)
      DW(K)=(ZERON(K)-STARN(K)/3+BETA*PRIME(K))*WCELL(K)*FACTOR
      PRIME(K)=PRIME(K)+DELT*(R*( GAMPR*STARN(K)-BEPR*PRIME(K))-(A+Z)*
     PPRIME(K)+EXPON*(GAMMA)*Z*(ZERON(K)+PLAIN(K)))
      ZERON(K)=ZERON(K)+DELT*(R*(BETA*PLAIN(K)-GAMMA*ZERON(K))+C(K)*
     P(STARN(K)/3.0-ZERON(K))+(2.0*BETA*A+BETA*Z)*(STARN(K)+PRIME(K))
     P-EXPON*Z*ZERON(K))
      STARN(K)=STARN(K)+DELT*(R*(BEPR*PRIME(K)-GAMPR*STARN(K))+C(K)*
     P(ZERON(K)-STARN(K)/3.0)-(A+Z)*STARN(K)+EXPON*BETA*Z*(ZERON(K)
     P+PLAIN(K)))
  100 PLAIN(K)=PLAIN(K)+DELT*(R*((GAMMA)*ZERON(K)-BETA*PLAIN(K))+
     P((1.0-2.0*BETA)*A+GAMMA*Z)*(STARN(K)+PRIME(K))-EXPON*Z*PLAIN(K))
      PULSE(J)  = WCELL(NDIV+1)
  200 CONTINUE
C   THIS DO LOOP PUTS THE TRANSMITTED PULSE ON THE SAME TIME AXIS
C   AS THE INPUT PULSE
      DO 600 J5=1,JJ
  600 PULSE(J5) = PULSE(J5+NDIV)
```

```
C   THIS DO LOOP GENERATES A TIME AXIS FOR PLOTTING
      DO 400 I1=1,JJJJ
  400 T(I1)= DELTL*I1/CL
      WRITE(6,440) ULAMB
  440 FORMAT('0IF LAMBERTS LAW-FRACTION=',E10.3)
      DIMENSION XAX(2), YAX(2)
C   DEFINE LABELS FOR AXES
      DATA XAX/'TIME'/,YAX/'W/CM2'/
      CALL PICTUR (6.,9.,XAX,4,YAX,5,T,W,J5,0.,KS,T,PULSE,J5,0.,KS)
      GO TO 300
  999 CALL ENDPLT
      CALL EXIT
      STOP
      END
```

Appendix 2

INFRARED SATURATION IN SULFUR HEXAFLUORIDE

I. Burak, J. I. Steinfeld and D. G. Sutton

J. Quant. Spectry. and Radiat. Transfer 9, 959 (1969)

J. Quant. Spectrosc. Radiat. Transfer. Vol. 9, pp. 959–980. Pergamon Press 1969. Printed in Great Britain

INFRARED SATURATION IN SULFUR HEXAFLUORIDE

I. BURAK, J. I. STEINFELD and D. G. SUTTON†

Department of Chemistry, Massachusetts Institute of Technology, Cambridge, Massachusetts 02139

(*Received* 5 *December* 1968)

Abstract—The saturation of absorption of a CW infrared laser beam by SF_6 has been measured as a function of pressure of SF_6 and added buffer gases (He, Kr, and C_2H_6). The results are interpreted by means of a four-state linear kinetic model for saturation of vibrational energy levels by intense infrared radiation, which predicts equalization of upper and lower level populations at power densities of approximately 10 W/cm^2. Vibrational and rotational deactivation cross sections are derived from these data with the aid of this model, which suggests that previously observed pulse transparency effects may be interpreted in terms of this same model.

1. INTRODUCTION

As COHERENT, high-power optical sources become available, a number of techniques hitherto limited to magnetic resonance and microwave spectroscopy become feasible in the optical region, such as double resonance and radiative echo formation. In order to extend these techniques into the infrared and optical regions of the spectrum, we must first know the response of molecular energy level populations to available power sources; an indicator of this response is the power saturation of absorbance.

The self-induced transparency of certain media to high-power infrared pulses is known,[1] and has been interpreted in terms of coherent optical excitation, according to the model of MCCALL and HAHN.[2] In this work, we develop a four-state kinetic model, which does not include coherent effects, to represent the steady-state saturation of the absorption of 10·59-μ laser radiation by sulfur hexafluoride, with and without added buffer gases. The population changes derived from this model are used to fit experimental power saturation data. These results are compared to the pulse transmission experiments and to related phenomena involving saturable-dye absorbers in the visible region; some practical consequences of these effects are also noted.

2. FOUR-STATE MODEL

In this section, we suggest a kinetic model for interpreting data on the attenuation of a CO_2 laser beam through the absorbing SF_6 gas which does not involve any coherent

† Work supported (in part) by Public Health Service Fellowship 1-F1-GM-39,059-01 from the National Institute of General Medical Science.

effects. The effects of an intense infrared laser beam on an absorbing gas are:

(a) changes in the populations in the various states of the gas molecules due to excitation;
(b) heating effects due to the relaxation of the excited molecules to lower energy levels.

When an absorbing gas is irradiated by the laser beam, molecules in certain rotational sublevels of the ground state are pumped to corresponding rotational sublevels in the vibrationally excited state. A molecule in one of the above excited states might return to the ground state by stimulated or spontaneous emission, or may suffer collisional transfer to another level. If we denote by 1 and 2 levels which are coupled by the electromagnetic field and by l any other level which is not coupled directly to the irradiation field then the effect of the radiation on populations is given in terms of the following master equation:

$$\frac{dN_1}{dt} = -B_{12}I(\nu)\left(N_1 - \frac{g_1}{g_2}N_2\right)\phi(\nu-\nu_0) + \sum_{j=1}^{n} k_{1j}N_j, \tag{1}$$

$$\frac{dN_2}{dt} = B_{12}I(\nu)\left(N_1 - \frac{g_1}{g_2}N_2\right)\phi(\nu-\nu_0) + \sum_{j=1}^{n} k_{2j}N_j, \tag{2}$$

$$\frac{dN_l}{dt} = \sum_{j=1}^{n} k_{lj}N_j \qquad (l = 3, 4, \ldots, n). \tag{3}$$

In each case, $k_{ll} = -\sum_{j \neq l} k_{lj}$ in order to conserve molecules and ensure a stochastic system of rate equations.[3] The first terms on the right-hand side of equations (1) and (2) are the difference between the pumping rate and the rate of stimulated emission. Both rates are proportional to the light intensity $I(\nu)$ and the lineshape factor $\phi(\nu-\nu_0)$, and N_j is the number density of molecules in the level j.

The terms $k_{lj}N_j$ represent the rate at which molecules are transferred from the jth level to the lth level due to collisional relaxation or spontaneous emission. n is the total number of levels involved in the above processes. The populations of the various levels under steady irradiation are given by the solutions of the homogeneous set of linear equations

$$\dot{\mathbf{N}} = \Pi\mathbf{N} = 0 \tag{4}$$

where $\mathbf{N}$ is a column vector of dimension n whose elements N_i are the number densities of molecules in the level i. Π is a square matrix of dimension n which consists of the various rate coefficients including radiation. Since some of the rate coefficients are light-intensity dependent, the solution $\mathbf{N}$ is a function of the intensity, i.e. $\mathbf{N} = \mathbf{N}(I)$. Since n, the number of the levels, might be very large and is usually not known in detail we have employed a simplified model in which the total number of levels is reduced to four.

The four-level model is represented schematically in Fig. 1. The molecules of the gas are divided into four groups. N_0 and N^* are the number densities of molecules in the ground state and in the excited state which are directly interacting with the electromagnetic field via absorption or stimulated emission. N and N' represent number densities of the rest of the molecules in the ground and excited states respectively. We take $N_0 = \beta N$ and $N^* = \beta N'$, with β to be determined. The following transitions are assumed to take place between the four levels.

(*a*) *Rotational transitions.* The transitions between the two levels in the ground state are assumed to take place via rotational energy transfer collisions [see Appendix 3]. We assume that the rate constant for rotational relaxation, R, is independent of the rotational level involved,

$$R = \sqrt{(2)}\pi\sigma_R^2\sqrt{\left(\frac{8kT}{\pi\mu}\right)}N_{\text{total}} \tag{5}$$

where σ_R^2 is a cross section applicable to all J levels, N_{total} is the total number density of molecules and μ is the reduced mass appropriate to the collision pair. The factor β, which is the ratio of level densities in N_0 relative to N, is also the probability that a rotational transfer collision involving a molecule of type N will result in a transition to a state included in N_0. Conversely, $(1-\beta)$ is the probability that the result of a collision of a molecule of type N_0 will be a transfer of this molecule to a state included in N. This definition ensures that at thermal equilibrium,

$$(1-\beta)RN_0^e = \beta RN^e.$$

(The superscript e denotes values at thermal equilibrium in the absence of radiation.) Thus

$$N^e/N_0^e = \beta/1-\beta$$

or

$$\beta = \frac{N_0^e}{N_0^e+N^e}. \tag{6}$$

If $h\nu \gg kT$ then $N_0^e+N^e = N_{\text{total}}$ and β is the fraction of the absorbing molecules in the sample at thermal equilibrium [see Appendix 3]. We assume that the same rate law with the same β and R parameters exists for the levels N^* and N' in the upper state.

(*b*) *Vibrational transfer mechanism.* Vibrational relaxation is allowed between the ground and excited levels. A vibrational relaxation rate constant is introduced:

$$Z_{\text{vib}} = \sqrt{(2)}\pi\sigma_v^2\sqrt{\left(\frac{8kT}{\pi\mu}\right)}N_{\text{total}}.$$

βZ_{vib} and $(1-\beta)Z_{\text{vib}}$ represent the rate constants for the transitions from the N^* states to N_0 states, and from the N' states to N states, respectively. The rates for the reverse reactions are obtained from the above rates by multiplying by the Boltzmann factor, $(g_2/g_1)e^{-h\nu/kT}$. This ensures detailed balancing.

(*c*) *Transitions coupled to the laser field.* The net rate of radiative transitions in an ensemble of $n_1+n_2 = N_{\text{total}}$ molecules is given by

$$+\frac{dn_2}{dt} = \left(n_1-\frac{g_1}{g_2}n_2\right)B_{12}I_\nu\phi(\nu-\nu_0)-A_{21}n_2. \tag{7}$$

Here, B_{12} is the Einstein absorption coefficient for this transition, A_{21} the corresponding emission coefficient ($A_{21} = 8\pi h\nu^3 g_1 B_{12}/g_2c^2$); g_1 and g_2 are the statistical weights of the ground and excited states, respectively. I_ν is the intensity of monochromatic light at frequency ν, and $\phi(\nu-\nu_0)$ is a lineshape factor to be considered in more detail below.

In order to get a value for the Einstein coefficient B_{12}, we make use of the expression[4]

$$\alpha(\nu) = -\frac{dI_\nu/dz}{I_\nu} = \left(n_1\frac{g_2}{g_1}-n_2\right)h\nu B_{12}\phi(\nu-\nu_0).$$

At low intensities where $n_2 \ll n_1$,

$$\alpha(\nu) = n_1 B_{12} h\nu \phi(\nu - \nu_0);$$

$\alpha(\nu)$ is determined experimentally as

$$\alpha(\nu) = \varepsilon(\nu) P_{SF_6},$$

thus

$$B_{12} = \frac{\varepsilon(\nu) P_{SF_6}}{n_1 h\nu \phi(\nu - \nu_0)}. \tag{8}$$

We can identify n_1 with N_0^e, which in turn is βN_{total}; also, n_2 is called N^* in our model.

The lineshape factor $\phi(\nu - \nu_0)$ can be related to the parameter β in the following way. If the dominant broadening mechanism is inhomogeneous (Doppler broadening), we then have a Gaussian lineshape,

$$\phi(\nu - \nu_0) = \sqrt{\left(\frac{\ln 2}{\pi}\right)} \frac{2}{\delta\nu_D} e^{-4 \ln 2 (\nu - \nu_0)^2/(\delta\nu)^2}.$$

If, on the other hand, the dominant mechanism is homogeneous (collision broadening), we have a Lorentzian lineshape,

$$\phi(\nu - \nu_0) = \frac{\delta\nu_L}{2\pi[(\nu - \nu_0)^2 + (\delta\nu_L/2)^2]}.$$

In either case, suppose that the laser coincides with the peak of some transition. We would then have

$$\phi(0) = 2\sqrt{\left(\frac{\ln 2}{\pi}\right)} (\delta\nu_D)^{-1} = 0{\cdot}94(\delta\nu_D)^{-1} \quad \text{(inhomogeneous)}$$

or

$$\phi(0) = \frac{2}{\pi}(\delta\nu_L)^{-1} = 0{\cdot}64(\delta\nu_L)^{-1} \quad \text{(homogeneous)}.$$

In either case, $\phi(\nu)$ is of the order of $(\delta\nu)^{-1}$ times some numerical factor of order unity. Equation (8) then becomes

$$B_{12} \approx \frac{\varepsilon(\nu) P_{SF_6} \delta\nu}{\beta N_{\text{total}} h\nu}.$$

The factor $(\delta\nu/\beta)$ can be separated to give

$$B_{12} \approx \frac{\overline{\varepsilon(\nu)}}{h\nu} \left(\frac{P_{SF_6}}{N_{\text{total}}}\right) \left(\frac{\delta\nu}{\beta}\right).$$

We could also have found B_{12} from

$$\int \varepsilon(\nu)\, d\nu = \frac{N_{\text{total}}}{P_{SF_6}} B_{12} h\bar{\nu};$$

and since $\int \varepsilon(\nu)\, d\nu \approx \overline{\varepsilon(\nu)}\Delta\nu$, where $\Delta\nu$ is the width of the entire absorption band, it is natural to regard $\delta\nu$ as $\beta\Delta\nu$. Thus the B coefficient is, as it must be, independent of β or $\delta\nu$. The pumping rate as given by equation (7) is, on the other hand, dependent on the quantity

$(B_{12}I_\nu/\beta)$. The linewidth $\beta\Delta\nu$ is compared to independent estimates of homogeneous broadening in Appendix 3.

Spontaneous emission returns excited molecules to both the N_0 and the N states. We should expect that the relative weighting of the two possible paths is not simply β to $(1-\beta)$, since selection rules will favor a return to the original state. We have assumed that the weighting can be given by $2\beta:(1-2\beta)$; this is actually unimportant to the final results, since the spontaneous emission rate is the slowest in the entire system ($A \sim 25\,\mathrm{sec}^{-1}$).

In these terms, the kinetic equations corresponding to the scheme shown in Fig. 1 become

$$\frac{dN_0}{dt} = R(\beta N-(1-\beta)N_0)+\frac{B_{12}I}{\delta\nu}\left(\frac{g_1}{g_2}N^*-N_0\right) +(2\beta A_{21}+\beta Z_{\mathrm{vib}})(N^*+N')-\frac{g_2}{g_1}e^{-h\nu/kT}Z_{\mathrm{vib}}N_0 \tag{9a}$$

$$\frac{dN^*}{dt} = R(\beta N'-(1-\beta)N^*)+\frac{B_{12}N}{\delta\nu}\left(N_0-\frac{g_1}{g_2}N^*\right) -(A_{21}+Z_{\mathrm{vib}})N^*+\frac{g_2}{g_1}e^{-h\nu/kT}\beta Z_{\mathrm{vib}}(N_0+N) \tag{9b}$$

$$\frac{dN'}{dt} = R((1-\beta)N^*-\beta N')-(A_{21}+Z_{\mathrm{vib}})N' +\frac{g_2}{g_1}e^{-h\nu/kT}(1-\beta)Z_{\mathrm{vib}}(N_0+N) \tag{9c}$$

$$\frac{dN}{dt} = R((1-\beta)N_0-\beta N)+((1-2\beta)A_{21}+(1-\beta)Z_{\mathrm{vib}})(N^*+N') -\frac{g_2}{g_1}e^{-h\nu/kT}Z_{\mathrm{vib}}N. \tag{9d}$$

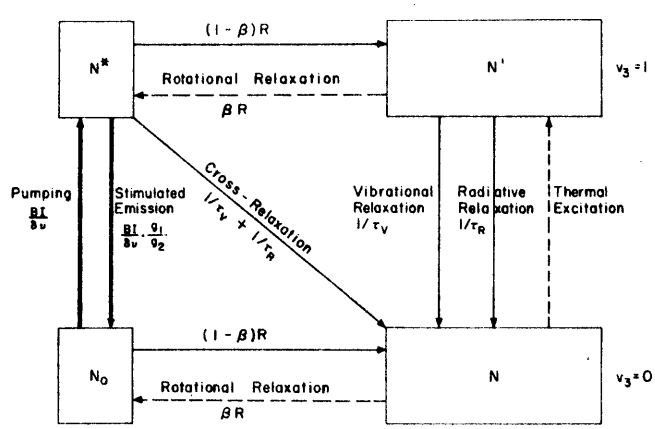

FIG. 1. Schematic four-state model used to calculate infrared saturation.

Applying the steady-state condition to equations (9a)–(9d) gives the system of linear equations indicated in equation (4), where Π has the explicit form

$$\Pi = \left\{ \begin{array}{c|c|c|c} -(1-\beta)R - \dfrac{B_{12}I}{\delta\nu} - \dfrac{g_2}{g_1}e^{-h\nu/kT}Z_{\text{vib}} & +\dfrac{B_{12}I}{\delta\nu}\dfrac{g_1}{g_2} + 2\beta A_{21} + \beta Z_{\text{vib}} & +2\beta A_{21} + \beta Z_{\text{vib}} & +\beta R \\ \hline +\dfrac{B_{12}I}{\delta\nu} + \dfrac{g_2}{g_1}e^{-h\nu/kT}\beta Z_{\text{vib}} & -\dfrac{B_{12}I}{\delta\nu}\dfrac{g_1}{g_2} - A_{21} - Z_{\text{vib}} - (1-\beta)R & +\beta R & +\dfrac{g_2}{g_1}e^{-h\nu/kT}\beta Z_{\text{vib}} \\ \hline +\dfrac{g_2}{g_1}e^{-h\nu/kT} \times (1-\beta)Z_{\text{vib}} & +(1-\beta)R & -\beta R - A_{21} - Z_{\text{vib}} & +\dfrac{g_2}{g_1}e^{-h\nu/kT}(1-\beta)Z_{\text{vib}} \\ \hline +(1-\beta)R & +(1-2\beta)A_{21} + (1-\beta)Z_{\text{vib}} & +(1-2\beta)A_{21} + (1-\beta)Z_{\text{vib}} & -\beta R - \dfrac{g_2}{g_1}e^{-h\nu/kT}Z_{\text{vib}} \end{array} \right\} \quad (10)$$

It can be seen that this satisfies the stochastic condition, $\Pi_{ll} = -\sum_{j \neq l} \Pi_{lj}$. This condition ensures that detailed balancing applies, i.e. $\Pi_{nm}N_m = \Pi_{mn}N_n$. In order to determine a particular solution of equation (10), we have to impose the additional mass balance condition,

$$N_0 + N^* + N' + N = N_{\text{total}} = \frac{P_{SF_6}}{kT}. \quad (11)$$

The effect of the temperature of the gas on the densities arises in several ways. First, and most obvious from equation (11), is the inverse dependence of density on temperature for a given pressure. In addition, the rate terms in (10) depend on temperature through the collision velocity and the Boltzmann factor for thermal excitation. In Appendix 1, we show that the passage of the laser beam through the gas produces considerable heating, and thus gives rise to radial temperature and density gradients. The temperature has been estimated for the various conditions of power and gas mixtures employed, and the corrected value used in the numerical evaluations of the model.

The quantity we observe which is sensitive to populations is the net absorption of laser light by the gas. The amount of light removed from a beam passing a distance δx through a sample of SF_6 is given by

$$\delta I = \left(\frac{g_2}{g_1}N_0 - N^*\right)\frac{c^2\phi(\nu-\nu_0)}{8\pi\nu^2}A_{21}I_\nu\,\delta x. \quad (12)$$

We have found that this is not adequate to account for the observed saturation behavior, particularly the limiting non-zero absorbance at high powers. This is attributed to residual absorption by the excited molecules at the laser frequency, which can be incorporated into equation (12) with the additional term

$$\delta I = \left(\frac{g_2}{g_1}N_0 - (1-\Phi)N^*\right)\frac{c^2\phi(\nu-\nu_0)}{8\pi\nu^2}A_{21}I_\nu\,\delta x. \tag{12a}$$

Since the beam intensity (and therefore the excited-state populations) will not be uniform down the length of the cell, we divide the cell into M slabs of thickness δx, such that $\delta I = I_\nu(x+\delta x) - I_\nu(x)$ is much less than I. In each slab, the populations N_0, N^*, N' and N are computed from equations (4), (10) and (11) for the appropriate values of I_ν, using σ_v^2, σ_R^2 and β as parameters. Using these populations, δI is calculated from equation (12a), with Φ as a parameter. The total emerging beam is

$$I_\nu(l) = I_\nu(0) - \sum_{i=1}^{M}\delta I_i,$$

When $N^* \to 0$, we of course regain Beer's law,

$$I_\nu(l) = I_\nu(0)e^{-\varepsilon_\nu P(SF_6)l}.$$

3. EXPERIMENTAL

Two different sets of apparatus were used for measurements of absorbance versus power in the SF_6 samples. Figure 2 is a block diagram of the first apparatus. It consists of a 20 W CO_2–He–N_2 laser incident on a 10 cm attenuation cell filled with dimethyl ether. After exiting from the attenuation cell the laser beam passes through a 10 cm absorption cell filled with the SF_6 mixture being studied. Both cells were equipped with NaCl windows normal to the incident laser ray. The beam was then chopped at 51 Hz and directed to the entrance slit of a Perkin–Elmer 12 spectrometer. The spectrometer was equipped with a fast (time constant of 20 msec) thermopile detector.[5] The thermopile output was coupled to a Model 120 PAR lock-in amplifier via an impedance matching transformer and a PAR Model 112 preamplifier. The lock-in amplifier was referenced to

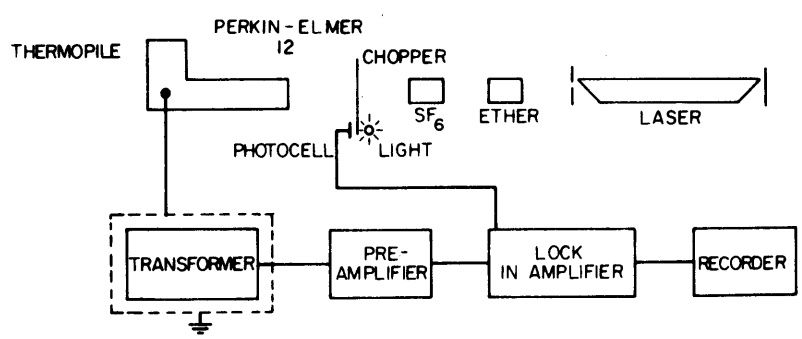

FIG. 2. Experimental setup for saturation measurements using a monochromator and a thermopile detector.

the chopping wheel by the periodic voltage generated by a photocell mounted opposed to a pea light but separated from it by the chopping wheel. The output of the lock-in was monitored by a Speedomax recorder after suitable attenuation by a Hewlett Packard Model 350BR attenuator set.

The second apparatus differed only in that a Coherent Radiation Laboratories Model 201 laser power meter and an impedance matching voltage divider replaced the chopper, spectrometer, lock-in amplifier and attenuator set.

Apparatus 1 was used to measure only the difference in power between the case when the absorption cell was in the laser path and when it was removed. (The residual power difference when the cell was completely evacuated served as a correction for losses due to the windows.) When difference measurements were being made with apparatus 1, the absolute power was determined with a water calorimeter. The power meter incorporated in apparatus 2 measured not only the power differences (cell in/cell out), but was also calibrated in absolute total power. A comparison of the power meter and the water calorimeter at 7·5 and 3·2 W agreed within experimental error. The beam spot diameter, required to convert power in watts to intensity in watts/cm^2, was estimated at 1–2 mm by imaging the unfocused beam on a piece of Transite and visual inspection of the resulting glowing spot.

A comparison of the data taken with the different apparatus showed agreement for a sample of pure SF_6. At high power apparatus 1 was, however, subject to much larger noise levels than apparatus 2, due to the wavelength discrimination of the spectrometer and the mode and frequency instability associated with the laser. Apparatus 1 monitored only one vibration–rotation transition while apparatus 2 averaged the output of the several lasing transitions. The results were the same for both sets of apparatus, since SF_6 has similar absorption coefficients for the lasing (P18)–P(24) transitions.[6] The data for pure SF_6 and SF_6–He mixtures was obtained mainly with apparatus 1. A data check on pure SF_6 and the data on all gas mixtures except SF_6–He was taken with apparatus 2.

Gas handling was accomplished with a standard glass and grease system equipped with a mercury diffusion pump and mechanical back-up pump. Pressures were measured with a dibutyl phthalate manometer which was monitored with a cathetometer, or with a McLeod gauge. All gases were supplied by the Matheson Co. Krypton and helium were research grade, guaranteed 99·995 per cent pure. Sulfur hexafluoride and ethane were guaranteed 98 and 99 per cent pure, respectively. SF_6, ethane and krypton were purified using a freeze, pump, thaw cycle repetitively. No precautions were taken to purify helium. SF_6–He mixtures were prepared by freezing the SF_6 in a sidearm of the absorption cell, adjusting the He pressure in the cell as desired, and then allowing the SF_6 to sublime. All other mixtures were prepared by expansion into calibrated volumes. The infrared absorption spectrum was monitored before and after adding the relaxing gas to check on the completeness of the mixing.

4. RESULTS AND DISCUSSION

The saturation effects observed in mixtures of SF_6 and helium are shown in Fig. 3. In order to interpret these in terms of the model discussed in Section 2, a knowledge of a number of parameters describing the absorption and relaxation properties of the saturating molecule is required.

(a) The absorption coefficient ε is determined by conventional absorption measurements at the laser frequency, which agree closely with the low-power limit of laser

transmission. We have used $\varepsilon(\nu_0) = 0{\cdot}46\,\mathrm{Torr}^{-1}\,\mathrm{cm}^{-1}$. This gives an Einstein coefficient $B_{12} = 1{\cdot}7 \times 10^7$ sec/g, with a corresponding radiative lifetime of 42 msec and transition dipole strength of 3×10^{-19} esu-cm.

(b) The fraction of molecules which absorb the laser radiation, β, determines the saturation threshold. The value of 0·003 assumed by PATEL[1] also gives good agreement with our experiments; any value in the range 0·001–0·005 gives nearly equivalent results. The equivalent homogeneous linewidth implied by this value is of the order of 10^8 Hz, which corresponds to estimates based on combined collision and saturation broadening (see Appendix 3).

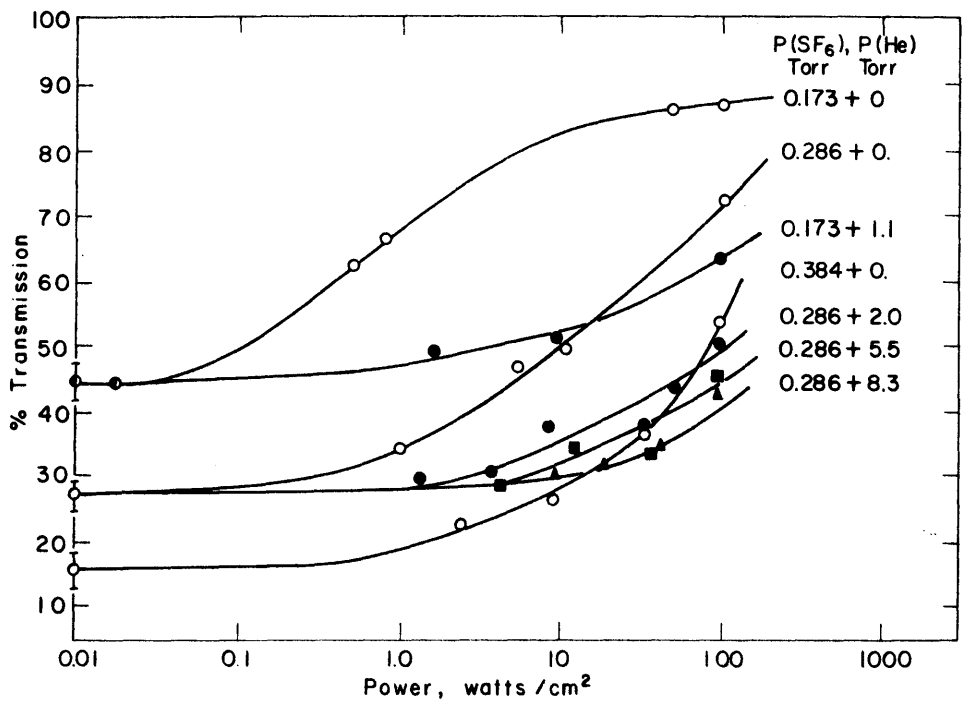

FIG. 3. Experimental saturation curves for pure SF_6 and SF_6–He mixtures.

(c) The residual fractional absorbance by excited molecules, Φ, is determined from the high-power limit of laser transmission to be $0{\cdot}3 \pm 0{\cdot}1$.

(d) The vibrationally inelastic cross sections, σ_v^2, for SF_6–SF_6 and He–SF_6 collisions make some contribution to the pressure dependence of the saturation, but are swamped by the rotationally inelastic processes. The best value for $\sigma_v^2(SF_6\text{–}SF_6)$ is of the order of 1 Å^2, which is about ten times larger than that for net vibrational deactivation of the lowest levels;[7] this can be interpreted as representing fast vibration–vibration transfer processes. The cross section for $\sigma_v^2(SF_6\text{–He})$ is not well determined from these experiments; we have used a value of 0·01 Å^2.

(e) The dominant relaxation pathway is rotational energy transfer. The value of $\sigma_R^2(SF_6\text{–}SF_6)$ which gives the best agreement lies in the range 15–50 Å^2, somewhat less

than that used by PATEL[8] to describe photon echo dephasing processes; it corresponds to rotational energy transfer on essentially every gas-kinetic collision. For $\sigma_R^2(SF_6\text{–He})$, we find 8 ± 3 Å^2, slightly smaller than the photon echo dephasing cross section,[8] but larger than the value estimated from the self-induced transparency experiments.[1]

In Figs. 4 through 10, predictions of the four-state model are compared with experiments on SF_6 and SF_6–He mixtures for the following range of parameters:

Set	β	Φ	$\sigma_v^2(SF_6)$	$\sigma_v^2(He)$	$\sigma_R^2(SF_6)$	$\sigma_R^2(He)$
1	0·01	0·3	0·1 Å^2	0·01 Å^2	105 Å^2	12 Å^2
2	0·004	0·3	0·1	0·01	105	12
3	0·002	0·3	0·1	0·01	105	12
4	0·004	0·3	1·0	0·01	105	12
5	0·004	0·3	1·0	0·01	50	12
6	0·004	0·3	1·0	0·01	15	12
7	0·004	0·3	1·0	0·01	15	6

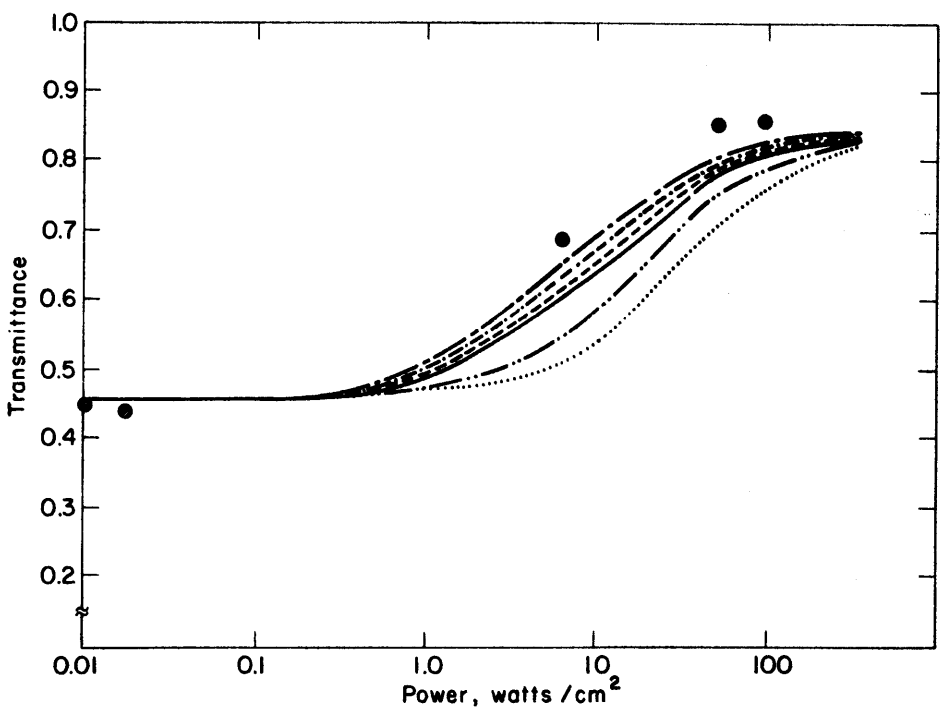

FIG. 4. Calculated saturation curves for $P(SF_6) = 0{\cdot}173$ Torr, $p(He) = 0$. Identification of curves with parameters [see table above] is as follows: (———), set 1; (- - - - -), set 2; (— — — — —), set 3; (· · · · ·), set 4; (— · · — · · — · · —), set 5; (- · - · - · - · - · -), set 6; (— — — — — — — — —), set 7.

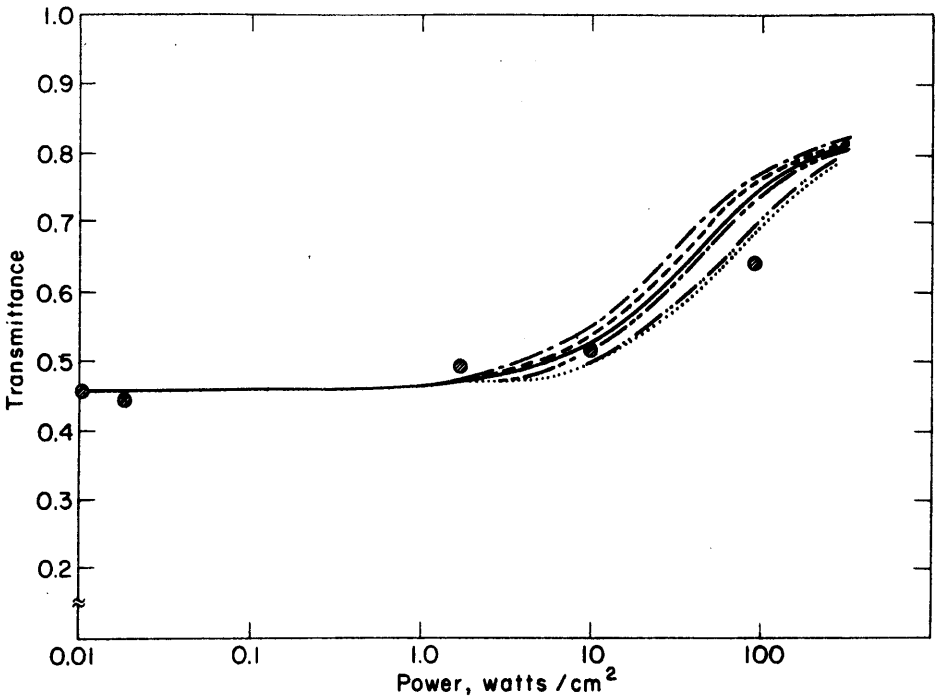

FIG. 5. Calculated saturation curves for $P(SF_6) = 0{\cdot}173$ Torr, p(He) = 1·1 Torr. For identification of curves, see caption to Fig. 4.

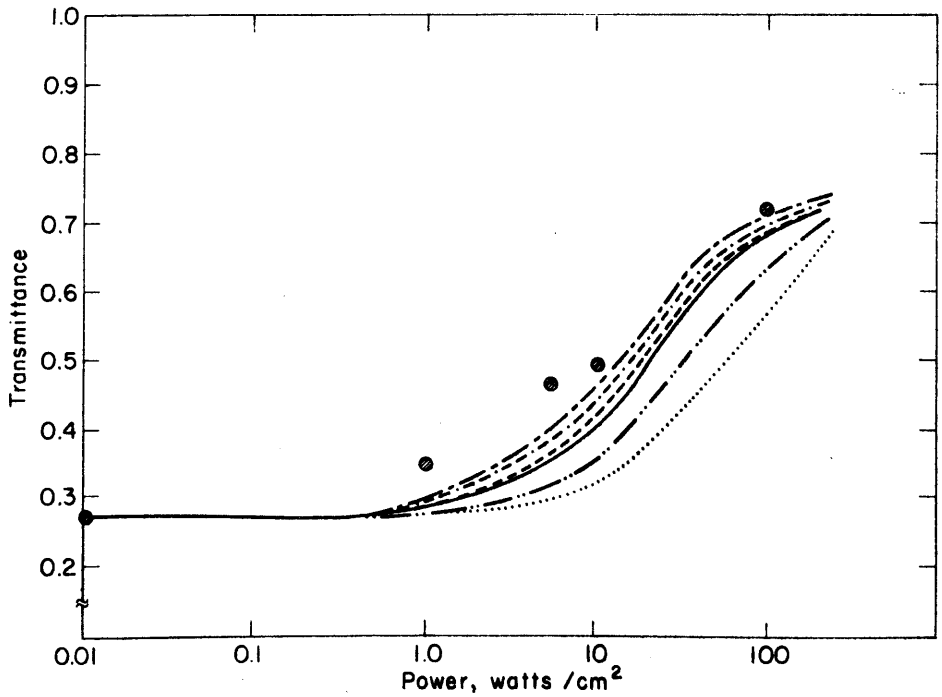

FIG. 6. Calculated saturation curves for $P(SF_6) = 0{\cdot}286$ Torr, p(He) = 0. See Fig. 4.

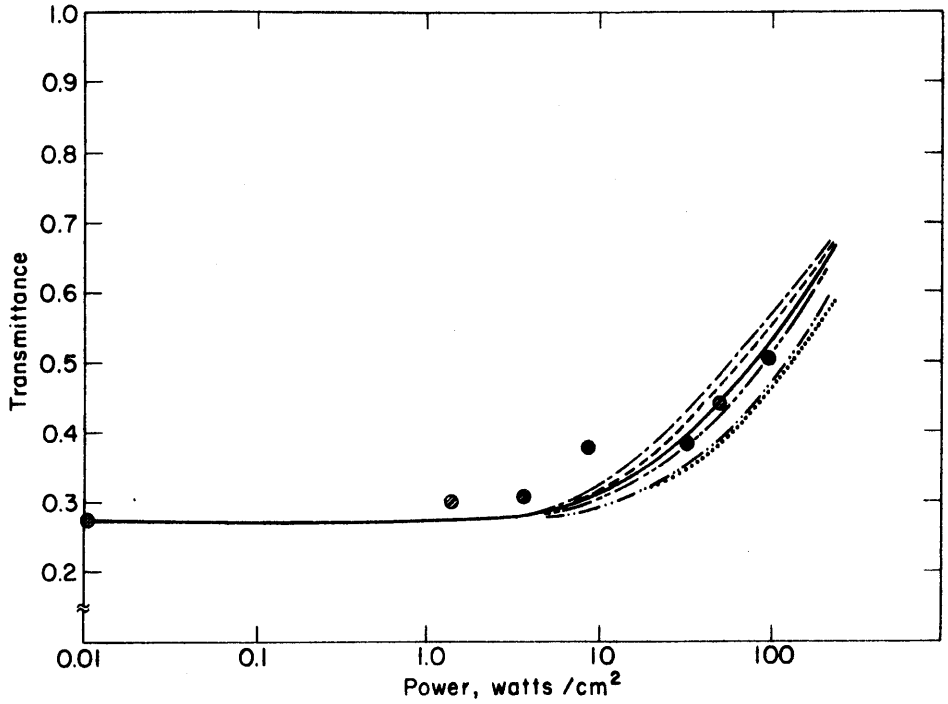

FIG. 7. Calculated saturation curves for $P(SF_6) = 0{\cdot}286$ Torr, $p(He) = 2{\cdot}0$ Torr. See Fig. 4.

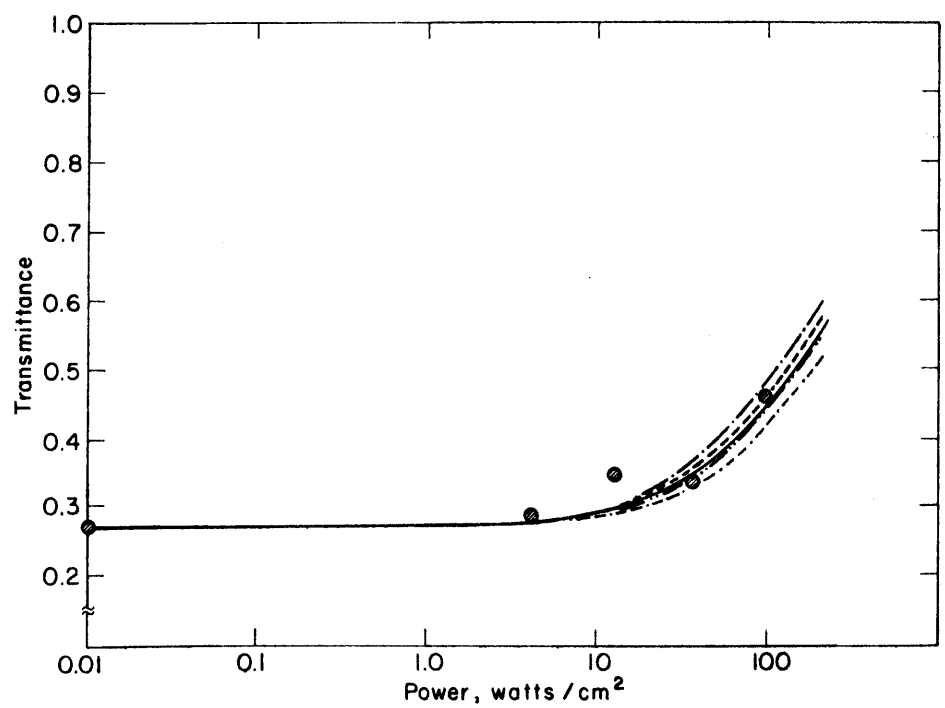

FIG. 8. Calculated saturation curves for $P(SF_6) = 0{\cdot}286$ Torr, $p(He) = 5{\cdot}5$ Torr. See Fig. 4.

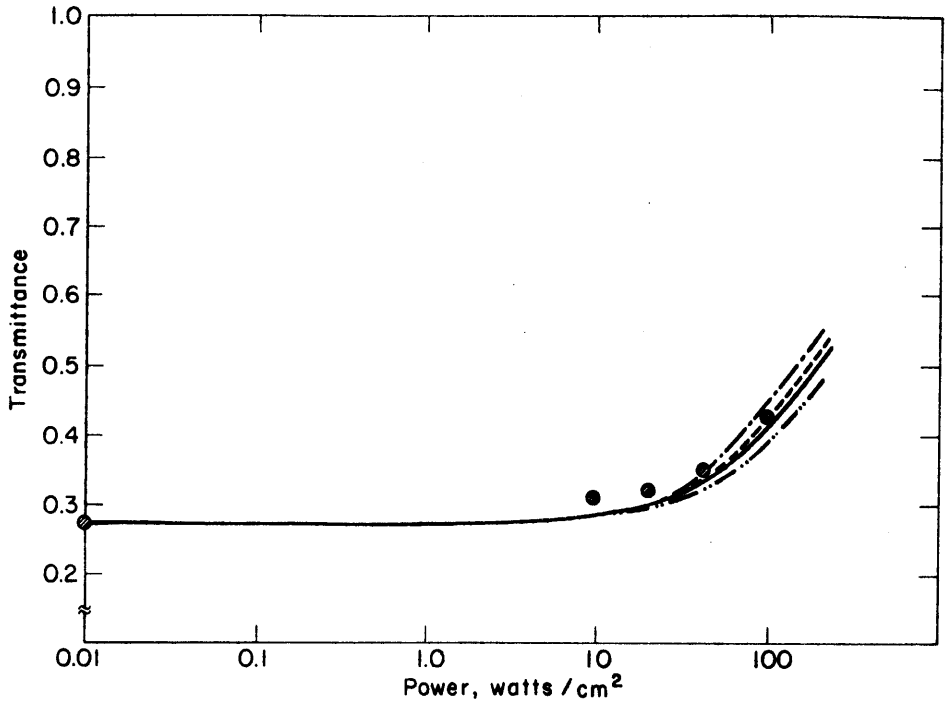

FIG. 9. Calculated saturation curves for $P(SF_6) = 0{\cdot}286$ Torr, p(He) = 8·3 Torr. See Fig. 4.

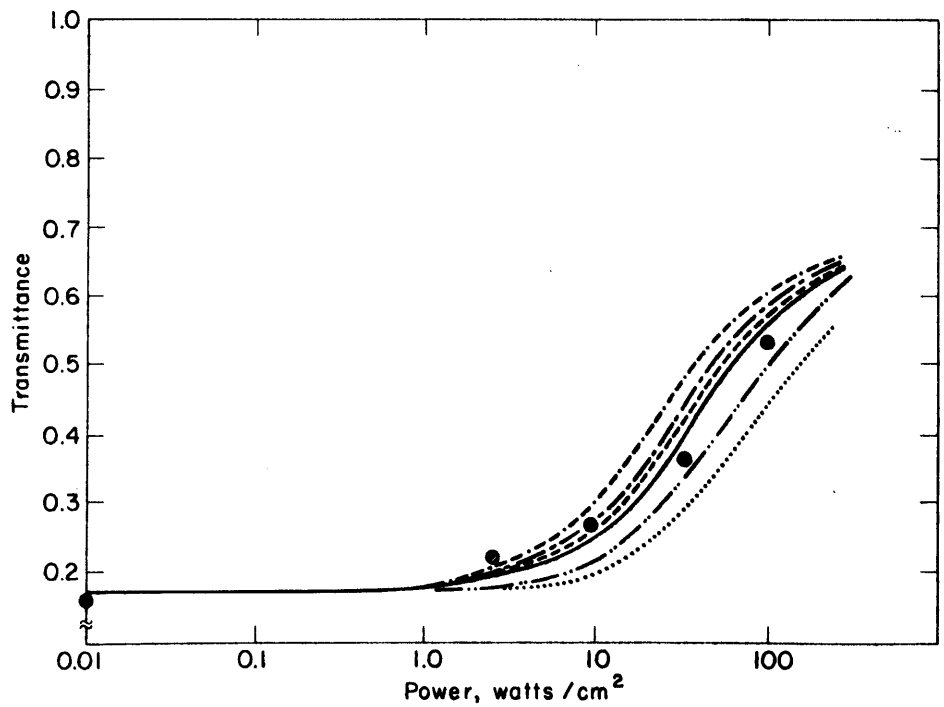

FIG. 10. Calculated saturation curves for $P(SF_6) = 0{\cdot}384$ Torr, p(He) = 0. See Fig. 4.

In these calculations, bulk heating effects are included (see Appendix 1), but radial diffusion effects are not (see Appendix 2).

The high-power limit of transmission in Fig. 4 permits an estimate of Φ to be made. The curves in Figs. 4, 6, and 10 were used to estimate best values for $\beta = 0{\cdot}004$, $\sigma_v^2(SF_6\text{–}SF_6) = 1{\cdot}0\,\text{Å}^2$, and $\sigma_R^2(SF_6\text{–}SF_6) = 15\text{–}50\,\text{Å}^2$. Using these values, the curves in Figs. 5, 7, 8, and 9 were used to establish $\sigma_R^2(SF_6\text{–}He)$ slightly larger than $6\,\text{Å}^2$. Other calculations indicated that $\sigma_v^2(SF_6\text{–}He)$ had to be small; the value of $0{\cdot}01\,\text{Å}^2$ is an order-of-magnitude estimate.

In order to distinguish clearly between relaxation and cooling effects, additional saturation experiments were carried out with ethane and krypton as added gases. The results, and corresponding calculations, are shown in Figs. 11 and 12. Although the thermal

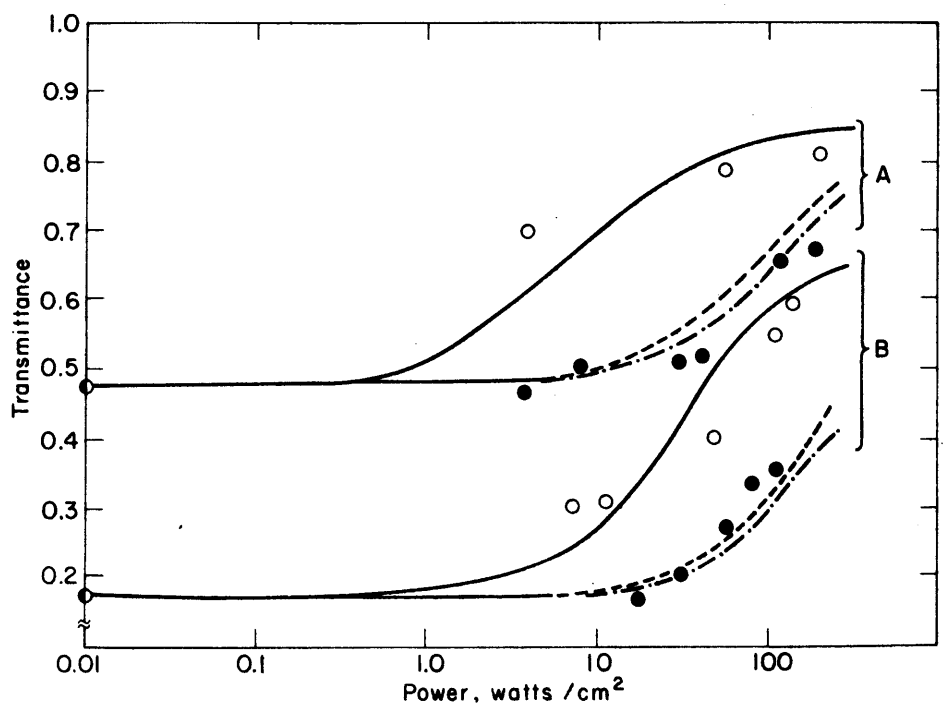

FIG. 11. Experimental points and calculated saturation curves for $SF_6\text{–}C_2H_6$ mixtures. ○ and (———), pure SF_6: ● and dashed curves, $SF_6 + C_2H_6$. Curve (- - - - - -) is calculated for $\sigma_v^2(SF_6\text{–}C_2H_6) = 0{\cdot}1\,\text{Å}^2$, while curve (—·—·—·—) is calculated for $\sigma_v^2(SF_6\text{–}C_2H_6) = 1{\cdot}0$ or $6{\cdot}0\,\text{Å}^2$. Set "A": $P(SF_6) = 0{\cdot}165$ Torr, $P(C_2H_6) = 2{\cdot}65$ Torr. Set "B": $P(SF_6) = 0{\cdot}39$ Torr, $P(C_2H_6) = 3{\cdot}4$ Torr.

conductivity coefficient of ethane is only twice that of krypton, ethane is nearly as effective as helium in reducing saturation. This can be attributed to large vibrational and/or rotational relaxation cross sections for $SF_6\text{–}C_2H_6$ collisions; the model does not distinguish clearly between the two. A large vibrationally inelastic cross section is to be expected for ethane, since it possesses an infrared-inactive vibration level ($993\,\text{cm}^{-1}$ (a_{1g})[9]) which is

near-resonant with the SF_6 level at 965 cm^{-1}. The values used in the calculations shown in Figs. 11 and 12 are:

$$\sigma_v^2(SF_6\text{–}C_2H_6) = 0{\cdot}1, 1, \text{and } 6\ \text{Å}^2 \quad \text{with} \quad \sigma_R^2(SF_6\text{–}C_2H_6) = 20\ \text{Å}^2$$
$$\sigma_v^2(SF_6\text{–}Kr) = 0{\cdot}01\ \text{Å}^2 \quad \text{with} \quad \sigma_R^2(SF_6\text{–}Kr) = 10\ \text{Å}^2.$$

The cross sections for $\sigma_v^2(SF_6\text{–}SF_6)$ and $\sigma_R^2(SF_6\text{–}SF_6)$ were set at 1·0 and 25 Å^2 in these particular calculations, and $\beta = 0{\cdot}003$ was used.

The response of the populations in each of the four states to varying levels of infrared power, for a typical set of conditions, is shown in Fig. 13. In pure SF_6 at low pressures, depletion of ground-state populations and corresponding enhancement of excited-state populations in the directly pumped levels begin to set in at $\sim$0·1 W/cm^2; these levels are

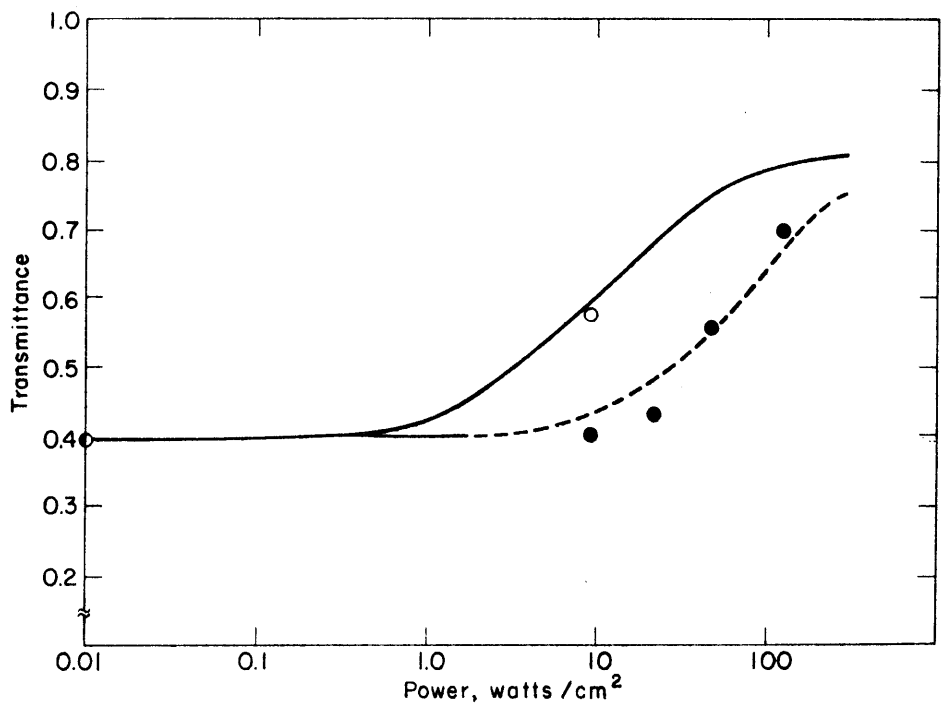

FIG. 12. Experimental points and calculated saturation curves for SF_6–Kr mixtures. ○ and (———), $P(SF_6)$ = 0·205 Torr, p(Kr) = 0; ● and (------), $P(SF_6)$ = 0·205 Torr, p(Kr) = 6·65 Torr.

essentially fully saturated at $\sim$50 W/cm^2. The states coupled by rotational relaxation approach equal population at the highest power level employed; their behavior is determined by the ratio of rotationally to vibrationally inelastic cross sections. When helium is added, approximately one order of magnitude higher power is required to reach the same level of saturation, as is reflected by the transmission curves in Fig. 3. In the low-power limit, the populations N^* and N' are determined by pure Boltzmann equilibrium. Note also that the ratios N^*/N' and N_0/N remain close to the equilibrium value β, at least at low powers. The decrease in all population densities at very high power is due to inclusion

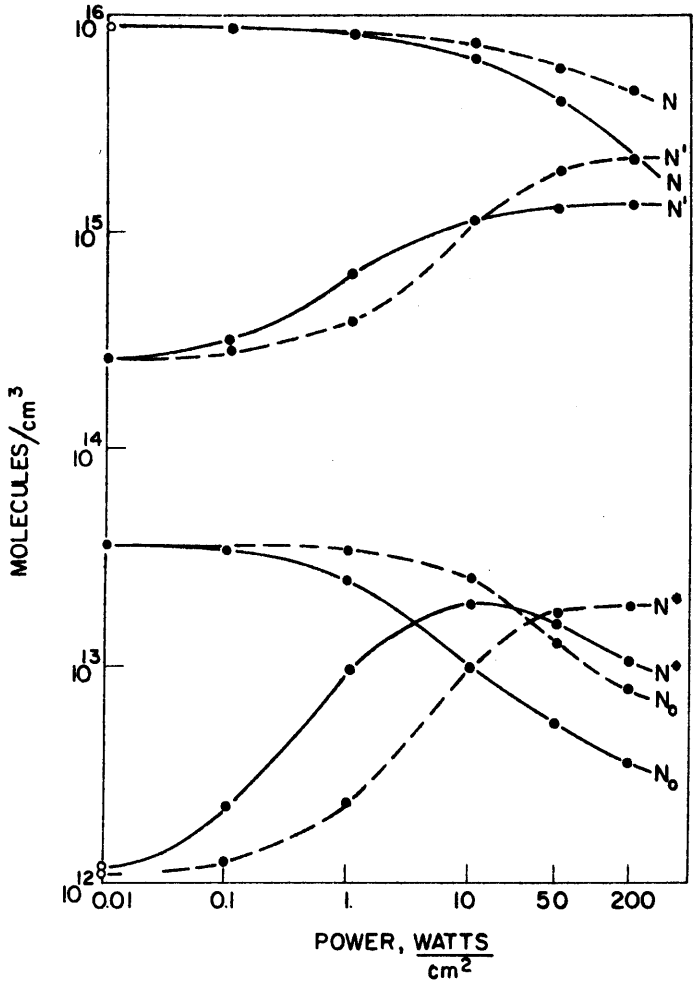

FIG. 13. Response of populations of various sublevels of SF_6 to infrared pumping. The curves were taken from calculations for $P(SF_6) = 0{\cdot}173$ Torr (solid curves), and for $P(SF_6) = 0{\cdot}173$ Torr with $p(He) = 1{\cdot}1$ Torr (dashed curves), using a set of relaxation parameters giving good agreement with the observed saturation.

of the bulk heating effect (Appendix 1) while assuming a constant pressure in the system.

These populations can be used to interpret the absorption intensity changes observed in infrared–microwave[10] and infrared–infrared[11] double resonance experiments; in each case, however, care must be taken to distinguish these effects from simple thermal population changes. The high population in the upper vibrational level is also consistent with the infrared fluorescence observed by RONN[12] although once more one must be careful to distinguish effects due to simple heating of the gas.

The time dependence of this population response to laser pumping is presently being investigated, and will be the subject of future publications. We may just comment at this point on the notable similarity of the values of β, inelastic cross sections, and saturation

threshold energy between this work and the self-induced transparency results of PATEL.[1] The latter deals with pulsed radiation, and was interpreted as a coherent optical effect using the model of MCCALL and HAHN;[2] but one must consider the possibility that this effect may be wholly interpretable in terms of a quasi-steady-state kinetic saturation model similar to the one proposed here. At the high power levels, the directly pumped levels have attained their new equilibrium values in times of the order of 10^{-8} sec, while the duration of the pulses used by Patel was of the order of 10^{-6} sec.

This model, of course, would still not explain additional effects, such as long pulse delays (as distinct from simple pulse narrowing) and the photon echo.[8]

The analysis employed in the evaluation of this model is very similar to that used in studies of saturable dye bleaching;[13,14] the behavior of SF_6 in these terms is that of "steady-state bleaching" rather than "hole-burning". One would expect "bleaching" behavior in all systems where rotational relaxation is more rapid than vibrational relaxation.

The considerations discussed here are not limited to laser sources, of course, but are applicable to any source having sufficiently high radiation density in a sufficiently narrow bandwidth. Since, however, the saturation threshold of ~ 1 W/cm^2 at 10·6 μ in a bandwidth of 10^8 Hz corresponds to a black-body temperature of $\sim 10^9$ °K, these effects are of practical importance only for lasers. They should be considered operative in such experiments as long-distance atmospheric concentration measurements by pulse attenuation, since peak pulse powers may be of the order of kilowatts/cm^2. Considerable deviations from Lambert's law propagation may also be found, as shown by the example in Fig. 14.

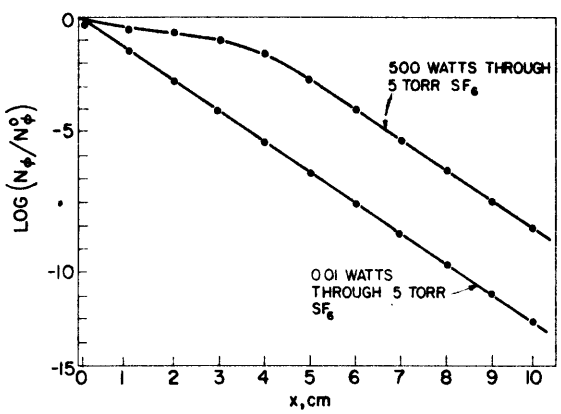

FIG. 14. Transmission curves for high- and low-power laser beams through 5 Torr of SF_6, showing deviations from Lambert's law. N_ϕ is the number of photons at distance x; N_ϕ^0 is $N_\phi(x = 0)$.

Acknowledgements—We would like to thank Mr. A. NOWAK for help with the experimental portion of this work and Mr. E. WEITZ for help with computer programming of the model. We have had helpful discussions with Profs. A. JAVAN, J. ROSS, and A. SZÖKE. This work was supported by a grant (GP-6504) from the National Science Foundation.

REFERENCES

1. C. K. N. PATEL and R. E. SLUSHER, *Phys. Rev. Letters* **19**, 1019 (1967).
2. S. L. MCCALL and E. L. HAHN, *Phys. Rev. Letters* **18**, 908 (1967).
3. R. G. GORDON, *J. Chem. Phys.* **46**, 4399 (1967).
4. A. YARIV, *Quantum Electronics*, p. 202, Wiley, New York (1968).

5. For a report on the characteristics of these atmospheric thermopiles see Bureau of Ships, Code 853, Contract numbers: NObsr 39069; NObs 25391, Task VIII; NObsr 52497; and NObsr 64540.
6. C. B. MOORE, private communication.
7. B. STEVENS, *Collisional Activation in Gases*, p. 221, Pergamon Press, Oxford (1967).
8. C. K. N. PATEL and R. E. SLUSHER, *Phys. Rev. Letters* **20**, 1087 (1968).
9. G. HERZBERG, *Infrared and Raman Spectra of Polyatomic Molecules*, p. 344, D. van Nostrand, Princeton, N.J. (1945).
10. A. M. RONN and D. R. LIDE, JR., *J. Chem. Phys.* **47**, 3669 (1967).
11. D. SUTTON, I. BURAK, A. V. NOWAK and J. I. STEINFELD, Paper 01, 23rd Symposium on Molecular Structure and Spectroscopy, Columbus, Ohio (1968).
12. A. M. RONN, *J. Chem. Phys.* **48**, 511 (1968).
13. C. R. GIULIANO and L. D. HESS, *I.E.E.E. J. Quant. Electr.* **QE-4**, 358 (1967).
14. M. HERCHER, W. CHU and D. L. STOCKMAN, *I.E.E.E. J. Quant. Electr.* (in press).

APPENDIX 1—BULK HEATING EFFECTS

In calculating the temperature distribution in the cell the following assumptions were made:

(1) A steady temperature distribution is established in the cell.

(2) Since the absorption cell is cylindrical and the laser beam density has a cylindrical symmetry in the cell the temperature distribution has the form:

$$T = T(r, z)$$

where r, z and ϕ are the cylindrical coordinates.

(3) As a further approximation we assume that the laser light is absorbed uniformly along the z axis. Since the heating effect is important only at high laser intensities where we observe saturation effects, this assumption is justified. If we neglect the heat conduction to the end windows of the cell T becomes independent of z. The temperature distribution in a uniformly heated infinitely long cylinder is given by[a]

$$T(r) = T(a) + \frac{1}{k}\left\{\log\frac{a}{r}\int_0^r q(r')r'\,\mathrm{d}r' + \int_r^a \log\left(\frac{a}{r'}\right) q(r')\,\mathrm{d}r'\right\} \tag{A1.1}$$

where a is the radius of the cell, $q(r)$ is the heating rate per unit volume, and k is the coefficient of thermal conductivity. We have taken the following form for $q(r)$:

$$q(r) = \begin{matrix} q_0 \\ 0 \end{matrix}\begin{cases} \text{for} \quad 0 \le r' \le b \\ \text{for} \quad b \le r' \le a \end{cases}$$

where b is the radius of the beam and q_0 is a constant.

This approximation involves the assumption that all the relaxation effects are taking place in the region of the beam. Neglecting spontaneous emission, the rate of heating in the steady state is equal to the rate of energy absorption. Thus the value of q_0 may be calculated from the experimental rate of energy absorption W_{abs}:

$$q_0 = \frac{W_{abs}}{\pi b^2 L}$$

where L is the length of the cell.

Equation (A1.1) may be simply integrated to give the temperature distribution

$$T(r) = \begin{cases} \dfrac{q_0 b^2}{2k} \ln\left(\dfrac{a}{r}\right), & b \le r < a \\ \dfrac{q_0}{k}\left[\dfrac{b^2}{2} \ln\left(\dfrac{a}{b}\right) - \dfrac{1}{4}(b^2 - r^2)\right], & 0 \le r < b \end{cases} \tag{A1.2}$$

if we take k as independent of temperature. This is not strictly true,[b] but including the explicit temperature dependence makes the integration (A1.1) extremely difficult; therefore, we have calculated upper limits for the temperature by using k for $T = 25°C$, since k increases as $T^{1/2}$. The thermal conductivities for pure SF_6 and SF_6–He mixtures were calculated by the procedures of HIRSCHFELDER, CURTISS and BIRD,[b] using the data summarized in the following table.

	σ, collision diameter[b]	ε/k, potential well depth[b]	$\tilde{C}_v$, heat capacity per mole[c,d]	k, thermal conductivity
SF_6	5·5 Å	20·1°K	$22 \frac{\text{cal}}{\text{mole-deg}}$	$23{\cdot}4 \times 10^{-6} \frac{\text{cal}}{\text{deg-cm-sec}}$
He	2·6	10·2	3	340
C_2H_6	4·4	230	9·5	45
Kr	3·6	190	3	20

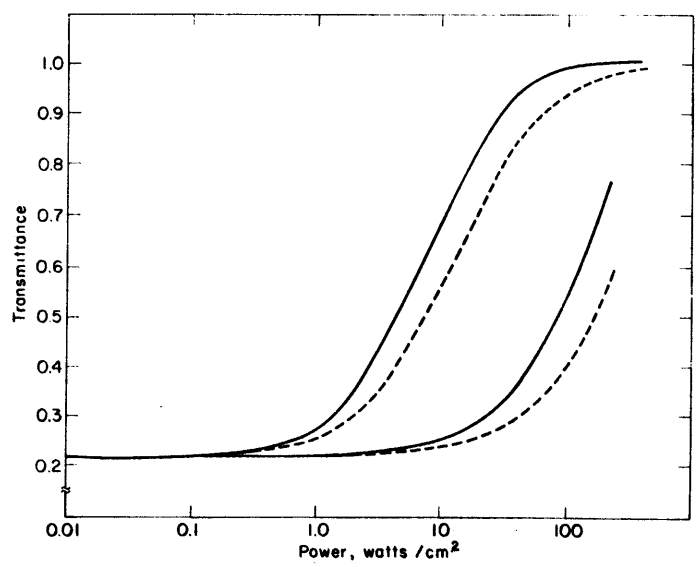

FIG. 15. Effect of heating on calculated saturation curves. The solid curve is for $T = 298°K$ at all powers, while the dashed curve uses the temperature appropriate to each power level, as estimated in this Appendix. These are taken from an earlier calculation, in which $\Phi = 0$ was used.

For SF_6–C_2H_6 and SF_6–Kr mixtures, the thermal conductivity was taken to be the same as in pure SF_6.

Using $a = 2$ cm, $b = 0{\cdot}1$ cm, $L = 10$ cm, and $W_{abs} = 1$ W, we find temperatures at the center of the laser beam of the order of 500°C in pure SF_6, and 76°C in a 10 per cent SF_6–90 per cent He mixture. These estimates are in agreement with some rough measurements carried out by irradiating a cell incorporating thermistors sealed through the cell body at several different values of r. It should be pointed out that this high internal temperature is obtained even while $T(a)$, the temperature of the boundary of the cell, is maintained at 25°C. These temperatures have been taken into account in the calculations described in Section 2.

REFERENCES

a. P. M. MORSE and H. FESHBACH, *Methods of Theoretical Physics*, p. 1190. McGraw-Hill, New York (1953).
b. J. O. HIRSCHFELDER, C. F. CURTISS and R. B. BIRD, *Molecular Theory of Gases*, p. 533. John Wiley, New York (1954).
c. *Handbook of Chemistry and Physics*, 39th ed., p. 2108, Chemical Rubber Publishing Co., Cleveland (1958).
d. *Landolt–Bornstein Physikalisch–Chemische Tabellen*, Springer-Verlag, Berlin (1923 *et seq*).

APPENDIX 2—RADIAL DIFFUSION EFFECTS

The considerable temperature and concentration gradients set up by the passage of a small-diameter laser beam through bulk gas may be expected to give rise to diffusion processes. The importance of these processes to saturation behavior may be estimated from Fick's first law of diffusion,

$$\frac{\partial N}{\partial t} = -D\frac{\partial N'}{\partial x},$$

where $\partial N/\partial t$ is the number of molecules crossing the area of the boundary per second. N' is the number density of these same molecules. The concentration gradient may be estimated by assuming that the radiation-induced population disequilibria, $N^*(0)-N^*(a)$ and $N_0(0)-N_0(a)$, fall to one-half their value in the space of one mean free path; the diffusion coefficient D is estimated as 50 cm^2/sec for SF_6 at *ca.* 0·7 Torr pressure. This gives a total flux of 9×10^{16} excited molecules leaving the pumped region per second. By comparison, the laser pumping rate (at 100 W/cm^2) is of the order of $1{\cdot}5\times10^{21}$ sec^{-1}; the total rotational relaxation rate is 5×10^{18} sec^{-1}, and vibrational relaxation is 5×10^{16} sec^{-1}, so that diffusion is comparable to vibrational relaxation in depopulation effectiveness. We have already seen that saturation behavior is relatively insensitive to assumed vibrational deactivation efficiencies.

Diffusion can be included explicitly in the four-state model by using Fick's second law of diffusion,

$$\frac{\partial N'}{\partial t} = D\nabla^2 N'.$$

A reasonable form for the concentration of various species outside the pumped region of the gas which includes collisional relaxation effects and conserves total density is, for $r \geq b$,

$$N_i'(r) = (\Delta N_i')e^{-r^2/\lambda^2 Z_i} + N_i'(a), \tag{A2.1}$$

where $\Delta N_i' = N_i'(0)-N_i'(a)$, λ is the mean free path, and Z_i is the number of gas-kinetic

collisions required to relax either rotational or vibrational levels, as appropriate. By applying ∇^2 in cylindrical coordinates to equation (A2.1) we may estimate the magnitude of $\nabla^2 N_i'$, and obtain

$$\frac{\partial N_i'}{\partial t} \simeq -D(\Delta N_i')\frac{6}{\lambda^2 Z}e^{-b^2/\lambda^2 Z}$$

at the boundary of the pumped region. These terms can then be added to the steady-state equations in N_i, and the model re-evaluated. This was done, with no resulting perceptible change in the steady-state concentration of the various species, in accord with the previous argument. It is therefore concluded that radial diffusion plays a minor role in this system, and may be neglected.

APPENDIX 3—HOMOGENEOUS LINEWIDTH AND IDENTIFICATION OF SATURATED TRANSITIONS

One of the key parameters in the description of a saturated system is the fraction of the total number of molecules present which can absorb the radiation, defined as

$$\beta = N_0/N.$$

From the definition of the absorption coefficient in terms of the lineshape $\phi(\nu-\nu_0)$, this quantity also appears as

$$\beta = \delta\nu/\Delta\nu, \tag{A3.1}$$

where $\Delta\nu$ is the total absorption band width and $\delta\nu$ is the effective absorber bandwidth. Since the laser bandwidth itself is negligible, of the order of a few Hz,[4] the main contributor to $\delta\nu$ is the homogeneous linewidth of the transition.

The magnitude of this linewidth can be estimated from lifetime considerations. At low powers, we have

$$\begin{aligned}\delta\nu_H \approx \langle\tau\rangle^{-1} &= \delta\nu_L + \delta\nu_N \\ &= \frac{1}{\pi}(Z_{\text{vib}} + Z_{\text{rot}}) + \frac{1}{2\pi\tau_{\text{rad}}}.\end{aligned}$$

When intense radiation is applied, the lifetime is further shortened and saturation broadening occurs, giving

$$\delta\nu_H \approx \delta\nu_L + \delta\nu_N + \frac{I_\nu B_{12}}{\delta\nu_H}.$$

Since the rate of pumping is itself dependent on the linewidth, a quadratic equation for $\delta\nu_H$ is obtained, which can be solved to give

$$\delta\nu_H = \tfrac{1}{2}\{(\delta\nu_L + \delta\nu_N) + [(\delta\nu_L + \delta\nu_N)^2 + 4I_\nu B_{01}/\pi]^{1/2}\}.$$

The natural linewidth $\delta\nu_N$ is negligible due to the long radiative lifetime; at the gas pressures and infrared intensities used in these experiments, values for $\delta\nu_H$ in the range $(0{\cdot}5\text{–}1{\cdot}5)\times 10^8$ Hz are obtained. This is greater than the Doppler width in this system, which suggests that molecules in states N_0 and N differ in rotational, rather than translational, states.

Since the total band width $\Delta\nu$ is of the order of $7\,\text{cm}^{-1}$, and the best value of β is

approximately 0·003, equation (A3.1) implies a $\delta\nu$ of about 6×10^8 Hz. That this is several times larger than $\delta\nu_H$ implies that several different transitions in the absorption band, each with linewidth $\delta\nu_H$, are being pumped simultaneously.

The question of which lines these are cannot be answered at the present time. The vibration itself is assigned f_{1u}, with $g_1 = 1$ and $g_2 = 3$. The absorption band is not resolved, however,[a] and thus must be rotationally analyzed by contour fitting, which is being carried out at this time. We may also note that essentially the same absorbance at a given wavelength was observed in pure SF_6 and mixed samples, using either a weak or a full-strength laser beam or the continuous source in a Perkin–Elmer 337B spectrometer. This shows that the SF_6 presents a very nearly continuous, structureless absorbance contour to the radiation. We can say, though, that the pumped lines cannot be very low-J transitions, since the Boltzmann factor for $J = 0$ or 1 is of the order of 10^{-5}, much smaller than β. The fractional populations in levels with $J \approx J_{max}$ $(= 47)$ is of the order of β, at room temperature. The most likely situation is that a combination of several medium-J transitions in SF_6 are pumped by the CO_2 laser.

REFERENCE

a. H. BRUNET and M. PEREZ, private communication.

Appendix 3

INFRARED DOUBLE RESONANCE IN SULFUR HEXAFLUORIDE

J. I. Steinfeld, I. Burak, D. G. Sutton, and A. V. Nowak

Journal of Chemical Physics 52, 5421 (1970)

Reprinted from THE JOURNAL OF CHEMICAL PHYSICS, Vol. 52, No. 10, 5421-5434, 15 May 1970
Printed in U. S. A.

Infrared Double Resonance in Sulfur Hexafluoride

J. I. STEINFELD,* I. BURAK, D. G. SUTTON,† AND A. V. NOWAK‡
Department of Chemistry, Massachusetts Institute of Technology, Cambridge, Massachusetts 02139
(Received 24 November 1969)

The relaxation of sulfur hexafluoride has been monitored by observation of infrared absorption intensities following passage of an infrared laser pulse through the gas. The laser pulse saturates a small number of rotational lines in the $\nu_3 \leftarrow 0$ transition of SF_6 at 944 cm^{-1}, producing a transient "hole" in the absorption spectrum at that frequency. This hole is filled in very rapidly by rotational relaxation processes. The specific vibrational excitation is, at essentially the same time, transformed into a vibrational temperature in excess of the gas's translational temperature, by means of very efficient vibration $\leftrightarrow$ vibration energy transfer collisions. The energy released in this step also heats the gas translationally by the order of 25°K. The vibrational temperature then relaxes to the translational temperature by a binary collision process, with $p\tau = (122 \pm 8)$ μsec·torr in pure SF_6. The rate-controlling step is concluded to be the vibration$\rightarrow$translation relaxation of the ν_6 level at 363 cm^{-1}. The mean efficiency per collision of this step has been measured for He, Ne, Ar, Kr, C_2H_6, $(CH_3)_2O$, CH_4, CH_3Br, CHF_2Cl, H_2O, H_2, N_2, and Cl_2, in addition to SF_6 itself. A transient absorption spectrum arising from the vibrationally hot SF_6 is also given. The slowest relaxation observed in the system is the bulk cooling of the translational temperature of the gas, which occurs in the order of milliseconds under typical experimental conditions. The dominant mechanism for this relaxation appears to be cooling by thermal conduction.

I. INTRODUCTION

The use of time-resolved spectroscopic behavior of molecules has become an important tool in the investigation of energy transfer and relaxation processes. If we ignore, for the moment, the domain of nuclear and electronic Zeeman spectroscopy and the classic photochemical technique of flash photolysis, we may enumerate the following experimental versions of this general approach:

(i) microwave double resonance,[1] in which intense microwave power at some absorption line is modulated, producing a change in the rotational distribution $f(J)$, which is observed as a change in absorption strength, ΔI, at some other line;

(ii) infrared-microwave double resonance,[2,3] in which the modulated pumping is carried out at infrared frequencies, and the ensuing population changes are monitored by microwave absorption;

(iii) infrared fluorescence,[4] in which a pulse of infrared radiation changes the vibrational distribution $f(v)$, and emission from the excess population of vibrationally excited molecules is monitored as a function of time;

(iv) infrared double resonance, in which the changes in vibration–rotation distributions $f(v, J)$ produced by the infrared pulse are monitored as an infrared absorption intensity. This method has been used to probe CO_2 itself,[5] using CO_2 lasers as pumping and monitoring sources. Its more general applicability has been demonstrated by recent experiments[6] on relaxation processes in SF_6. In this paper, we present complete details of these experiments and our conclusions regarding the relaxation processes occurring in this system.

The choice of SF_6 as a model system is attributable primarily to its intense infrared absorption at the 944-cm^{-1} laser frequency and the ease of handling this material. These factors are doubtless what has led to over a dozen different studies of the effects of CO_2 laser radiation on SF_6, which we summarize below:

(i) self Q switching of a CO_2 laser by incorporating a cell containing SF_6 into the laser cavity[7];

(ii) passive mode locking of a CO_2 laser, by the same technique[8];

(iii) self-induced transparency of SF_6 to CO_2 laser pulses[9];

(iv) infrared photon echo in SF_6[10,11];

(v) transmission of CO_2 laser pulses through SF_6[12,13];

(vi) saturation of infrared absorption in SF_6 by a cw CO_2 laser beam[14–16];

(vii) fluorescence of SF_6 excited by a CO_2 laser pulse[16–18];

(viii) adiabatic inversion of vibrational level populations[19];

(ix) transient nutation impressed onto CO_2 laser pulses by SF_6,[20] although the origin of this effect has been questioned[21];

(x) use of SF_6 in a CO_2 laser cavity to tune the output wavelength[22];

(xi) cross saturation of laser signals by SF_6[23];

(xii) cavity dumping by saturable resonators.[23a]

A thorough study of the relaxation behavior of SF_6 is thus required, if for no other reason than to provide an interpretation to all these (sometimes conflicting) experimental studies.

II. EXPERIMENTAL

A. Apparatus

The basic experimental method involves superimposing a pulsed infrared pumping beam with a stable, monochromatic cw monitoring beam. This was accomplished by the apparatus shown in Fig. 1.

The infrared pulses are produced by a 2-m CO_2 laser,

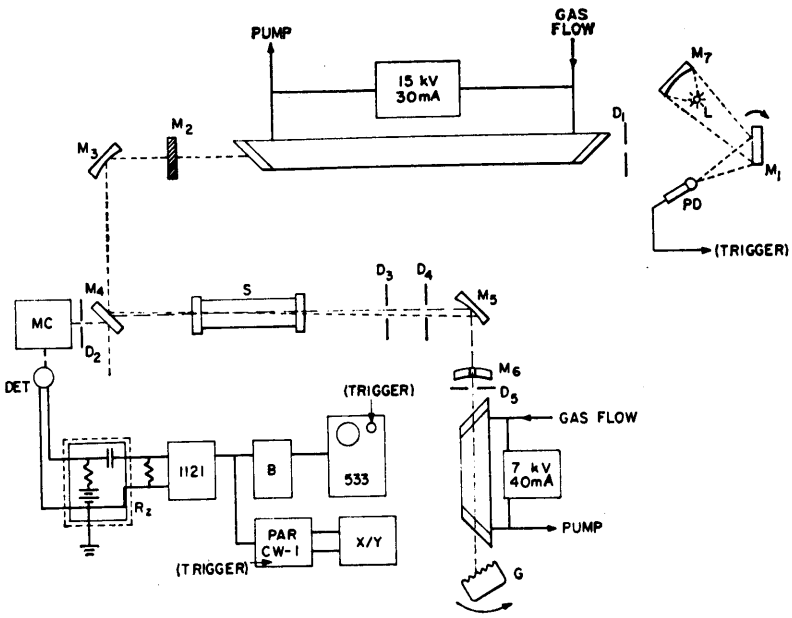

FIG. 1. Block diagram of infrared double resonance apparatus.

operating on a 15-kV, 30-mA discharge through a flowing mixture of 1.5 torr N_2, 0.5 torr CO_2, and $\approx$8 torr He. The laser is Q switched by a rotating mirror M_1, producing a 10-kW, 0.3-μsec pulse every 9 msec. The diaphragm D_1 is used to control the pulse width—when D_1 is fully opened, a train of pulses lasting 1–2 μsec is produced, which is most effective in producing excess vibrational population. A small tungsten lamp, L, is focussed by M_7 and reflected off M_1 to a photodiode PD (RCA 845TL), which gives a triggering pulse to the detection electronics. The triggering is stable to 0.1 μsec because of the small size of the photodiode. The Q-switched pulses are coupled out of the cavity through a germanium mirror, M_2, which reflects about 60% at 10.6 μ from the uncoated inner surface.

The monitoring beam is produced by a 1-m CO_2 laser, operating at 7 kV and 40 mA through a gas mixture similar to that used in the Q-switched laser. A current regulator is placed in series with the plasma tube and high voltage supply in order to eliminate instability and ripple arising in the power source. Wavelengths are selected by a grating (Ealing 26-1057, 1500 lines/in.) in the cavity; oscillation can be obtained on the $P(8)$ through $P(34)$ lines of the $00^01 \rightarrow 10^00$ transition, at 954–931 cm^{-1}, respectively, on several R-branch lines near 975 cm^{-1}, and on several lines of the $00^01 \rightarrow 02^00$ transition near 1045 cm^{-1}. The laser has also been operated with a flowing N_2O discharge, using a gold-coated mirror in place of the grating; several lines near 920 cm^{-1} were obtained. The diaphragm D_5 serves both to limit the output to a single CO_2 rotational transition and to the TEM_{00} cavity mode, which is important for the stability of the output power level. Power is coupled out through a 1/8-in. diam. hole in mirror M_6. Approximately 0.3 W are obtained with the grating in place; higher power levels than this are not desired, in order to avoid saturation effects in the SF_6 sample.[14]

The superposition of the two beams is accomplished by the remaining optical elements. The pulsed beam is deflected by a weakly focusing gold-coated mirror M_3 onto a germanium beamsplitter, M_4. Both these elements are gimbal mounted, with micrometer adjustments. The monitoring beam is deflected by mirror M_5, through diaphragms D_4 and D_3. The two beams are made to coincide in the volume of the sample cell S; the cell itself, which has sodium chloride end windows, is tilted at an angle to eliminate back reflections of the infrared pulse. The monitoring beam passes through the beamsplitter (the rear side of which is antireflection coated), through the diaphragm D_2, and into the monochromator MC.

Optimum results were obtained by making the beams not completely coaxial between M_4 and M_5, but crossing at a slight angle as shown. It is well known[24,25] that shining one CO_2 laser beam into the active discharge of a second laser changes the gain, and therefore the output intensity, of the latter. Any such effects would appear as spurious double resonance signals. The presence of diaphragms D_3 and D_4 prevented most of the pulsed beam from reaching the cw laser and thus eliminated nearly all such unwanted effects.

The double resonance signal, which is carried on the cw laser beam, passes through the monochromator (Bausch & Lomb 250-mm, with 30 line/mm grating) to the liquid nitrogen-cooled gold-doped germanium detector. Both a Raytheon QKN1568 and a Santa Barbara Research Corporation detector were used interchangeably, with equivalent results. The detector is

capacitor-coupled (0.1 μF) to a Tektronix 1121 preamplifier (60-dB gain, 10 MHz bandwidth); sometimes two amplifiers in series were used. When the input impedance of the amplifier itself was used as a load (1 MΩ) instrumental time constants of the order of 10 μsec were obtained, as determined by inspection of the reflected Q-switched pulse. This was reduced to less than 1 μsec by addition of a 2 kΩ resistive load, R_Z, in parallel. The amplified signal was then sent either to a Tektronix 533 oscilloscope with type B preamplifier, for photographing, or to a PAR Model CW-1 boxcar integrator for signal averaging. Both devices were triggered by the signal from photodiode PD.

B. Sample Handling and Experimental Procedure

Gas handling was accomplished with a standard glass and grease system equipped with a mercury diffusion pump and a mechanical backup pump. Pressures were measured with a mercury or dibutyl phthalate manometer monitored with a cathetometer, or with a McLeod gauge. Gases were supplied by the following companies —guaranteed percent purities are included in parentheses:

Matheson Company: SF_6 (98%), C_2H_6 (99%), $(CH_3)_2O$ (99%), CH_4 (99.97%), CH_3Br (99.5%), CHF_2Cl (99.9%), H_2 (99.95%), N_2 (99.987%), Cl_2 (99.5%), He (99.995%);

Airco: Ne (99.9995%), Ar (99.9995%), Kr (99.995%);

Lif-O-Gen Incorporated: SF_6(99.9%).

Water was taken from the distilled water line, pumped to eliminate air, then put through the freeze–pump–thaw cycle repetitively. SF_6, $(CH_3)_2O$, and Cl_2 were also put through the freeze–pump–thaw cycle before use. No purification procedures were used on the other gases. Gas mixtures were prepared by freezing the SF_6 in a sidearm of the absorption sell, isolating the sidearm adjusting the pressure of the other component in the cell and then allowing both components to mix.

III. TRANSIENT ABSORPTION EFFECTS

As previously reported, three different sorts of absorption changes may be seen in SF_6, depending on the relation between the frequencies of the pumping and monitoring radiation.

(i) When the monitoring laser line is either the $P(18)$ [945.9 cm^{-1}], $P(20)$ [944.2 cm^{-1}], or $P(22)$ [942.4 cm^{-1}], a sharp decrease in absorption appears, which appears and disappears at essentially the same time as the laser pulse itself; this is shown in Fig. 2(a). These frequencies are those at which the Q-switched laser has its strongest output; therefore, this effect is interpreted as burning a "hole" into the absorption spectrum by local saturation of those rotational fine-structure levels which are directly pumped by the laser. When the system is properly aligned, the hole completely disappears when the SF_6 is pumped or frozen out

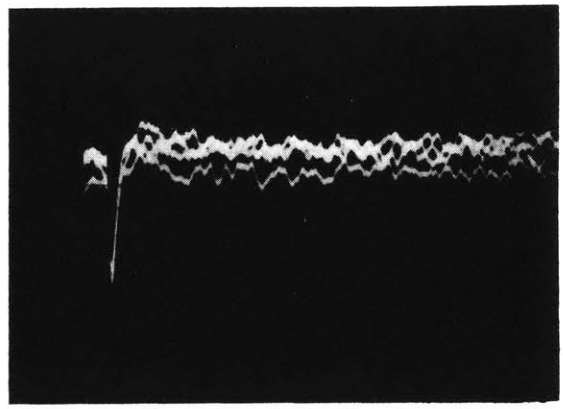

(a)

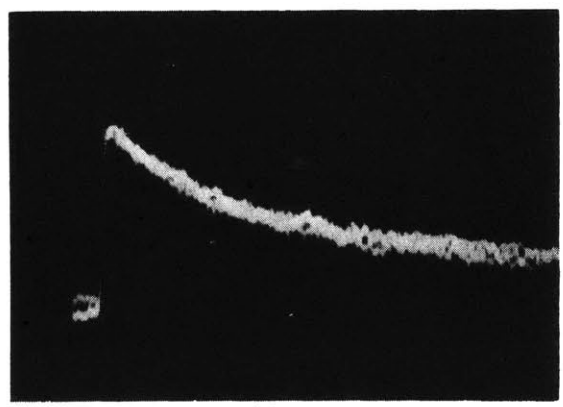

(b)

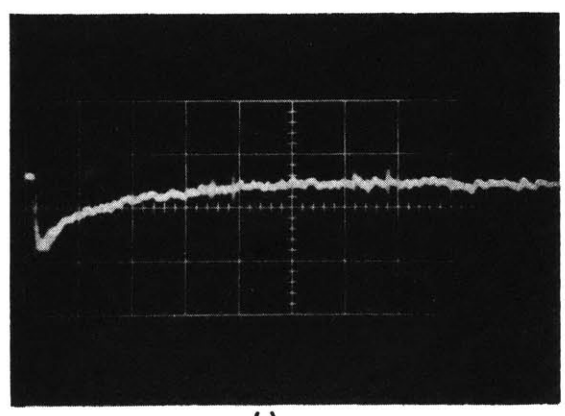

(c)

FIG. 2. Representative infrared double resonance signals in SF_6. (a) "Hole" at 944 cm^{-1} in 0.28 torr SF_6; sweep 100 μsec/cm. (b) Transient absorption at 938.7 cm^{-1} in 0.6 torr SF_6; sweep 100 μsec/cm. (c) Depletion of ground-state absorption at 948 cm^{-1} in 0.25 torr SF_6; sweep 200 μsec/cm.

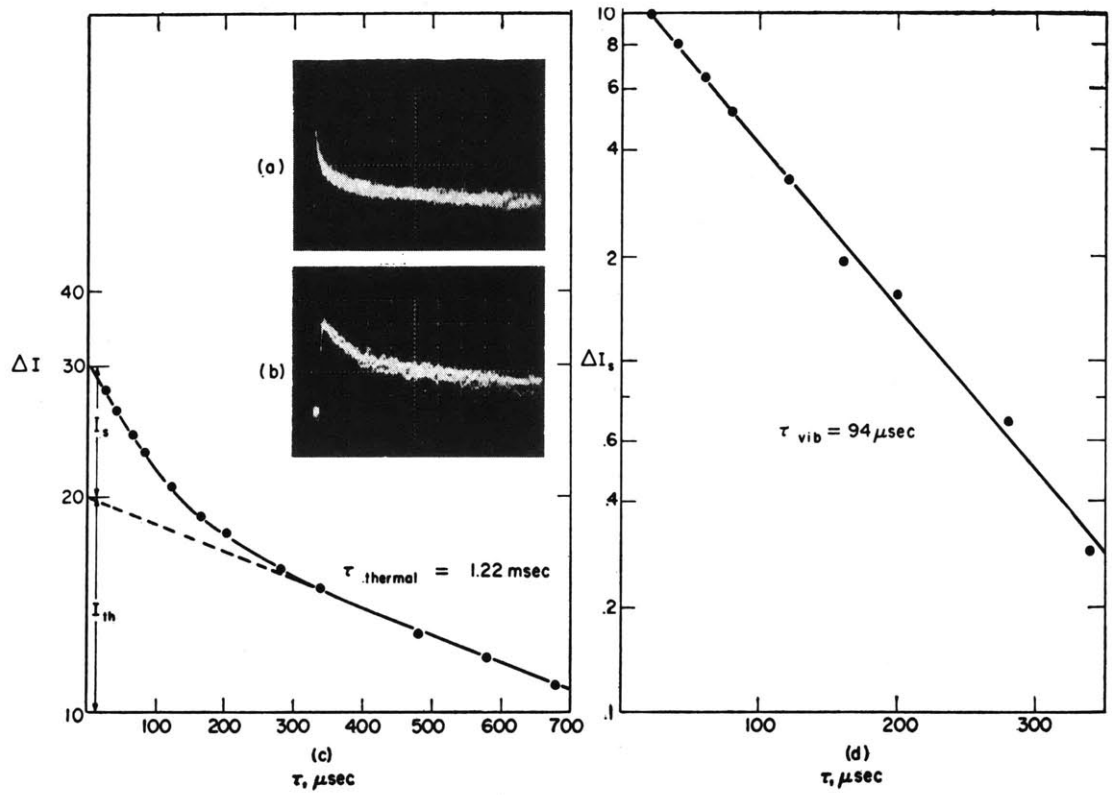

FIG. 3. Analysis of absorption transients at 938.7 cm^{-1}. (a) Signal in 1.15 torr SF_6 at 1 msec/cm. (b) Same at 100 μsec/cm. (c) Semilogarithmic plot of data from (b). (d) Isolation of short relaxation time.

of the sample cell, showing that the signal is not due to a reflected pulse or to the pulse getting into the cw laser and changing its gain characteristics. A similar-appearing effect has recently been seen[26] in a two-photon optical experiment, which is due to sample fluorescence. This possibility can also be dismissed since there is no signal when the cw monitoring beam is blocked.

The relaxation time of the hole is not greater than 0.3 μsec·torr, which sets an upper limit of $Z=2$ for the average number of SF_6–SF_6 collisions required to relax the nonequilibrium rotational distribution produced by the laser. The width of the hole must be at least 40 MHz since the two lasers used in the experiment are not frequency locked to any extent other than the Doppler width of the CO_2 gain profile, which is 40 MHz under discharge conditions. This is reasonable since the homogeneous linewidth of a saturated SF_6 absorption line has been estimated at 100 MHz.[14] Broad-band electro-optic tuning of the probe laser frequency will be required, if the profile of the hole is to be explored in detail.

(ii) When the monitoring laser line is at a *lower* frequency than the pumping line, a transient increase in absorption occurs, as shown in Fig. 2(b). The amplitude of this increase is a function of the monitoring wavelength employed; from this dependence, the absorption spectrum of the excited states produced by the laser pulse can be obtained. This is done in Sec. IV.B, below. The risetime of this transient absorption is of the same order of magnitude as that with which the "hole" is filled in, viz. less than 0.3 μsec·torr. This will be interpreted as indicating that vibration ↔ vibration energy transfer proceeds as efficiently as rotation ↔ translation processes, i.e., on essentially every gas-kinetic collision.

In many cases, the excess absorption decays with two relaxation times. A similar type of behavior has been observed in CO_2 fluorescence experiments.[27] A typical example is shown in Fig. 3, for pure SF_6 at a pressure of 1.15 torr. The fast and slow relaxation times appear clearly in Fig. 3(a); the data are actually obtained from Fig. 3(b), in which the time base has been expanded by a factor of 10. Figure 3(c) shows a semilogarithmic plot of this decay curve, from which a long relaxation time of 1.22 msec is obtained. This is extrapolated back to zero time to resove the short relaxation time of 94 μsec, in Fig. 3(d). When the beamsplitting mirror M_4 is misaligned just enough to cause the two beams to be no longer coaxial but to lie just alongside each other in the volume of gas, the short-time effect disappears, but the long-time effect remains essentially unchanged. For this, and other reasons to be adduced later, we attribute the slow relaxation to a bulk gas temperature cooling,

and the fast relaxation to a specific vibration→translation energy transfer process.

(iii) When the monitoring laser line is at a *higher* frequency than the pumping line, a transient decrease in absorption occurs, as shown in Fig. 2(c), which decays exponentially with time constants comparable to those for the transient increased absorption noted above. This effect is attributed to a depletion of the lower vibrational states in SF_6, just compensating for the increase in the higher states populated by the laser pulse.

All the observed relaxation times are summarized in Table I. The data for the short times in pure SF_6 are shown in Fig. 4. The scatter in the experimental data for mixtures was comparable to that for pure SF_6. To eliminate the considerable scatter, caused by the appearance of the long thermal relaxation time, several runs were carried out on SF_6–Kr mixtures, and the relaxation times extrapolated to $p(\mathrm{Kr})=0$, using the formula

$$(\tau_{\mathrm{obs}})^{-1}=[p(\mathrm{Kr})/p\tau_{\mathrm{Kr}}]+[p(\mathrm{SF_6})/p\tau_{\mathrm{SF_6}}]. \quad (1)$$

These data are shown in Fig. 5, and the extrapolated values of τ^{-1} shown as the crosses in Fig. 4.

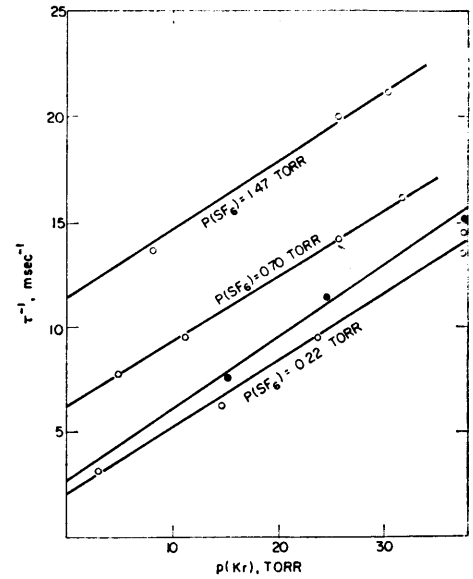

FIG. 5. Relaxation time data for SF_6–Kr mixtures; the extrapolated values for pure SF_6 are included in Fig. 4. ○, data taken at 938.7 cm^{-1}, $P(SF_6)$ as indicated; ●, data taken at 952.9 cm^{-1}, $P(SF_6)=0.19$ torr.

IV. SPECTROSCOPIC CONSIDERATIONS

A. Assignment of Pumped Levels

The dominant output of the Q-switched $He/N_2/CO_2$ laser is at the $P(18)$, $P(20)$, and $P(22)$ lines of the $00^01\rightarrow10^00$ transition in CO_2, lying at 945.9, 944.2, and 942.4 cm^{-1}, respectively. This falls in the center of the ν_3 (f_{1u}) fundamental vibration of SF_6—an extremely strong infrared transition, with $\mu_{if}\sim3\times10^{-19}$ esu·cm.[14] A much more difficult problem, however, is that of specifying exactly which rotational components of the band are coupled to the laser radiation. There are a number of indications that several SF_6 transitions are involved, so that the molecular absorption presents an essentially smooth, structureless contour to the laser radiation. These include the observation that the linear absorption coefficients measured for the laser lines are nearly the same as those measured on a conventional, low-resolution infrared spectrophotometer set to the corresponding wavelength[14]; consideration of extensive second-order Coriolis splittings[28]; interpretation of photon echo experiments, in which the model of a continuous frequency distribution of dipole strength is assumed[13]; and cross-saturation[23] and Lamb Dip[29] experiments. Shimizu[30] has measured linear absorption of laser radiation by SF_6, while scanning the line frequency across the 40-MHz CO_2 Doppler width by means of longitudinal cavity tuning. He finds a factor-of-2 variation in absorption strength over this range. This also argues in favor of several overlapping lines since a resolved SF_6 fine-structure line would be expected to show a large variation in intensity over its own Doppler width, which is of the order of 25 MHz. Finally, analysis of the saturation experiments[14] indicates that 0.3% of the molecules can directly absorb laser radiation, again requiring the participation of several J states to make up this much population.

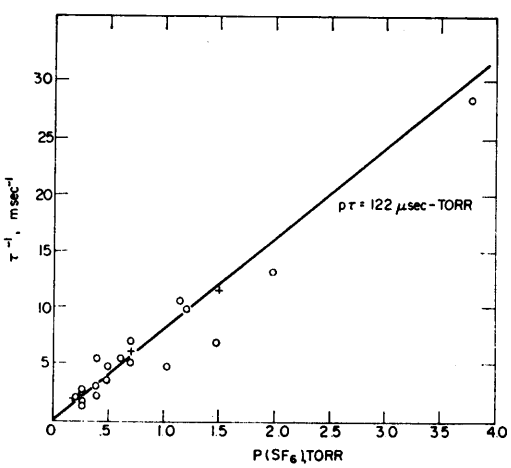

FIG. 4. Test of $p\tau$ relationship in SF_6. ○, data for pure SF_6; +, data for SF_6–Kr mixtures extrapolated to $p(\mathrm{Kr})=0$.

Thus, we attribute the absorption of CO_2 laser radiation by SF_6 to several overlapping fine-structure lines. The question of exactly which J, K levels are involved, however, must be deferred until a band contour analysis can be completed.

TABLE I. Observed vibrational relaxation in SF_6 mixtures.

System	Run	$P(SF_6)$ (torr)	P(gas) (torr)	$\bar{\nu}_{obs}$ (cm^{-1})	τ_1 obs (μsec)	τ_1 calc (μsec)	τ_2 obs (msec)	Notes[a]
Pure SF_6	5	0.21		936.8	505	581	...	*
	38	0.25		936.8	354	488	...	
	143	0.25		938.7	634	488	...	
	162	0.25		938.7	591	488	...	High-purity SF_6
	3	0.39		936.8	476	313	...	*
	4′	0.39		936.8	330	313	...	
	39	0.48		936.8	274	254	...	
	6	0.48		938.7	260	254	1.85	*
	21a	0.60		938.7	180	203	1.08	
	1a	0.70		938.7	195	174	1.40	
	2a	0.70		938.7	143	174	1.01	
	184	0.87		938.7	115	140	0.5	High-purity SF_6
	51	1.02		938.7	209	120	0.72	*
	82	1.15		938.7	94	105	1.22	
	1	1.20		936.8	101	102	1.89	*
	7a′	1.47		938.7	144	83	0.71	
	185	1.56		938.7	100	78	0.49	High-purity SF_6
	85	1.98		936.8	76	62	2.74	
	183	2.39		938.7	35	51	1.4	High-purity SF_6
	31	3.77		938.7	35	32	≈4.5	
	142	0.25		952.9	488	488	...	
	152	0.42		952.9	266	290	...	
	153	0.42		952.9	300	290	...	
	154	0.42		952.9	374	290	...	
	155	0.66		951.2	330	185	...	Misaligned (see text)
	156	0.66		952.9	256	185	...	
	157	0.66		952.9	390	185	...	
	52	1.08		952.9	137	113	0.61	
SF_6+He	12	0.21	0.95	938.7	34.7	40.2	...	*
	11	0.24	1.23	938.7	32.5	31.3	...	*
	45	0.21	1.85	938.7	18.8	21.3	...	
	10	0.21	2.46	938.7	17.3	16.2	...	*
	9	0.21	3.08	938.7	16.0	13.0	...	*
	44	0.21	4.73	938.7	7.2	8.5	...	
	69′	0.22	1.78	952.9	32.5	22.1	...	
SF_6+Ne	71′	0.21	3.79	938.7	40	47	...	
	72	0.21	3.79	938.7	47	47	...	
	74	0.17	10.2	938.7	20	18.5	...	
	73	0.21	3.79	952.9	51	47	0.66	
SF_6+Ar	75	0.17	7.46	938.7	58	58	...	
SF_6+Kr	146	0.25	1.57	938.7	346	390	...	
	58	0.22	3.13	938.7	300	353	2.68	
	148	0.25	6.0	938.7	274	248	...	
	61	0.20	14.8	938.7	159	153	...	
	67	0.19	24.	938.7	122	106	...	
	68	0.19	24.	938.7	102	106	...	
	63	0.18	38.	938.7	77	71	...	
	3a	0.70	4.5	938.7	180	138	3.1	
	4a	0.70	4.5	938.7	137	138	3.27	
	5a	0.69	11.6	938.7	97	106	0.75	
	7a	0.63	32.	938.7	68.5	64	...	
	12a	1.2	8.5	938.7	87	79	3.2	
	8a	1.47	31.	938.7	37.5	45	...	
	9a	1.47	31.	938.7	43	45	...	
	59	0.22	3.13	952.9	245	353	...	
	60	0.22	3.13	952.9	185	353	0.88	

TABLE I (*Continued*)

System	Run	$P(SF_6)$ (torr)	P(gas) (torr)	$\bar{\nu}_{obs}$ (cm^{-1})	τ_1 obs (μsec)	τ_1 calc (μsec)	τ_2 obs (msec)	Notes[a]
SF_6+Kr	62	0.2	14.8	952.9	130	153	...	
	66	0.19	24.	952.9	87	106	...	
	65	0.18	38.	952.9	65	71	...	
$SF_6+C_2H_6$	46	0.22	2.39	938.7	7.8	3.6	...	
	47	0.22	0.79	938.7	11.5	10.7	...	
	48	0.23	0.33	938.7	22.5	24.8	...	
$SF_6+(CH_3)_2O$	69	0.41	0.77	938.7	5.9	6.7	...	
	69a	0.41	0.77	936.8	7.8	6.7	...	
	70	0.13	0.60	938.7	6.0	8.8	...	
	76	0.20	0.50	938.7	10.1	10.4	...	
	77	0.13	0.57	938.7	9.4	8.8	...	+15.0 torr Kr
SF_6+CH_4	116	0.22	0.37	938.7	48	49	0.43	
	118	0.22	0.37	938.7	35	49	0.87	
	117	0.22	0.96	938.7	20	20	...	
SF_6+CH_3Br	113	0.22	0.22	938.7	49	57	0.71	
	114	0.23	0.65	938.7	24	21	0.24	
SF_6+CHF_2Cl	120	0.20	0.23	938.7	46	72	0.42	
	119	0.25	0.90	938.7	18	20	0.09	
	124	0.20	0.23	940.6	42	72	0.49	
	166	0.23	0.165	938.7	57	95	2.1	
	169	0.15	0.78	938.7	23	24	0.41	
	174	0.21	0.78	938.7	33	23	0.52	
	176	0.21	0.78	938.7	26	23	0.27	
	121	0.20	0.23	952.9	112	62	...	
	123	0.25	0.90	952.9	69	17	...	
SF_6+H_2O	130	0.23	0.39	938.7	27	27	...	
SF_6+H_2	129	0.20	0.16	938.7	55.7	58.1	...	
	128	0.23	0.23	938.7	37.7	37.6	...	
	125	0.22	0.43	938.7	18.8	20.8	...	
SF_6+N_2	127	0.23	0.38	938.7	190	179	...	
	125	0.23	0.76	938.7	98.5	108	...	
	126	0.23	1.70	938.7	56	54	...	
SF_6+Cl_2	138	0.25	0.87	938.7	82	78	4.6	
	139	0.25	0.87	938.7	75	78	2.0	
	136	0.21	2.0	938.7	36	37	1.6	

[a] Asterisk indicates boxcar integrator used to process data.

B. Transient Absorption Spectrum

It is evident, from the spectroscopic changes being observed, that the laser pulse is pumping a substantial fraction of the SF_6 molecules from lower to higher vibrational levels. The identification of these levels is crucial to the interpretation of the experimental results. On the basis of evidence to be described in the following sections, we suggest that the levels being depleted are those having less than 1000-cm^{-1} vibrational energy content, and that the corresponding increase in population is therefore in levels having greater than 1000-cm^{-1} vibrational energy content. Let us denote the partial pressure of the former group of molecules by p_0, with an absorption coefficient α_0, and the partial pressure of the latter group by p^*, with an absorption coefficient α^*. Then the total linear optical absorption at any wavelength λ is given by

$$\ln(I_0/I)_\lambda = \alpha_0(\lambda)\, p_0 l + \alpha^*(\lambda)\, p^* l, \qquad (2)$$

where α is in $torr^{-1}\cdot cm^{-1}$. If the populations are changed by some amount Δp, the new absorption will be given by

$$\ln(I_0/I')_\lambda = \alpha_0(\lambda)\,(p_0-\Delta p)\, l + \alpha^*(p^*+\Delta p)\, l.$$

The absorption decrease at the $P(10)$, $P(12)$, and $P(14)$ laser lines was used to obtain Δp. These measurements indicated that approximately 20% of the total number of SF_6 molecules in the light beam were removed from the lower vibrational states and thus placed in the states absorbing at longer wavelengths.

A check on $\Delta p/p_0$ can be found by simply measuring

TABLE II. Excitation of SF_6 by laser pulses.

$P(SF_6)$, (torr)	$\langle I_{in}\rangle_{Av}$ (W)	% absorbed (exptl)	$\langle I_{abs}\rangle$ (W)	E_{abs} (erg)	Number of photons absorbed	$N(SF_6)$ (7.0 cm³)	Per cent excitation
0.28	0.09	22	0.02	2×10^2	1×10^{16}	7×10^{16}	17
0.43	0.08	50	0.04	4	2	10	22
0.83	0.085	99	0.084	8.4	4.2	20	21

the amount of radiation absorbed from each pulse by the SF_6 sample; this is done in Table II. The pulses were taken to have a 100-Hz repetition rate, in order to convert from average power to energy/pulse. The beam area was estimated at (0.23 ± 0.03) cm², by means of thermal imaging, to give an absorbing volume of 7.0 cm³ in a 30-cm path. The fraction of molecules excited on a one-photon-per-excitation basis, is in excellent agreement with that estimated above from ΔI. It is also about the same as previously calculated to explain infrared saturation effects[14]; the difference, as we shall see in the next section, is that the vibrationally excited molecules are distributed over a large number of levels, rather than all remaining in the ν_3 level.

Using these values of Δp, and Eq. (2), the absorption curve $\alpha^*(\bar{\nu})$ which is shown in Fig. 6 was obtained. The open circles are values of $\alpha_0(\bar{\nu})$ which were measured as a check against the known infrared spectrum of SF_6 in the absence of pumping. Good agreement is obtained, except that the structure between 945 and 949 cm⁻¹ is not well reproduced. Two different path-length–pressure combinations were used for measurements at the $P(20)$ and $P(24)$ laser lines; the difference in the values of α_0 and α^* obtained at these points gives an idea of the accuracy of the measurements. The peak of α^* is shifted 8 cm⁻¹ to the red, as would be expected from anharmonicity. The integrated area

$$\int\alpha^*(\bar{\nu})\,d\bar{\nu}$$

is 1.15 times the area of

$$\int\alpha_0(\bar{\nu})\,d\bar{\nu};$$

a value of 2.0 would be expected if the transient absorption were attributable to the $2\nu_3\leftarrow\nu_3$ transition. No transient absorption was seen below 931 cm⁻¹; the probe laser was also run with a $N_2O/N_2/He$ mixture, giving output at 920 cm⁻¹, but no double resonance was observed at this frequency either.

The value of $\Delta p/p$ found above is also needed to determine the limits over which we may safely linearize the absorption in determining time constants. That is, we wish to have

$$\Delta I\simeq(\text{const.})\,\Delta p,$$

so that a logarithmic plot of the oscilloscope trace itself, on which the voltage change is directly proportional to the infrared intensity change, may yield the time constant directly. If we expand

$$I/I_0=e^{-\alpha pl}$$
$$=1-\alpha pl+[(\alpha pl)^2/2!]\cdots,$$

we find for the variation in I,

$$\Delta I/I_0=-\alpha l(\Delta p)+\tfrac{1}{2}(\alpha l)^2(\Delta p)^2\cdots. \qquad (3)$$

If $\Delta p/p$ is of the order of 20%, then neglecting the quadratic and higher terms in Δp introduces only a 1% error if $\alpha pl=0.1$, 5% if $\alpha pl=0.5$, and 9% if $\alpha pl=0.9$. Since the net absorbance on all the experimental runs was within these limits, the linearization could be safely carried out.

V. RELAXATION MODEL

A. Vibrational Temperatures

We now wish to interpret these observations in terms of detailed molecular processes taking place in the gas. In our prior study of cw saturation in SF_6,[14] a simplified model was proposed in which four subsets of molecules were distinguished. These were n_0 and n^*, the ground and vibrationally excited states, respectively, which could be directly coupled by the laser radiation, and which amounted to only about 0.3% of the total; and n and n', the ground and excited states having rotational quantum numbers different from those in n_0 and n^*. Good agreement with experiment could be obtained by solving the steady-state rate equations for this four-

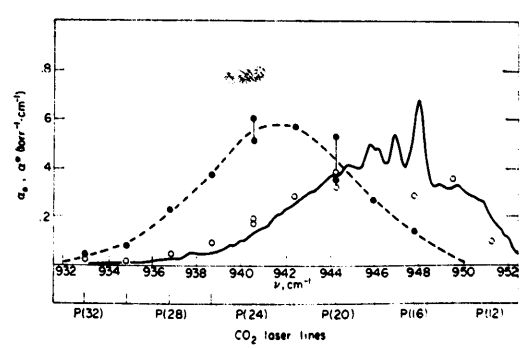

FIG. 6. Absorption spectra of normal and vibrationally pumped SF_6. ○, $\alpha_0(\lambda)$; ● and - - -, $\alpha^*(\lambda)$. The ground-state absorption curve is taken from Szöke and Rhodes (Ref. 13). The total spectrum of the gas would be the weighted sum of the two curves.

level system, using a rotational relaxation cross section of the order of 50 Å²; however, the system was not sensitive to the details of the processes by which molecules were removed from the n^* levels.

On the basis of the experiments reported here, we now propose a generalization of this model, shown in Fig. 7. The generalization consists of treating the vibrationally excited molecules as not exclusively in $v_3=1$, but in a complete distribution of vibrational states from $v_6=1$ on up, all of which are in very rapid equilibrium with each other. These levels can thus be described by an effective vibrational temperature, which need not be the same as the translational and rotational temperature of the system.

The experiment we are carrying out thus consists of:

(i) laser-pumping a small fraction of the SF_6 molecules to a specified rotational level(s) of the $v_3=1$ state;

(ii) these levels are rapidly coupled by *both* rotation ↔ translation and near-resonant vibration ↔ vibration energy transfer processes to the complete set of excited vibrational levels in SF_6, among which an equilibrium is reached in a few microseconds;

(iii) the excess vibrational temperature relaxes back to the translational temperature, and the rate-limiting process for this to occur is the vibration ↔ translation deactivation of the ν_6 level at 363 cm⁻¹;

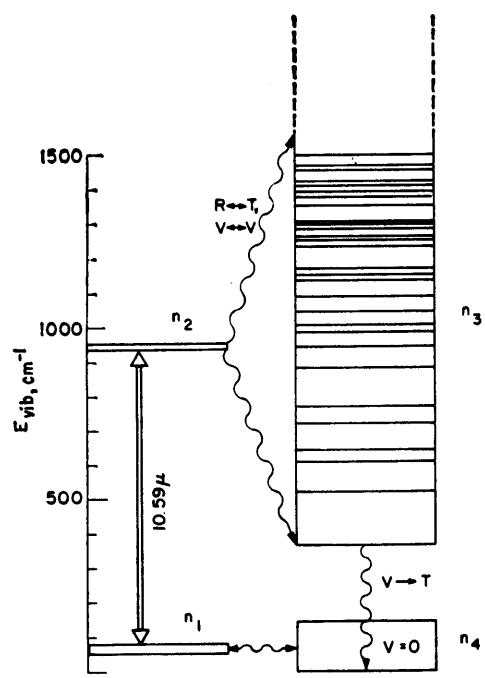

FIG. 7. Relaxation model for SF_6. The levels on the left-hand side represent those rotational components of $\{v_i\}=0$ and $v_3=1$ that can be directly coupled by CO_2 laser radiation. The stack of vibrational levels in the upper right-hand part of the diagram are assumed to be in rapid equilibrium; specific levels only up to 1500 cm⁻¹ are shown.

TABLE III. Relaxation amplitudes in SF_6–Kr mixtures.

$P(SF_6)$ (torr)	$P(Kr)$ (torr)	I_{th}/I_s	$C_{vib}(SF_6)^a/C_{total}$
1.47	0	0.6	0.7
1.20	8.5	0.44(±0.06)	0.29
1.47	31	0.12	0.17

[a] A value of 14 cal/mole·deg is taken for $C_{vib}(SF_6)$ at 300°K.

(iv) meanwhile, the energy released in steps (ii) and (iii) has heated the entire gas translationally; this cools back to the ambient temperature by some combination of diffusion and conduction, giving rise to the long relaxation time seen in the system.

We may cite several points in support of this mechanism.

(i) Most important is the ratio of the amplitudes of the "short" to the "long" relaxation times, indicated as I_s and I_{th}, respectively, in Fig. 3. If the transient absorption at λ(probe) > λ(pump) were due to the $2\nu_3 \leftarrow \nu_3$ transition alone, then the amplitude of the thermal part of the relaxation should be much smaller than that of the faster part since the $v_3=1$ level never accounts for more than 1.2% of the total population at any temperature (see Fig. 8[31]). Rather than this, we attribute the absorption to a superposition of many excited vibrational levels, each absorbing one quantum of ν_3; as may be seen from Fig. 8, the levels whose population increase with increasing temperature are all those lying above 1000 cm⁻¹ in energy. This also implies that the fluorescence observed in Refs. (16) and (17) arises from only a small fraction of the molecules in the system. The recent observation of fluorescence from shock-heated SF_6 is in agreement with this point of view. A numerical check of this point may be made by looking at the ratio I_{th}/I_s for various SF_6–Kr mixtures; the ratio should be the same as $C_{vib}(SF_6)/C_{total}$, where C is the constant-volume heat capacity. This comparison is made in Table III, and good agreement is found. A direct comparison of this sort cannot be made for SF_6 pressures below 1 torr, because of nonlinear absorption in this region.

Another numerical consistency check involves the degree of excitation in the sample, $\Delta p/p_0$, which was found to be 20% from the change in absorption. From Fig. 8 a 20% decrease in the population of the $\{v_i\}=0$ level corresponds to a temperature rise of about 25°C. If we use the figures previously adopted, viz. 2×10^{-4} J absorbed per pulse by a total of 6×10^{16} SF_6 molecules with a heat capacity of 20 cal/mole·deg, we calculate a temperature rise of 24°C, exactly as required.

(ii) The $V\rightarrow T$ relaxation time found in this work is within 25%–30% of the ultrasonic relaxation time [see Table V] which is known to be a measure of the ν_6 deactivation rate.

(iii) The mass dependence of the $V\rightarrow T$ relaxation

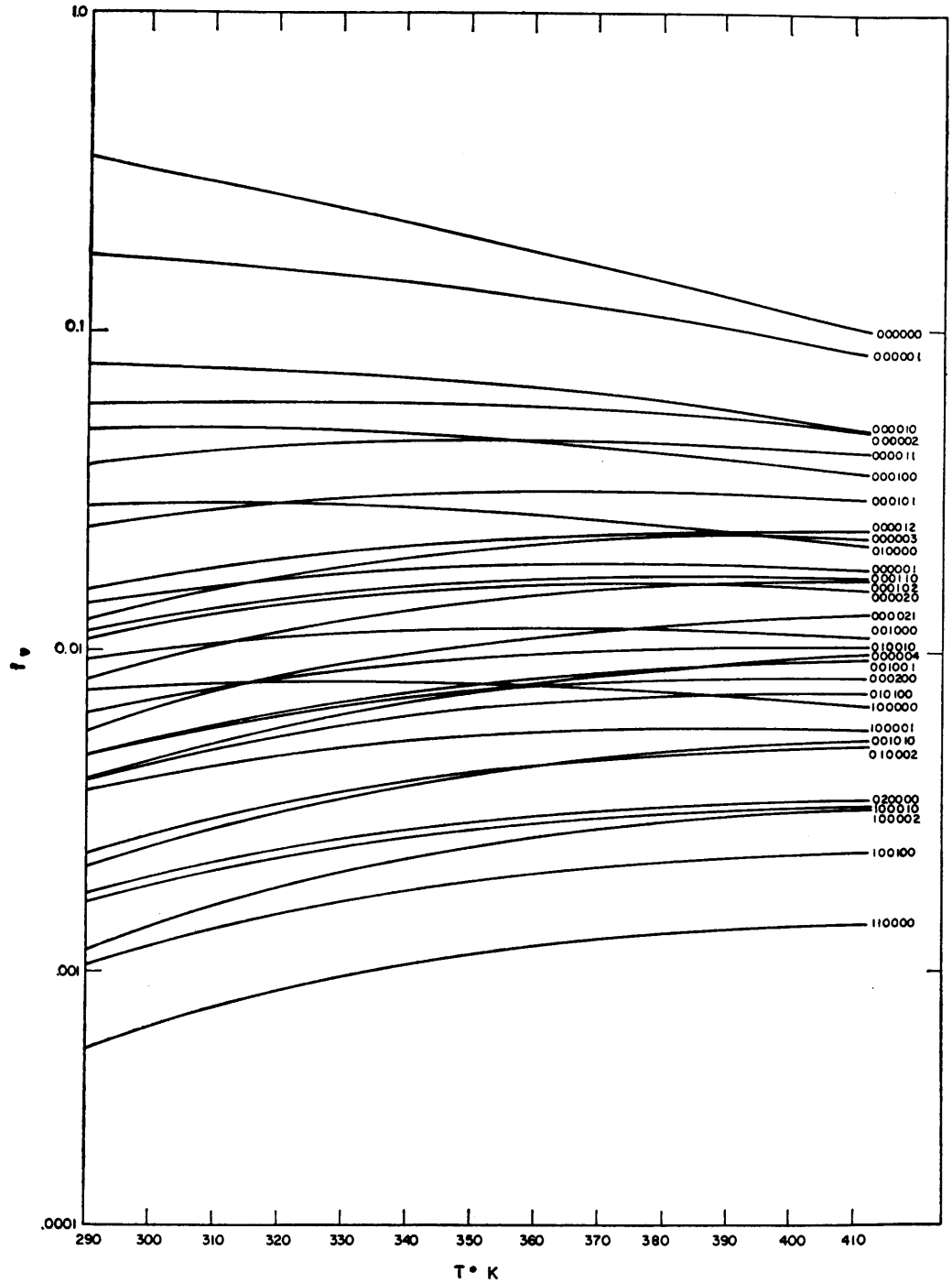

FIG. 8. Fractional population in all SF_6 vibrational levels up to 1500 cm^{-1}, assuming equilibrium between the levels.

time for SF_6–rare-gas mixtures, when calculated by Moore and Yardley's expression,[32] can be fit only if ΔE_{vib} is of the order of 300 cm^{-1}. The $\nu_6 \rightarrow 0$ spacing is 363 cm^{-1}, while the $\nu_3 \rightarrow 0$ spacing is 945 cm^{-1}.

(iv) The integrated area of the excited state absorption curve is only slightly larger than that of the ground state, which indicates that only a small component of the excited molecules are in the $v_3 = 1$ state, for which

TABLE IV. Time dependence of populations.

Pressure of SF_6 = 0.20 torr at 300°K.
$V \leftrightarrow V$ rate constant is 7.83×10^5 sec^{-1}
$V \leftrightarrow T$ rate constant is 1.07×10^3 sec^{-1}

	Power = 0 (W/cm²)			Power = 1000 (W/cm²)		
Eigenvalues (sec^{-1})[a]	λ_1 -1.64×10^3	λ_2 -7.84×10^5	λ_3 -7.84×10^5	λ_1 -3.99×10^3	λ_2 -3.61×10^8	λ_3 -7.84×10^5
Eigenvector for						
n_1	−0.003	+0.004	+1.000	−0.000	+0.707	+0.229
n_2	+0.003	+0.707	+0.000	+0.000	−0.707	+0.688
n_3	+1.000	−0.707	−0.000	+1.000	+0.002	−0.688
Steady-state populations (fractional) in						
n_1	0.0019			0.0008		
n_2	0.0010			0.0022		
n_3	0.3405			0.5797		
n_4	0.6566			0.4173 ($\Delta n_4 = -24\%$)		

[a] $\lambda_4 = 0$, in both cases (see text).

the oscillator strength for $\Delta v_3 = +1$ would be twice that of any state with $v_3 = 0$.

B. Solution of the Master Equation

The relaxation behavior of the model proposed in Fig. 7 is governed by the equation

$$d\mathbf{n}/dt = \mathbf{A}\cdot\mathbf{n}, \tag{4}$$

where the concentration vector $\mathbf{n} = (n_1, n_2, n_3, n_4)$ and $\mathbf{A}$ is the 4×4 matrix of rate coefficients previously described in the work on infrared saturation.[14] Since the matrix elements of $\mathbf{A}$ satisfy the stochastic condition,

$$-a_{ii} = \sum_{i\neq j} a_{ij},$$

one of the eigenvalues of $\mathbf{A}$ is zero.[30] To avoid numerical difficulties introduced by this fact into the diagonalization of $\mathbf{A}$, the problem was reduced to a three-dimensional form,

$$d\mathbf{n}'/dt = \mathbf{A}'\cdot\mathbf{n}' + \mathbf{c}, \tag{5}$$

where

$$\mathbf{n}' = (n_1, n_2, n_3),$$

$$\mathbf{A}' = \begin{pmatrix} a_{11}-a_{14} & a_{12}-a_{14} & a_{13}-a_{14} \\ a_{21}-a_{24} & a_{22}-a_{24} & a_{23}-a_{24} \\ a_{31}-a_{34} & a_{32}-a_{34} & a_{33}-a_{34} \end{pmatrix},$$

and $\mathbf{c} = (N_{\text{total}})^{-1}\,(a_{14}, a_{24}, a_{34})$; we normalize by taking $N_{\text{total}} = 1$.

If we diagonalize the 3×3 problem, viz,

$$\mathbf{A}'\mathbf{R}_i = \lambda_i\mathbf{R}_i \qquad (i = 1, 2, 3), \tag{6}$$

where the R_i are the normalized eigenvectors of the problem, then the solutions to the time-dependent concentrations are

$$\mathbf{n}'(t) = \sum_{i=1}^{3} \alpha_i\mathbf{R}_i \exp(\lambda_i t) - (\mathbf{A}')^{-1}\cdot\mathbf{c}. \tag{7}$$

The coefficients α_i are found by solving the set of inhomogeneous equations

$$\mathbf{n}'(0) = \sum_i \alpha_i\mathbf{R}_i - (\mathbf{A}')^{-1}\cdot\mathbf{c}, \tag{8}$$

where $n'(0)$ is the set of concentrations before the infrared pulse is applied. Inverting this gives

$$\alpha_i = \mathbf{R}_i^{-1}\cdot[\mathbf{n}'(0) + (\mathbf{A}')^{-1}\cdot\mathbf{c}]. \tag{9}$$

If we let $t \to \infty$ in Eq. (7), and note that the λ_i are all negative, we see that

$$\mathbf{n}'(\infty) = -(\mathbf{A}')^{-1}\cdot\mathbf{c};$$

this is just the steady-state solution to the saturation problem which was considered in Ref. 14.

Some numerical results for a typical set of experimental conditions are given in Table IV. In the absence of radiation, i.e., after the pulse has been applied, the population of vibrationally excited molecules which we are observing (n_3) relaxes with a decay time governed almost completely by the specific $V \leftrightarrow T$ rate constant for the lowest level, as was assumed in setting up the model. The observed relaxation time is given by $\tau^{-1} = k_{VT}[1 + 3\exp(-h\nu_6/kT)]$. During the pulse, this population equilibrates more rapidly, because of the radiation coupling between n_1 and n_2. The steady-state populations found in the latter case are just those appropriate to a saturated system: $n_2/n_1 \approx g_2/g_1 = 3$, and the population n_3 has increased relative to n_4.

The calculation for 1000 W/cm² impinging on 0.20 torr of SF_6 yields a value of $\Delta p/p_0$ of 24%, close to the measured 20%. In general, however, this fully saturated condition is not reached during a typical Q-switched pulse, because of the time lag in populating n_3 from n_2. The depletion of n_1 and buildup of n_3 is shown in Fig. 9; while the depletion of the directly pumped level (i.e., the formation of the "hole" in the absorption spectrum) is ≈80% complete in the first 100 nsec of the pulse, the overpopulation of n_3 (i.e., the buildup of the transient

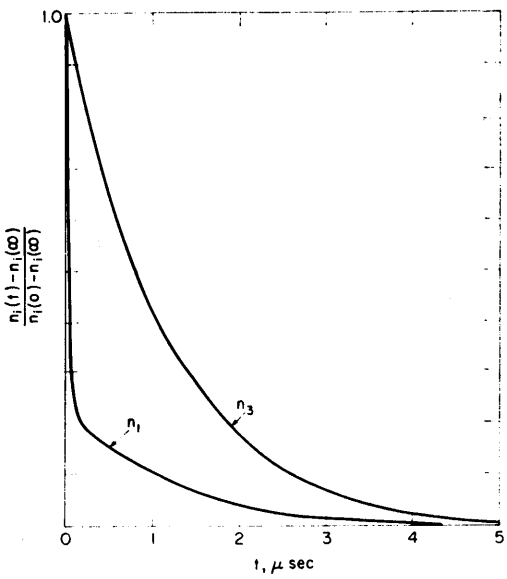

FIG. 9. Response of populations n_1 and n_3 to 1000 W/cm² of infrared radiation, in 0.20 torr pure SF_6. The populations are plotted on a common scale, giving the fractional deviation from the full difference between the populations prior to the pulse ($t=0$) and at complete saturation ($t=\infty$).

absorption) has reached only 20% of its fully saturated value in the duration of a single Q-switched pulse, of the order of 300 nsec. A train of pulses lasting 3 μsec can bring n_3 to ≈90% of its fully saturated value, in accord with experimental observations, namely, that the amplitude of the transient absorption is nearly independent of peak pulse power over the range 0.1→1.0 kW, but is strongly dependent on the duration of the pulse.

VI. COLLISIONN UMBERS AND DE-EXCITATION EFFICIENCY RATIOS

The results of Sec. V.B show that after the Q-switched pulse has passed through the cell the gas relaxes as an effective two-state system. Therefore, it is appropriate[34] to calculate the collision number, Z_{10}^1 from the observed relaxation time as follows:

$$Z_{10}^1 = Z\beta[1+3\exp(-h\nu_6/kT)], \qquad (10)$$

where β is the *experimental* relaxation time at unit pressure. The factor of 3 arises from the three-fold degeneracy of the ν_6 normal mode. The gas-kinetic collision number is given by[34]

$$Z = 4n\sigma^2[\Omega^{(2,2)*}(kT/\epsilon)](\pi kT/m)^{1/2}, \qquad (11)$$

where n is the molecular density at unit pressure; σ and ϵ are the Lennard-Jones cross section and well depth parameters, respectively; $\Omega^{(2,2)*}(kT/\epsilon)$ is the usual collision integral[35]; m is the mass of the SF_6 molecule, and $T=300°K$ in all calculations.

For gas mixtures, the ratio

$$Z\beta/Z_x\beta_x = P_{10}(SF_6-x)/P_{10}(SF_6-SF_6)$$

is tabulated, where

$$Z_x = 2n_x[\tfrac{1}{2}(\sigma+\sigma_x)]^2\Omega^{(2,2)*}[kT/(\epsilon\epsilon_x)^{1/2}] \times[2\pi kT(m+m_x)/(mm_x)]^{1/2}; \qquad (12)$$

n_x, σ_x, ϵ_x, and m_x are the density, gas-kinetic cross section, potential well depth, and mass, respectively, for buffer gas x. β_x would be the relaxation time for SF_6 infinitely dilute in x. It is determined from the observed relaxation time, τ_{obs}, by the relation

$$\tau_{obs}^{-1} = (P_{SF_6}/\beta_{SF_6}) + (P_x/\beta_x).$$

This relation was found to be obeyed by all the SF_6–buffer-gas mixtures studied, even for CHF_2Cl, for which Lambert *et al.*[36] found a nonlinear dependence of τ^{-1} on P_x.

The SF_6 relaxation times, collision numbers, and de-excitation efficiency ratios are given in Table V. Also included for comparison are ultrasonic data, where available. The discrepancy in the relation between Z_{10}^1 and $p\tau$ for pure SF_6 arises from the general use of the relation

$$Z_{10}^1 = Z\beta[1-3\exp(-h\nu_6/kT)]$$

for interpreting ultrasonic experiments. This would be appropriate for a harmonic oscillator built on the ν_6 fundamental; our model implies the use of Eq. (10)

TABLE V. Relaxation times and collisional deactivation efficiencies for SF_6.

Gas	$p\tau$ (μsec·torr)	Z_{10}^1	$\frac{P_{10}(SF_6-x)}{P_{10}(SF_6-SF_6)}$	Ref.
Pure SF_6	122	2240		a
	182	1560		b
	137	1140		c
He	41		1.83	a
Ne	194		0.78	a
Ar	470		0.37	a
Kr	3040		0.071	a
C_2H_6	8.6		14.5	a
$(CH_3)_2O$	5.3		29	a
			13	d
CH_3Br	14		15.7	a
CHF_2Cl	19		10	a
			20	d
H_2	9.3		5.2	a
N_2	103		1.36	a
Cl_2	80		2.2	a
H_2O	11.3		13	a
CH_4	20.		5.4	a

[a] This work.
[b] Reference 34.
[c] C. L. O'Connor, J. Acoust. Soc. Am. 26, 361 (1954).
[d] Reference 36.

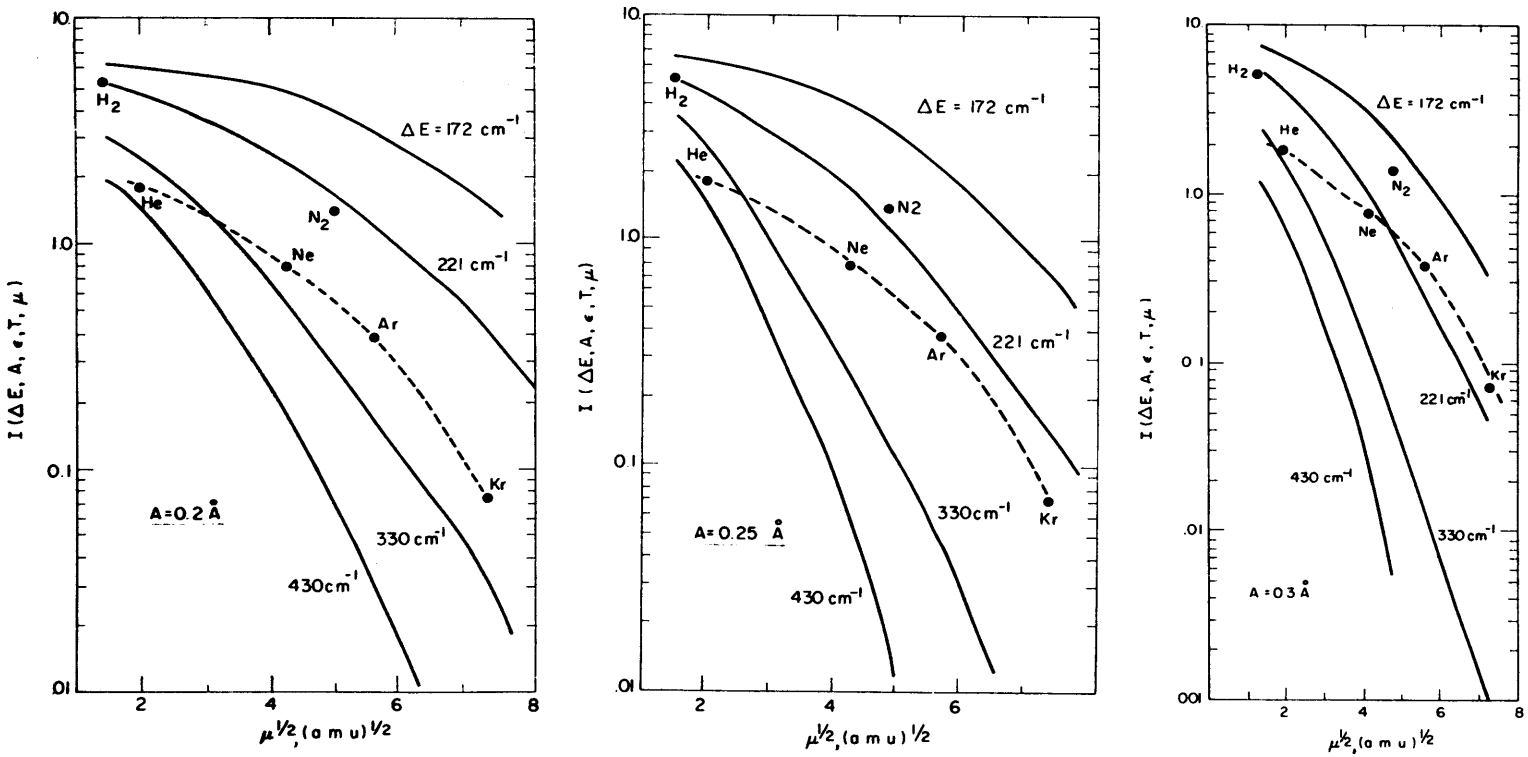

FIG. 10. Comparison of experimental data (●) for SF_6–buffer-gas relaxation with Tanczos' breathing-sphere model. Parameters used were (a) $A=0.2$ Å, (b) $A=0.25$ Å, and (c) $A=0.3$ Å, and $\Delta E(\text{vib}\rightarrow\text{trans})=172$, 221, 330, and 430 cm^{-1}.

instead. Further evidence for attributing the relaxation to the $\Delta\nu_6 = -1$ process is obtained from a consideration of the breathing sphere theory of molecular energy transfer developed by Tanczos[37] and Stretton[38] and used by Yardley and Moore[32] to explain their CO_2–rare-gas data. According to this theory, the probability per rare gas collision for removing energy ΔE from a vibrating molecule is proportional to

$$I(\Delta E, A, \epsilon_0, T, \mu) = \frac{256\pi^6 A^4 \mu^2 (\Delta E)^2}{h^4} e^{-\epsilon/kT} \int_0^\infty \frac{\exp(4\pi^2 A\mu v\{1-[1+(2\Delta E/\mu v^2)]^{1/2}\}h^{-1})(\mu v/kT)\exp(-\mu v^2/2kT)dv}{[1-\exp(4\pi^2 A\mu v\{1-[1+(2\Delta E/\mu v^2)]^{1/2}\}h^{-1})]^2}. \quad (13)$$

A is the repulsive exponential potential range parameter, μ the collision reduced mass, ϵ is the Lennard-Jones well depth, and v is the relative velocity of the collision partners.

The above expression was integrated numerically for several values of A, ΔE, and μ. The results are shown in Figs. 10(a)–10(c), where $\log I$ is plotted as a function of $\mu^{1/2}$. The experimental points for He, Ne, Ar, Kr, N_2, and H_2 are also shown, scaled to fit on the $\log I$ plot. Values for ϵ were computed from the values tabulated in Ref. 35 according to the formula $\epsilon_{SF_6-x} = (\epsilon_{SF_6}\epsilon_x)^{1/2}$. T was set equal to 300°K.

It is apparent from these graphs that for reasonable values of the exponential range parameter the experimental results are consistent with an energy transfer of 200–300 cm^{-1} per effective collision. We believe this is consistent with our model which requires 360 cm^{-1} to be removed from vibration upon an effective collision. It is also apparent that H_2 and N_2 are more effective in removing vibrational energy from the SF_6 molecule than one would predict by considering them to be noble gases. Considering the very high vibrational frequencies of these molecules (especially H_2), leads us to conclude that this result is evidence for vibration–rotation energy transfer. A similar effect is surely taking place in collisions with such gases as CH_4 and H_2O, which possess no low-lying vibrational levels which could accept energy from the SF_6. The high relaxation efficiencies in C_2H_6, $(CH_3)_2O$, CH_3Br, and CHF_2Cl may be due to a combination of $V \leftrightarrow R$ and $V \leftrightarrow V'$ processes.

ACKNOWLEDGMENTS

This work was supported by the National Science Foundation and the North Atlantic Treaty Organization. We thank Miss Irene Platzblatt for programming a number of calculations, and Professor A. Szöke, Professor C. B. Moore, and Professor G. Flynn for helpful discussions.

* Alfred P. Sloan Research Fellow.

† N.I.H. Predoctoral Fellow, supported by P.H.S. Fellowship 1-F1-GM-30959-02.

‡ N.D.E.A. Predoctoral Fellow.

[1] T. Oka, J. Chem. Phys. **49**, 4234 (1968); earlier references therein.

[2] A. M. Ronn and D. R. Lide, Jr., J. Chem. Phys. **47**, 3669 (1967).

[3] J. Lemaire, J. Houriez, J. Bellet, and J. Thibault, Compt. Rend. **B268**, 922 (1969).

[4] C. B. Moore, Accounts Chem. Res. **2**, 103 (1969), and references therein.

[5] C. Rhodes, M. J. Kelly, and A. Javan, J. Chem. Phys. **48**, 5730 (1968).

[6] I. Burak, A. V. Nowak, J. I. Steinfeld, and D. G. Sutton, J. Chem. Phys. **51**, 2275 (1969).

[7] O. R. Wood and S. E. Schwarz, Appl. Phys. Letters **11**, 88 (1967).

[8] O. R. Wood and S. E. Schwarz, Appl. Phys. Letters **12**, 263 (1968).

[9] C. K. N. Patel and R. E. Slusher, Phys. Rev. Letters **19**, 1019 (1967).

[10] C. K. N. Patel and R. E. Slusher, Phys. Rev. Letters **20**, 1087 (1968).

[11] J. P. Gordon, C. H. Wang, C. K. N. Patel, R. E. Slusher, and W. J. Tomlinson, Phys. Rev. **179**, 294 (1969).

[12] C. K. Rhodes, Ph.D. thesis, Massachusetts Institute of Technology, 1969.

[13] A. Szöke and C. K. Rhodes (unpublished).

[14] I. Burak, A. V. Nowak, J. I. Steinfeld, and D. G. Sutton, J. Quant. Spectry. Radiative Transfer **9**, 959 (1969).

[15] H. Brunet and M. Perez, Compt. Rend. **B267**, 1084 (1968).

[16] O. R. Wood, P. L. Gordon, and S. E. Schwarz, IEEE J. Quantum Electron. **5**, 502 (1969).

[17] G. Flynn (private communications).

[18] H. Brunet, Compt. Rend. **B264**, 1721 (1967).

[19] E. B. Treacy, Phys. Letters **27A**, 421 (1968).

[20] G. B. Hocker and C. L. Tang, Phys. Rev. Letters **21**, 591 (1968).

[21] A. Szöke (private communication).

[22] I. Burak, J. I. Steinfeld, and D. G. Sutton, J. Appl. Phys. **39**, 4464 (1968).

[23] R. L. Abrams and A. Dienes, Appl. Phys. Letters **14**, 237 (1969).

[24] T. D. Carroll and S. Marcus, Phys. Letters **27A**, 590 (1968).

[25] P. K. Cheo and R. L. Abrams, Appl. Phys. Letters **14**, 47 (1969).

[26] D. S. Kliger and A. C. Albrecht, J. Chem. Phys. **50**, 4109 (1969).

[27] W. A. Rosser, Jr., A. D. Wood, and E. T. Gerry, J. Chem. Phys. **50**, 4996 (1969).

[28] H. Brunet, Compt. Rend. **B268**, 1750 (1969).

[29] P. Rabinowitz, R. Keller, and J. T. La Tourrette, Appl. Phys. Letters **14**, 276 (1969).

[30] F. Shimizu, Appl. Phys. Letters **14**, 378 (1969).

[31] The populations in Fig. 8 have been calculated on the assumption of an equilibrium vibrational temperature in the system. For this purpose, the degeneracy of multiply excited levels is given by

$$g_{vib} = \prod_{i=1}^{6} \frac{(n_i+g_i-1)!}{g_i!n_i!},$$

where n_i is the number of quanta excited, and g_i the degeneracy, of the ith vibrational mode.

[32] J. T. Yardley and C. B. Moore, J. Chem. Phys. **46**, 4491 (1967).

[33] K. E. Shuler, Phys. Fluids **2**, 442 (1959).

[34] T. C. Cottrell and J. C. McCoubrey, *Molecular Energy Transfer in Gases* (Butterworth, London, 1961), p. 75.

[35] J. O. Hirschfelder, C. F. Curtiss, and R. B. Bird, *Molecular Theory of Gases and Liquids* (Wiley, New York, 1954).

[36] J. D. Lambert, D. G. Parks-Smith, and J. L. Stretton, Proc. Roy. Soc. (London) **A282**, 380 (1964).

[37] F. I. Tanczos, J. Chem. Phys. **25**, 439 (1956).

[38] J. L. Stretton, Trans. Faraday Soc. **61**, 1053 (1965).

Appendix 4

STATISTICAL WEIGHTS FOR ROVIBRATOR LEVELS OF SF_6

APPENDIX 4: STATISTICAL WEIGHTS FOR ROVIBRATOR LEVELS OF SF_6

The method of Wilson[1] can be used to calculate statistical weights for the rotational levels of all the vibrational states of a spherical top molecule. This was done for SF_6 in the course of computing a band synthesis. Since this computation represents a considerable effort, and since a need has already been demonstrated for these numbers,[2] the results are included here in tabular form.

The symbols A_1, A_2, E, T_1, and T_2 represent the various summetry species of the rotational subgroup O of the point group O_h. An example of the use of this table follows. Suppose that one wished to know the rotational degeneracy of the J = 40 rotational level of the ground electronic and vibrational state of SF_6. First note that J = 6(6) + 4 and that the direct product of $\psi_{ELECTRONIC} \otimes \psi_{VIBRATIONAL} = A_{1g} \otimes A_{1g} = A_{1g}$ which corresponds to the A_1 species of the rotational subgroup. Then proceed to the row labeled A_1, and find the entry under the column headed by J = 6p + 4 (p even). The result in this case is found to be that the degeneracy of the 40th rotational level is

$$[2(40) + 1]\cdot[32(6) + 30] = 17,982$$

---

1. E. B. Wilson, Jr., J. Chem. Phys. 3, 276 (1935).

2. J. C. Stephenson and C. Bradley Moore, J. Chem Phys. 52, 2333 (1970).

Statistical Degeneracies of Rovibrator Levels of SF_6[1]

(Multiply Each Weight by 2J + 1)

Symmetry of $\psi_E \otimes \psi_V$	J = 6p		J = 6p + 1		J = 6p + 2		J = 6p + 3		J = 6p + 4		J = 6p + 5	
	p even	p odd	p even	p odd	p even	p odd	p even	p odd	p even	p odd	p even	p odd
A_1	32p+10	32p+6	32p+6	32p+2	32p+14	32p+18	32p+14	32p+18	32p+30	32p+26	32p+26	32p+22
A_2	32p+2	32p+6	32p+6	32p+10	32p+14	32p+10	32p+22	32p+18	32p+22	32p+26	32p+26	32p+30
E	64p+8	64p+8	64p+12	64p+12	64p+32	64p+32	64p+32	64p+32	64p+52	64p+52	64p+56	64p+56
T_1	96p+6	96p+2	96p+30	96p+26	96p+34	96p+38	96p+58	96p+62	96p+70	96p+66	96p+94	96p+90
T_2	96p+6	96p+10	96p+22	96p+26	96p+42	96p+38	96p+58	96p+54	96p+70	96p+74	96p+86	96p+90

1. An approximate value for any J may be attained by computing the value $\frac{8}{3}(2J+1)^2 \cdot g_v$, where $g_v = 1$ for A_1, A_2; 2 for E; 3 for T_1, T_2. Indeed, the values in the table average to this quantity.

BIOGRAPHICAL NOTE

The author is the son of George P. and Marjorie H. Sutton of Maxwell, California; he was born in San Francisco on April 17, 1944. He attended Maxwell Grammar and High Schools where he received a diploma from Maxwell Union High School in June, 1962.

In September 1962, he enrolled at the University of California at Berkeley receiving a B. S. in chemistry with honors in December 1966. In January 1967 he entered the graduate school in chemistry at the Massachusetts Institute of Technology under the supervision of Professor Jeffrey I. Steinfeld. In 1968 he was awarded a graduate fellowship by the National Institutes of Health.

He married the former Sandra M. Vierra of Maxwell, California in 1963, and they became the parents of Gregory D. Sutton in 1964.

His efforts as a graduate student have contributed toward the following publications:

1. CO_2 Laser Output Tuning by Selective Intracavity Absorption, I. Burak, J. I. Steinfeld, and D. G. Sutton, J. Appl Phys. 39, 4464 (1968).
2. Infrared Saturation in Sulfur Hexafluoride, I. Burak, J. I. Steinfeld, and D. G. Sutton, J. Quant. Spectry. and Radiat. Transfer 9, 959 (1969).
3. Infrared-Infrared Double Resonance, I. Burak, A. V. Nowak,

J.I. Steinfeld, and D.G. Sutton, J. Chem. Phys. 51, 2275 (1969).

4. Infrared Double Resonance in Sulfur Hexafluoride, J.I. Steinfeld, D.G. Sutton, I. Burak, and A.V. Nowak, J. Chem. Phys. 52, 5421 (1970)

He is presently a full member of the Society of Sigma Xi and a member of the American Physical Society.